THE INFLUENCE OF PH AND CHEMICAL DENATURANTS ON METAL BINDING AND STRUCTURE OF ANTHRAX LETHAL FACTOR

By

Becky Suet Yan Lo

A thesis submitted in partial fulfillment of the requirements for the degree of Master of Science (M.Sc.) in Chemical Sciences

The Faculty of Graduate Studies

Laurentian University
Sudbury, Ontario, Canada

THESIS DEFENCE COMMITTEE/COMITÉ DE SOUTENANCE DE THÈSE
Laurentian Université/Université Laurentienne
Faculty of Graduate Studies/Faculté des études supérieures

Title of Thesis Titre de la thèse	THE INFLUENCE OF PH AND CHEMICAL DENATURANTS ON METAL BINDING AND STRUCTURE OF ANTHRAX LETHAL FACTOR
Name of Candidate Nom du candidat	Lo, Suet
Degree Diplôme	Master of Science
Department/Program Département/Programme	Chemical Sciences
Date of Defence Date de la soutenance	February 15, 2017

APPROVED/APPROUVÉ

Thesis Examiners/Examinateurs de thèse:

Dr. Stefan Siemann
(Supervisor/Directeur(trice) de thèse)

Dr. Aseem Kumar
(Committee member/Membre du comité)

Dr. Amadeo Parissenti
(Committee member/Membre du comité)

Dr. Mazdak Khajehpour
(External Examiner/Examinateur externe)

Approved for the Faculty of Graduate Studies
Approuvé pour la Faculté des études supérieures
Dr. David Lesbarrères
Monsieur David Lesbarrères
Dean, Faculty of Graduate Studies
Doyen, Faculté des études supérieures

ACCESSIBILITY CLAUSE AND PERMISSION TO USE

Abstract

Bacillus anthracis is the causative agent of anthrax, and secretes a three-component toxin consisting of protective antigen (PA), edema factor (EF), and lethal factor (LF). LF is a zinc-dependent metallopeptidase responsible for cleaving mitogen-activated protein kinase kinases in the cytosol. To reach the cytosol, LF must be unfolded to pass through the narrow lumen of the PA channel embedded in the endosomal membrane. Whether the metal-binding motif in LF remains intact, and the Zn^{2+} ion is co-translocated along with the protein is currently unknown. Using a combination of intrinsic tryptophan fluorescence spectroscopy and chelator studies to probe the unfolding and metal status of LF, this study shows that acidification from pH 7 to pH 5 leads a marked destabilization of LF's native fold, and a significantly increased degree of Zn^{2+} accessibility (to chelation) and release. Furthermore, red-edge excitation shift studies show that LF still retains a partial fold even when exposed to low pH and high concentrations of denaturants. Taken together, these results provide insights into the structure and metal status of LF under conditions similar to those encountered during translocation *in vivo*, and they suggest that LF's Zn^{2+} ion is likely lost during PA-mediated translocation.

Acknowledgements

First and foremost, I sincerely thank my supervisor (Dr. S. Siemann) for his guidance, help, and the opportunities that he has given me over the years (before and during my Master's studies). I also thank the committee members, Dr. A. Kumar and Dr. A. Parissenti, for their time and advice on this project.

I also thank my labmates for their company and support. A special thanks goes to those who helped me with some of the experiments, including Ananya Beruar (LF aggregation), Carter Hayes (chelation studies), and Calvin Young (LF isolation). Lastly, I would like to show my appreciation to all professors and technicians of the Chemistry and Biochemistry department at Laurentian University.

Table of Contents

List of Tables

List of Figures

List of Abbreviations

Å	Ångström
AD	Alzheimer's disease
AMT buffer	Acetic acid, MES, Tris three-component buffer
APS	Ammonium persulfate
ATP	Adenosine triphosphate
ATR	Anthrax toxin receptor
BclA/B	*Bacillus anthracis* glycoprotein A/B
C	Cysteine
c	Concentration
cAMP	Cyclic adenosine monophosphate
CDC	Cholesterol-dependent cytolysin
CMG2	Capillary morphogenesis gene-2
C_{mid}	Midpoint concentration
Complex III	Cytochrome c reductase
Complex IV	Cytochrome c oxidase
Cr	Core
Ct	Coat
Cx	Cortex
D	Aspartate
DMSO	Dimethyl sulphoxide
DNA	Deoxyribonucleic acid
E	Glutamate
EF	Edema factor
ERK	Extracellular receptor kinase
Exo	Exosporium
Fl	Fluorescence intensity
Gdm^+	Guanidinium ion
GdnHCl	Guanidine hydrochloride
GdnSCN	Guanidine thiocyanate
H	Histidine
HEPES	*N*-2-Hydroxyethylpiperazine-*N*'-2-ethanesulfonic acid
I	Ionic strength
I	Intermediate state
JNK	Jun N-terminal kinase
K_d	Dissociation constant
kDa	Kilodalton
LF	Lethal factor
m	Denaturant dependence of ΔG°
MAPKK	Mitogen-activated protein kinase kinase
MES	2-(*N*-morphoplino)ethanesulfonic acid
MIDAS	Metal ion-dependent adhesion site
MRN	Mre11-Rad50-Nbs1
MT	Metallothionein

mV	Millivolt
N	Native state
NATA	*N*-acetyl-L-tryptophanamide
NLRP1	NOD-like receptor pyrin domain containing 1
O.D.	Optical density (absorbance)
p38 MAPK	p38 mitogen-activated protein kinase
PA	Protective antigen
PAR	4-(2-pyridylazo)resorcinol
PEG	Polyethylene glycol
PFT	Pore-forming toxin
Phe	Phenylalanine
PKA	Protein kinase A
pK_a	Acid dissociation constant
PMF	Proton motive force
R	Gas constant
REES	Red-edge excitation shift
rpm	Revolutions per minute
s.d.	Standard deviation
SASPs	Small acid-soluble proteins
SDS	Sodium dodecyl sulfate
SOD	Superoxide dismutase
S-*p*NA	Lethal factor substrate II (Ac-GYβARRRRRRRRVLR-*p*NA,*p*NA=*para*-nitroanilide)
T	Temperature
TEM8	Tumor endothelial marker 8
TEMED	*N,N,N'N'*-Tetramethylethylenediamine
Tris	Tris(hydroxymethyl)aminomethane
U	Unfolded state
UV	Ultra-violet
v/v	Volume by volume
W	Tryptophan
w/v	Weight by volume
WHO	World Health Organization
Y	Tyrosine
Zincon	2-Carboxy-2'-hydroxy-5'-sulfoformazylbenzene
ZIP	Zrt/Irt-like protein
ZnF	Zinc finger
βCD	β-cyclodextrin
ΔG°	Gibbs free energy
ΔpH	Proton gradient
λ_{exc}	Excitation wavelength
λ_{max}	Emission/absorption maximum
$\times g$	Relative centrifugal force

1 Introduction

1.1 Biological roles of metals

1.1.1 General considerations

Metals are essential to life, and many biological processes require metals such as sodium (Na), potassium (K), magnesium (Mg), calcium (Ca), vanadium (V), molybdenum (Mo), tungsten (W), manganese (Mn), iron (Fe), cobalt (Co), nickel (Ni), copper (Cu), and zinc (Zn) for function (1). The abundance of transition metals is in the following order for eukaryotes: Fe> Zn> Cu> Mn> Mo and Co (2). Functions such as muscle contraction, signal transduction, cellular respiration and metabolism rely on metals. In plants and some microorganisms, photosynthesis requires metals to produce carbohydrates (1). In addition, in recent decades, metals have been widely used in the medical field in the form of metal-based compounds for anticancer therapy, and in the form of metal isotopes in radio imaging (3,4). It is believed that ~ 30% of all proteins and 40% of all enzymes contain at least one metal ion. Owing to a metal's unique chemical characteristics, it fulfills and carries out many specific biological functions (see Table 1.1).

Table 1.1: Biological functions of selected metal ions. The same metal can carry out diverse biological functions, and different metals can perform the same task. This table was modified from (1).

Metal	Biological functions
Sodium	Charge carrier, osmotic balance
Potassium	Charge carrier, osmotic balance
Magnesium	Hydrolase, isomerase, structure
Calcium	Charge carrier, trigger, structure
Vanadium	Oxidase, nitrogen fixation
Molybdenum	Oxidase, nitrogen fixation, oxo transfer
Tungsten	Dehydrogenase
Manganese	Oxidase, photosynthesis, structure
Iron	Oxidase, dioxygen transport and storage, nitrogen fixation, electron transfer
Cobalt	Oxidase, alkyl group transfer
Nickel	Hydrogenase, hydrolase
Copper	Oxidase, dioxygen transport, electron transfer
Zinc	Hydrolase, structure

1.1.2 Metals as cofactors

Metals can carry out diverse physiological functions in proteins as cofactors because of the metals' different characteristics (5,6). For instance, metals can form bonds that are stronger than hydrogen bonds but weaker than covalent bonds, an aspect that is very beneficial to reversible reactions. Secondly, metal binding can be ligand-specific, as only the right combination of ligands and metal can facilitate reactions. Thirdly, metal-ligand bonds can be made or broken in response to external factors such as pH or temperature. In addition, metals can be involved in redox reactions either in enzymes or as electron carriers (1,5). There are different classes or families of metalloproteins which are classified according to their function (see Figure 1.1) (6).

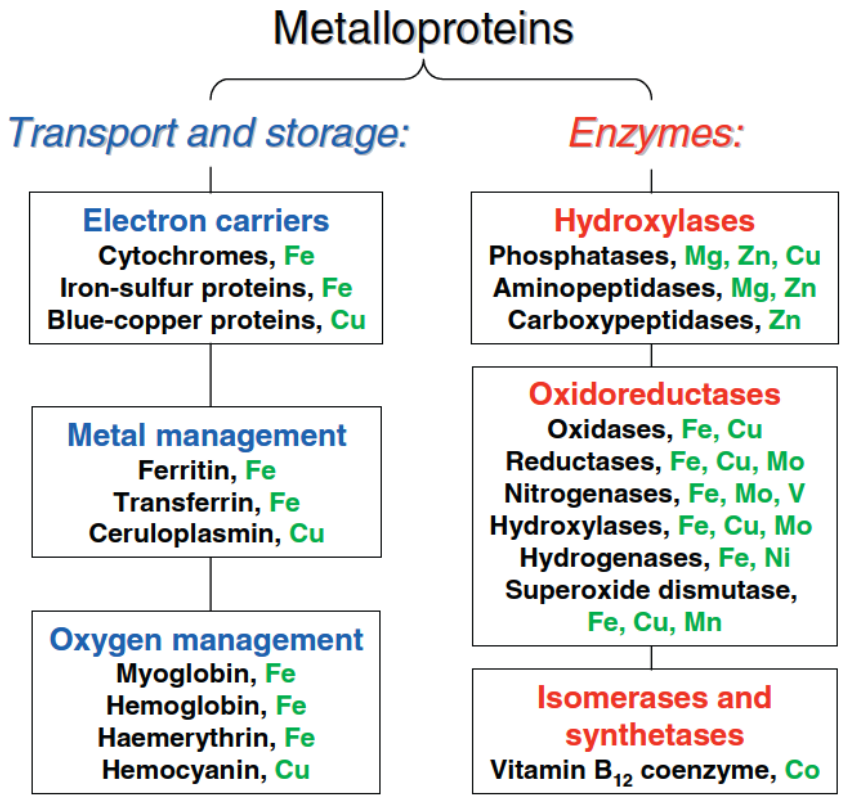

Figure 1.1: Classification of metalloproteins. Some of the metalloproteins can be classified as enzymes (red), while others are involved in transport and storage (blue). Metals utilized in each group are shown in green. This figure was adapted from (6) with permission from Cambridge University Press.

It is not surprising that some of the metalloproteins have been studied extensively given their importance in facilitating fundamental biological processes (1,2). In eukaryotes, cytosolic Cu/Zn superoxide dismutase (SOD), for instance catalyzes the disproportionation of the superoxide radical (O_2^-) into oxygen (O_2) and hydrogen peroxide (H_2O_2), hence preventing cells from oxidative damage (7). Nitrogenase expressed by some bacteria, contains Fe and Mo to reduce atmospheric nitrogen (N_2) to ammonia (NH_3), which is subsequently used as a source of nitrogen in the formation of amino acids and nucleic acids (8). In vertebrates, hemoglobin, a Fe-heme protein, functions in red blood cells to transport oxygen (9). Cytochrome c reductase (complex III) uses a Fe-S cofactor to transfer electrons to cytochrome c oxidase (complex IV), a process required for ATP production (10). Plastocyanin contains Cu^{2+} to function as an electron carrier necessary for photosynthesis (1). Zinc fingers (ZnF) are structural motifs in transcription factors which stabilize DNA during transcription (11).

1.1.3 Effect of metals on protein folding

In addition to the aforementioned roles in biological systems, metals can also direct the assembly and folding of proteins (5,6,12). The role of metals in protein folding has been studied using demetallated and metal-reconstituted proteins, by monitoring structural changes upon metal insertion. One of the most studied copper proteins is azurin, an electron carrier isolated from *Pseudomonas aeruginosa* (6). In the unfolded state, it binds to Cu^{2+}in milliseconds. In contrast, the process of metal binding to folded apo-azurin requires minutes to complete. In addition, when Cu^{2+} binds to the unfolded state of azurin, the formation of an active holo-azurin is 4000 times faster compared to its formation via the folded apo-state (see Figure 1.2). The metal in azurin is typically Cu^{2+}, but it can be replaced by other metals such as Zn^{2+}. However, its binding affinity for Zn^{2+} is 17,000-fold lower than that for Cu^{2+}.Another example illustrating the role of metals in protein folding is cytochrome c because in the absence of Fe^{2+}, the unfolded apoprotein cannot fold into its native state (6). In conclusion, metals can stabilize proteins prior to their folding, hence playing an essential role in protein assembly.

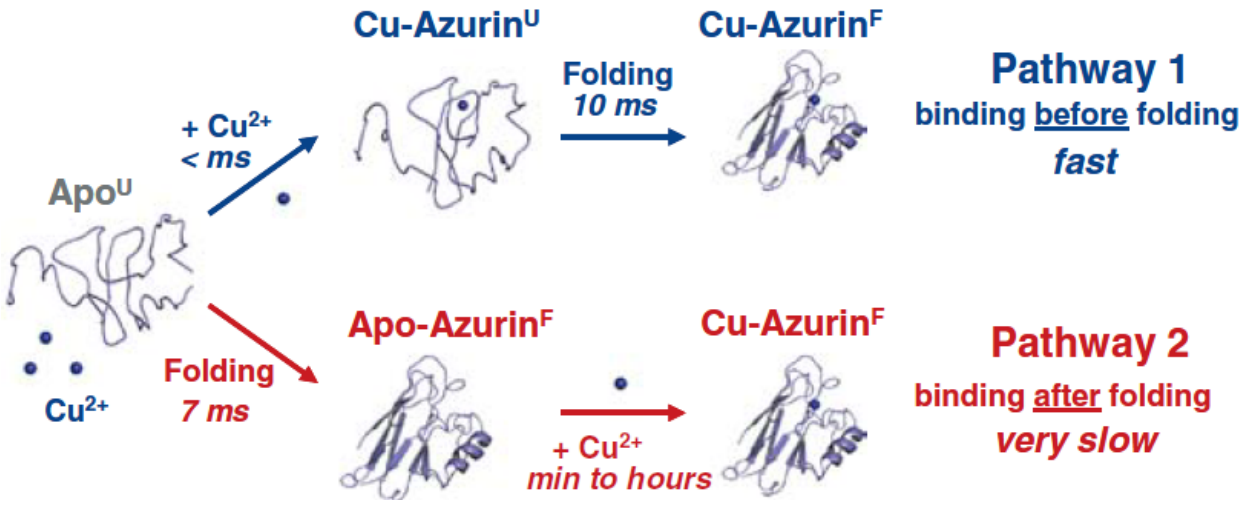

Figure 1.2: Time scale for the formation of Cu-azurin. Two pathways account for the formation of active azurin. In pathway 1 (blue), the Cu^{2+} ion binds to the unfolded protein almost instantaneously. The folding of Cu-azurin then proceeds within ~10 ms. On the other hand, when the protein folds first, the binding of the Cu^{2+} ion requires minutes to hours to complete (pathway 2 in red). This figure was adapted from (6) with permission from Cambridge University Press.

Metals are linked to neurodegenerative diseases such as Alzheimer's disease (AD), Parkinson's disease, and prion diseases, which are characterized by the presence of misfolded proteins such as amyloid-β peptides in AD that bind to the metals, thus increasing the levels of Cu^{2+}, Fe^{2+}, Zn^{2+} ions in the brain (13,14). Whether the metals are the cause or the consequence of these diseases is unknown, but the Cu/Zn-amyloid-β complex is only detected in AD patients, and metals are known to accelerate the aggregation of amyloid-β to form amyloid plaques (15-17).

1.1.4 Zinc

Compared to other trace metals, Zn^{2+} is a strong Lewis acid but does not undergo redox reactions. Its roles are to promote hydrolysis reactions, as well as to provide structural support in proteins (18). It represents the 2nd most abundant transition metal in the human body (11). Although the total weight of Zn in the human body is less than 0.01%, at least 10% of the genome encodes Zn proteins. Over 300 zinc-dependent enzymes have been discovered

covering all classes of enzymes (11,18,19). According to the Irving-Williams series (Mn< Fe< Co< Ni< Cu > Zn), Zn^{2+} is only second to Cu^{2+} in terms of forming very stable metal-protein complexes (20); therefore, the majority of Zn^{2+} in cells form complexes with proteins rather than being present as the free ions. The cytosolic free Zn^{2+} concentration is in the picomolar range, as compared to the total cellular Zn^{2+} concentration which is in micromolar range (18). In addition, Zn^{2+} has multiple crucial roles in eukaryotes. It is a neurotransmitter which is involved in extracellular cell-to-cell communication, and it functions as the secondary messenger important for DNA synthesis (21). Given its role in many biological processes it is not surprising that zinc is important to our nutrition. According to the World Health Organization (WHO), zinc deficiency affects more than 25% of the world's population, mostly in the undeveloped countries (21,22). It is important for an adult to consume ~ 15 mg of Zn per day in order to maintain good health, and proper brain and immune system function (11,22).

1.1.5 Zn^{2+} binding sites

There are five classes of Zn^{2+} binding sites (see Figure 1.3). The amino acid residues typically used for Zn^{2+} binding are histidine (H), aspartate (D), glutamate (E), and cysteine (C) (23,24). The first class is the catalytic Zn^{2+} site which contains one Zn^{2+} ion binding to three ligands and one water molecule (see Figure 1.3a). Catalytic Zn^{2+} sites are found in anthrax lethal factor (LF), thermolysin, alcohol dehydrogenase, carboxypeptidases, and many other hydrolases. The water molecule in catalytic sites functions as the nucleophile during catalysis (23). The second and third class of Zn^{2+} sites are structural and clustered Zn^{2+} binding sites which are predominated by cysteine (C) as the metal ligand (see Figure 1.3b and Figure 1.3c). An example of a structural Zn^{2+} site is a Zn finger (ZnFs) which structurally supports DNA transcription. Clustered Zn^{2+} sites are found in metallothioneins (MTs) which can bind multiple Zn^{2+} ions per site, and are involved in metal detoxification and metal storage (12,23). The fourth class of Zn^{2+} sites is related to transport, and can be found in Zn transporters such as the Zrt/Irt-like (ZIP) protein (see Figure 1.3d). In this case, the Zn^{2+} ions are loosely bound and no cysteine residue serves as a metal ligand in this class (23). Lastly, the interprotein Zn^{2+} binding site is the least studied class. It contains one Zn^{2+} ion

coordinating to at least two polypeptides (see Figure 1.3e). An example is the Rad50 protein, in which the Zn^{2+} ion functions to mediate the homodimerization of the Mre11-Rad50-Nbs1 (MRN) complex regulating the detection of DNA damage and repair (25). This class of Zn^{2+} site can fulfill all sorts of functions such as structural, regulatory, and catalytic roles (23).

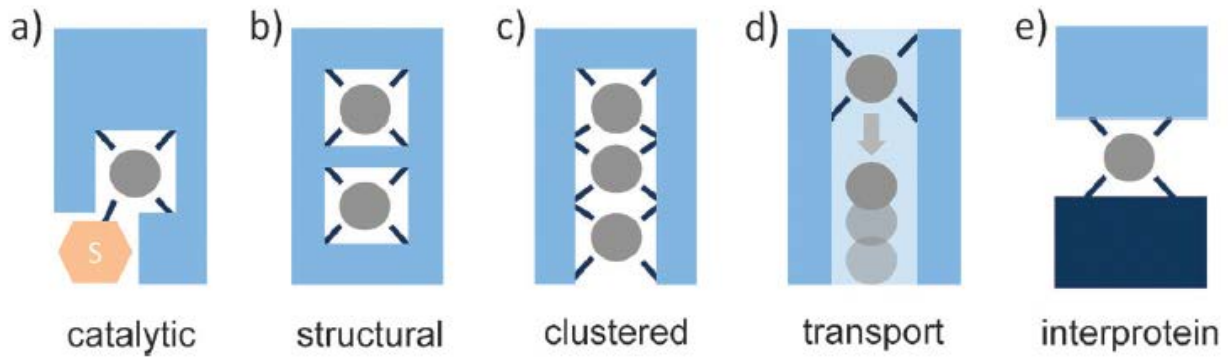

Figure 1.3: Five classes of Zn^{2+} binding sites. Five classes of Zn^{2+} binding sites have been identified based on their functions and the nature of the primary ligands. This figure was adapted from (23) with permission from The Royal Society of Chemistry.

1.2 Anthrax

1.2.1 A brief history of anthrax and its use as an agent of bioterrorism

Anthrax is a devastating, often lethal disease that has threatened public health on a global scale. It is caused by the rod-shaped, aerobic, spore-forming Gram-positive bacterium *Bacillus anthracis* (26-28). The earliest record of anthrax originated in Egypt and Mesopotamia around 5000 BC, and an incident of the disease may have been described in the Bible (Chapters 7 - 9 in the Exodus) (26,29). Since then, cases of anthrax from all over the world have been documented including its use as a modern biological warfare agent (30). Prior to the late 19th century, anthrax represented the major cause of death in animal livestock and a deadly disease in humans. The word "anthrax" derives from the Greek word *anthrakis*, which describes the black coat on skin lesions observed in infected individuals (29,30).

The inhalational form of anthrax has a very high mortality rate in humans (45 - 80%) which is caused by the spores produced by *B. anthracis*. The spores are extremely resistant to harsh environments (26,31). Anthrax has become one of the most dangerous biological weapons since World War I and II. It was estimated by the World Health Organization (WHO) that anthrax can kill as many people as a nuclear weapon (28). In fact, the use of biological weapons preceded the discovery of microorganisms by many centuries. For instance, in the early 14th century, European Tatar soldiers delivered the corpses of plague (caused by *Yersinia pestis*) victims to their enemy's towns to spread the disease (29). Anthrax, plague and cholera were the most popular agents of biological warfare. In Canada, the use of anthrax was promoted by Nobel laureate Frederick Banting to defend against foreign biological weapons (28). The most notorious human experimentation involving anthrax was performed by the unit 731 of the Japanese military in China, causing thousands of deaths in the 1930s. The former Soviet Union secretly conducted spore production and research for military purposes from 1973 to 1992 (28,29). The most recent bioterrorism attack was in 2001, where anthrax spores were deliberately dispersed in the mail, raising public safety concerns in the United States. It also highlighted the economic impact because the US government spent nearly $2 billion US dollars on medical treatments and decontamination (28).

1.2.2 Germ theory of disease

In the 1870s, Robert Koch had identified the life cycle of *B. anthracis*, and discovered their spore production as the only source for anthrax infection (see Figure 1.4). This discovery represents the first time in history that a direct link between microorganisms and disease had been established. It was called the germ theory of disease (28,29).

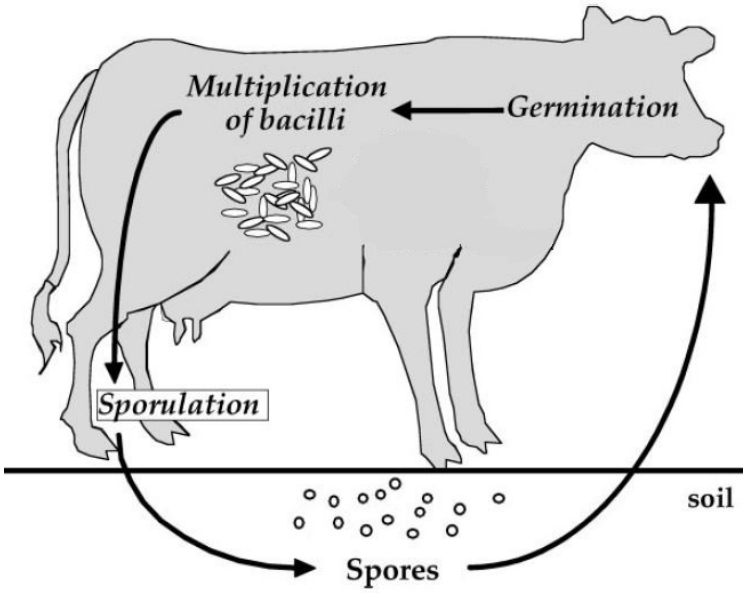

Figure 1.4: The life cycle of *Bacillus anthracis.* *B. anthracis* is the Gram-positive bacterium responsible for anthrax. The bacteria can produce spores that can persist in contaminated soil for decades until ingested by warm-blooded animals. The spores germinate into vegetative cells and multiply in the host (26,30,32). The vegetative bacteria produce virulence factors which eventually cause the death of the host. Upon death, sporulation is triggered by the presence of free oxygen leading to the initiation of another round in the life cycle of *B. anthracis*. This figure was modified from (27).

Louis Pasteur was not convinced of Koch's germ theory, until he had prepared the first anthrax vaccine himself in the 1890s by injecting an attenuated *B. Anthracis* strain into animals (29,30). Koch's findings were confirmed, and vaccinations were widely used in animal farming representing a milestone in vaccine research. After vaccine distribution, the loss of animal livestock decreased from 14% to 0.54% during 1897/98 in the United States (29). However, the first anthrax vaccine for humans was not developed successfully until the 1950s by the US Amy Corps. The safety and effectiveness of anthrax vaccines on human are not guaranteed even today, where only a small amount of people such as those in the military can receive vaccination in the U.S (29,30). Unfortunately, it was reported that ~ 7.9% of individuals who received vaccinations suffer from adverse reactions like memory loss, reduction in eyesight, muscle twitches, and hair loss. A considerable number of these side effects are reported to be the consequence of a zinc deficiency (33).

1.2.3 Spores

Anthrax spores are the metabolically inactive form of *B. anthracis* that is essential for its survival (34). The vegetative bacteria grow best aerobically at 37 °C, but they can form spores when growth factors are not abundant (26,34). Spores are highly resistant to chemical agents, heat, pressure, ionizing and UV radiation (26). Their high tolerance to adverse environments can be attributed to the anatomy of *B. anthracis* (see Figure 1.5). The bacterium is composed of four layers: the core (Cr), the cortex (Cx), the coat (Ct), and the exosporium (Exo) (see Figure 1.5b). Chromosomes are packed and protected in the core by small acid-soluble proteins (SASPs). Cx represents the second inner layer which keeps the core dehydrated. The third layer (Ct) is comprised of ridges and valleys preventing the entry of microbes and toxin molecules. The most outer layer is Exo which contains surface glycoprotein BclA and BclB, which communicate the environmental factors and are crucial for germination. In addition, these proteins are the target for vaccination (34). There are three routes of spore entry into the host: cutaneous, inhalational, and gastrointestinal (26,31). Cutaneous cases account for ~ 95% of naturally occurring anthrax, whereas the inhalational form is rather rare, and acquired mostly by deliberate anthrax dispersal (31). Gastrointestinal anthrax often occurs in developing countries following ingestion of meat from infected animals (35). It represents the least common form of anthrax. Spores germinate into vegetative cells in the presence of amino acids, ribonucleoside, and peptidoglycan fragments, which are detected by receptors located in the spore's inner membrane (28,34).

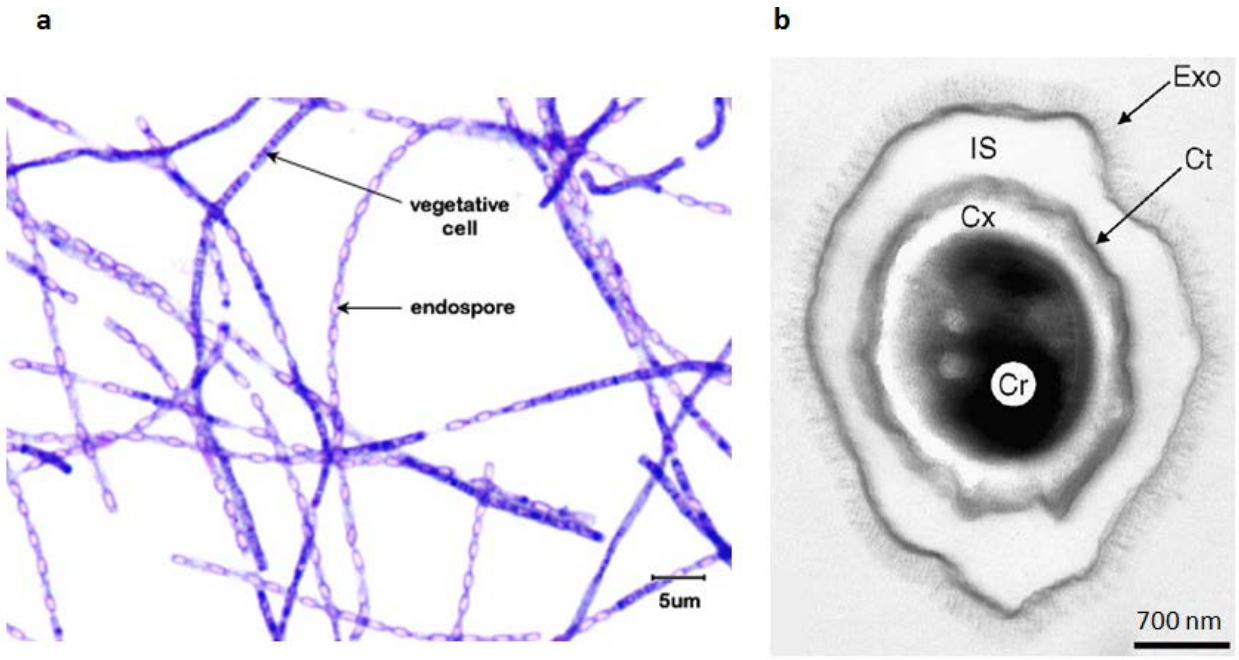

Figure 1.5: Anatomy of *Bacillus anthracis* spores. a.) Micrograph of vegetative cells and endospores. *Bacillus anthracis* bacteria are rod-shaped with spores developing inside the cells. b.) Cross-section electron micrograph of a spore showing the layered structures: Core (Cr), cortex (Cx), coat (Ct), interspace (IS), and exosporium (Exo). The figure was modified from (34) with permission from Elsevier.

1.2.4 Pathogenesis

There are two major virulence factors of *Bacillus anthracis*: the capsule and the anthrax toxin (27,36). The capsule is a negatively charged poly-D-glutamic acid sheath protecting bacteria from phagocytosis, and is encoded on the pXO2 plasmid (27,36-38). The anthrax toxin, which is encoded on the pXO1 plasmid, is comprised of protective antigen (PA), lethal factor (LF), and edema factor (EF) (27,37,38). PA is a pore-forming protein involved in the translocation of LF/EF into the cytosol of host cells. In the absence of PA, both LF and EF are non-cytotoxic (36). LF and EF exhibit enzymatic activities which target primarily signalling proteins. They weaken and deteriorate the immune system and organs of the host systematically (see Figure 1.6) (36). More specifically, LF cleaves almost all types of mitogen-activated protein kinase kinases (MAPKKs) in humans, and appears to activate the inflammasome sensor NLRP1 in rodents (36). On the other hand, EF is a calmodulin-activated adenylyl cyclase which converts massive amounts of ATP into cyclic adenosine monophosphate (cAMP)

(36,39). These actions impair various downstream signalling pathways. For example, LF can inactivate extracellular receptor kinase (ERK), Jun N-terminus kinase (JNK), p38 mitogen-activated protein kinase (p38 MAPK), and the proteins that are responsible for the secretion of pro-inflammatory cytokines (36,37). One molecule of EF depletes cellular ATP at 2000 molecules per second, and the resulting production of cAMP leads to excess cellular fluid, organ bleeding, activation of protein kinase A (PKA), and inhibition of cytokine receptors (36,40). Overall, PA, EF, and LF work together to disable the immune response to promote pyroptosis, leading to haemorrhage, edema, necrosis and death if not treated rapidly (36,37).

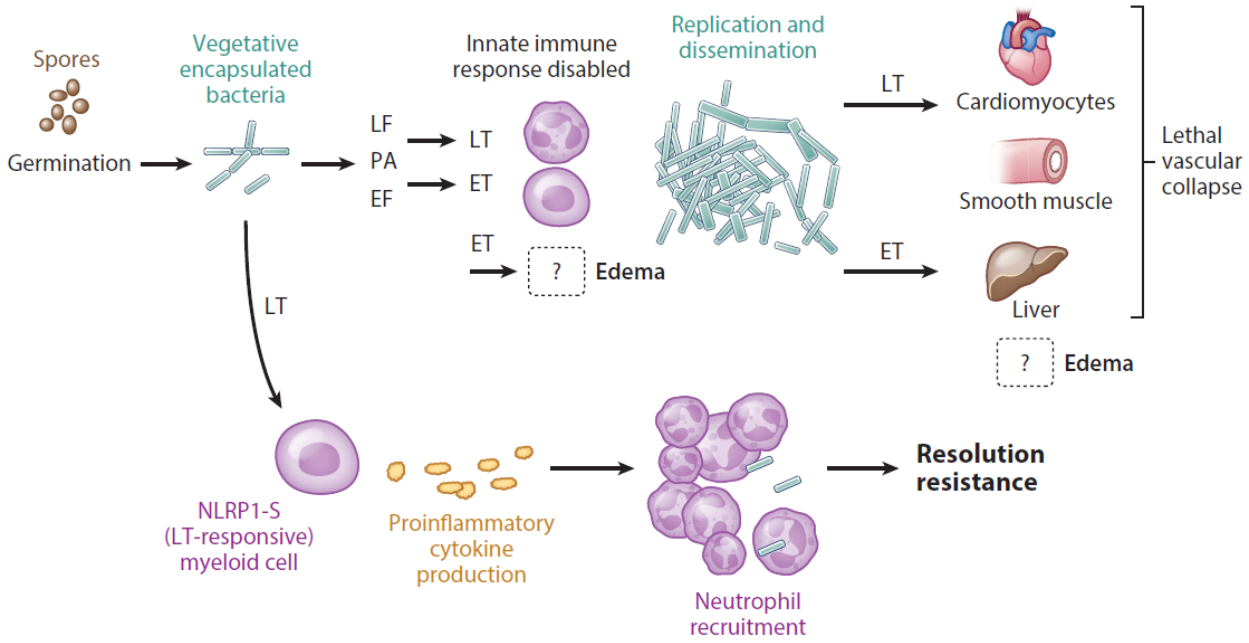

Figure 1.6: Anthrax pathogenesis. Spores germinate into vegetative encapsulated *B. anthracis*, and secrete toxins such as PA, LF, and EF inside the host. LF and EF work to disable the innate immune response, allowing bacteria to replicate and disseminate through the blood stream. Eventually, LF and EF target vital organs such as heart and liver (36). In addition, LF activates NLRP1 proteins on (rodent) macrophages to increase the production of pro-inflammatory cytokines leading to neutrophil recruitment (36,39). This figure was taken from (36).

1.2.5 Treatments

Anthrax is still a lethal disease (26,31). Early diagnosis of anthrax is crucial for a patient's survival. The symptoms of different forms of anthrax (cutaneous, inhalational, and

gastrointestinal) vary, and a proper diagnosis is often delayed especially for inhalational anthrax where the symptoms are similar to that of the flu (41). According to the US Center for Disease Control (CDC), anyone who is suspected of having anthrax should be treated with antibiotics and be vaccinated for 60 days (42). *B. anthracis* is susceptible to most antibiotics such as doxycycline, penicillins, levofloxacin, and ciprofloxacin. However, any internalized LF/EF continues to display enzymatic activities for weeks (41). There are commercially available neutralizing agents which block the entry of toxins or inhibit the activities of LF/EF directly (see Figure 1.7). Currently, Abthrax is the only FDA-approved monoclonal antibody which binds to the domain 4 of PA, preventing it from interacting with the anthrax toxin receptor (43). Enzymatic activity inhibitors such as Adefovir dipivoxyl are small compounds that can penetrate the cell membrane and inactivate EF in the cytosol. Small polyvalent peptide-like β-cyclodextrins can compete with LF/ EF for binding to the PA (41). There are treatments and drugs in development, but clinical trials are required to test whether they are functional *in vivo* (41,43,44).

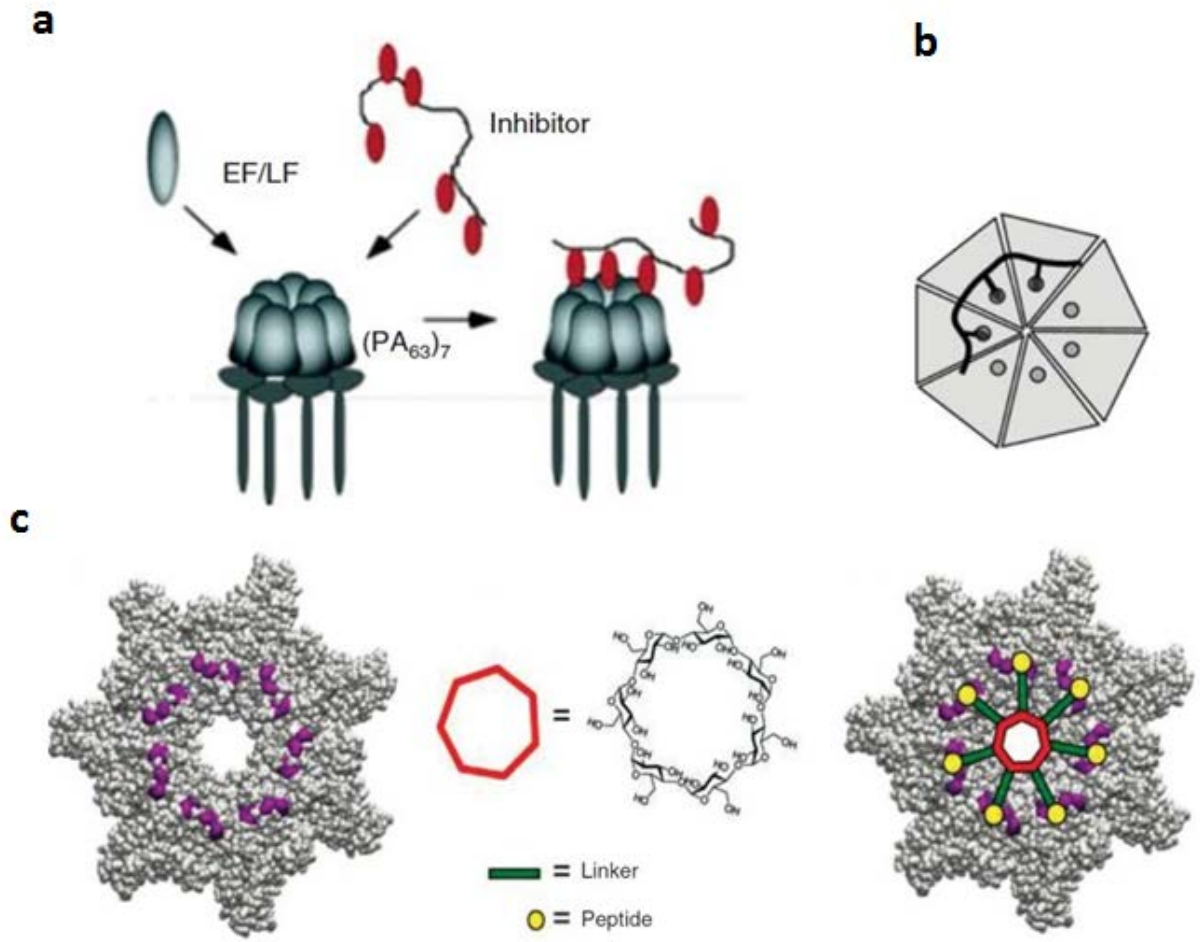

Figure 1.7: Anthrax-neutralizing agents. a.) Peptide-based inhibitor. The peptide-based polyvalent inhibitor binds to the PA_{63} heptamer preventing the entry of LF/ EF into the cell. b.) Cross-section of the PA_{63} heptamer showing the peptide binding sites (grey circles) interacting with the polyvalent peptide inhibitor (black). c.) Structure-based design inhibitor. For example, β-cyclodextrin (βCD) has a 7-fold symmetry (orange), and it can bind to the binding sites on PA (purple) via polyethylene glycol (PEG) linkers (green). The figure was modified from (41).

1.2.6 Anthrax toxin entry into host cells

The entry of the anthrax toxin components LF and EF into the cytosol requires that they must penetrate the cell membrane (see Figure 1.8) (27,38,45). Many pathogenic bacteria produce pore-forming toxins (PFT) to translocate their toxins into the cytosol or release nutrients from their host to counteract immune defense mechanisms. Bacterial toxins such as

Staphylococcus δ-haemolysins, cholesterol-dependent cytolysins (CDCs), and the PA component of the anthrax toxin form β-barrels in the host cell membrane (46). As shown in Figure 1.8, *B. Anthracis* secretes PA which binds to the membrane-associated anthrax toxin receptor (ATR) through a metal ion dependent adhesion site (MIDAS) on the cell membrane (38,47,48). There are two ATRs including the tumor endothelial marker 8 (TEM8) and the capillary morphogenesis gene-2 (CMG2). Upon binding to the ATR, PA (83 kDa) is activated by furin proteases (by removal of a 20 kDa fragment from the N-terminus), a feature which facilitates the assembly of a heptameric or octameric state (36,38,45). In this state, PA can bind three to four LF/EF molecules. The prepore-LF/EF complex is then internalized by receptor-mediated endocytosis. Endosomes are integral components of a cellular pathway which allows for the internalization of nutrients or antigens from the cell surface. After sorting and trafficking, antigens eventually are sent to lysosomes which contain the necessary hydrolases for their degradation (49). However, the anthrax toxin has evolved to escape from endosomes (into the cytosol) early, before reaching the lysosomes.

The low endosomal pH (pH 6.0 – 5.0) triggers the formation of the PA pore. The PA pore consists of a long β-barrel stem that penetrates the endosomal membrane, allowing the unfolded chains of LF/EF to enter the cytosol one at a time (50). Upon the arrival, LF/EF refolds back into the native state to display its enzymatic activity (51,52). The mechanism of translocation is not fully understood. For example, neither the degree of protein unfolding nor the fate of LF's catalytic Zn^{2+} (whether the metal binding site is disrupted and leads to the loss of the metal ion) during translocation is known (53).

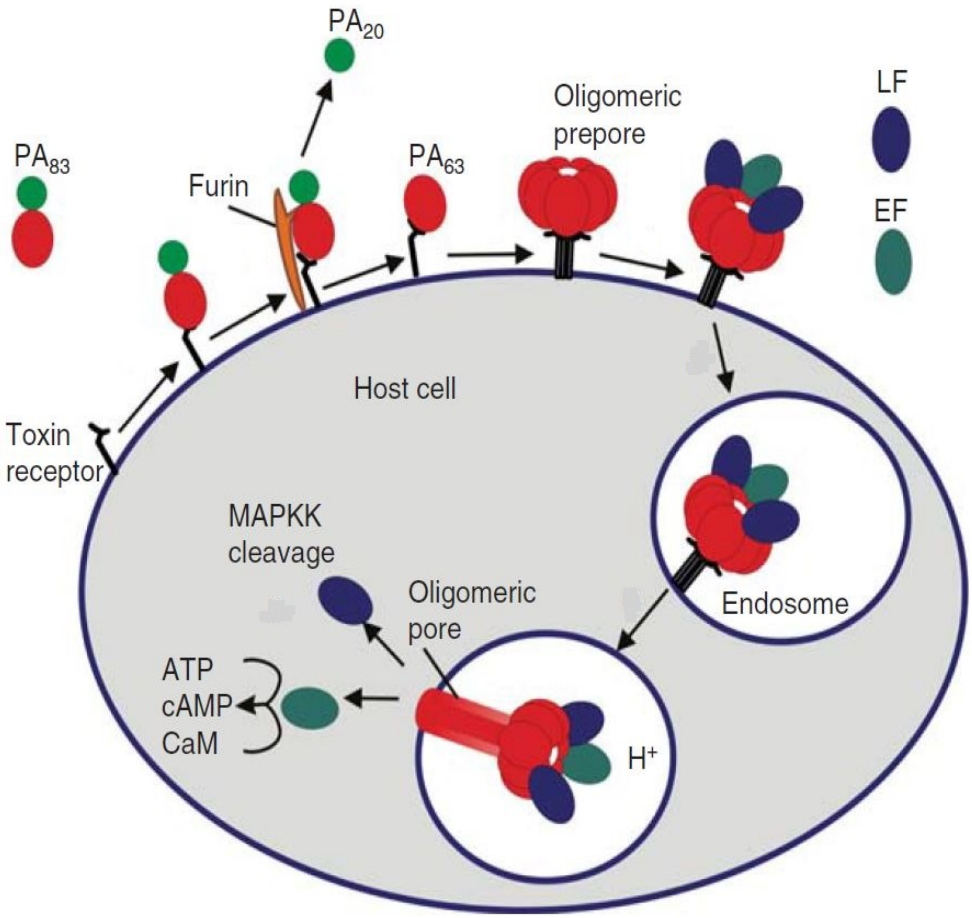

Figure 1.8: Delivery of the anthrax toxin components LF and EF to the cytoplasm. PA_{83} binds to the ATR, and is then proteolytically cleaved by furin proteases into a 20 kDa (PA_{20}) and a 63 kDa fragment (PA_{63}) (27,38). PA_{63} remains bound to the ATR, forming a PA prepore (heptamer or octamer) by oligomerization. The prepore binds up to 3 - 4 LF/EF molecules, and the LF/EF-prepore complex is then internalized through endocytosis. The acidic pH of the endosome triggers the conversion of the PA prepore to the PA pore, initiating the translocation of LF/EF into the cytosol (27,38,45). This figure was taken from (41).

1.2.7 Protective antigen (PA)

As mentioned above, PA is the pore-forming protein responsible for LF/EF translocation. The X-ray crystal structure of the PA pore is shown in Figure 1.9. The overall structure is 180 Å long and 160 Å wide. It is mushroom-shaped with two openings in the pore (51). There are four domains in PA, and each is responsible for different functions during the translocation event (38,51). Domain 1 contains a RKKR sequence which is targeted by furin proteases. It also contains a LF/EF binding site (α-clamp) at the entrance of the PA pore (38). Domain 2 forms the β-barrel penetrating the endosomal membrane, and contains a 2β10 - 2β11 loop which functions as a pH sensor for the conversion of the prepore to the pore (51). Domain 3 is highly hydrophobic, and is involved in the formation of PA oligomers. Domain 4 binds to the ATR. There is a constriction site in the heptameric PA pore (ϕ-clamp), which is 6 Å in diameter, and consists of seven Phe427 residues. During LF/EF translocation, the chemical gradient between the endosome and the cytosol is blocked at the ϕ-clamp (52). The α-clamps and ϕ-clamp are the major LF/EF binding sites which have been identified in the PA channel (51,54).

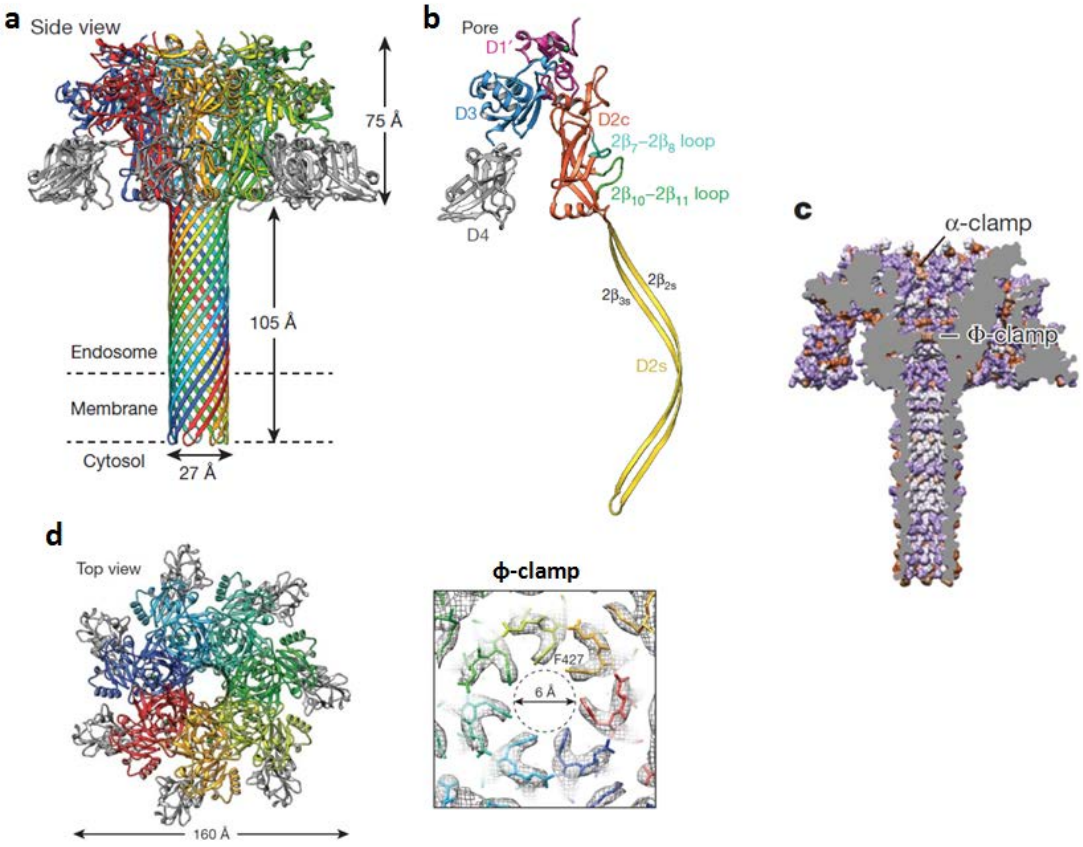

Figure 1.9: Atomic structure of the PA pore. a.) Overall dimension of the PA pore. The PA pore forms a β-barrel penetrating the endosomal membrane b.) The four-domain monomeric unit of the PA pore. Domain 1 (D1) binds to LF/EF. Domain 2 (D2) contains a pH sensor (2β10-2β11 loop) responsible for enforcing conformational changes in PA necessary for membrane insertion. c.) Cross-section of the PA pore. The α-clamp and ϕ-clamp are hydrophobic (orange) while the rest of the PA pore lumen is mostly hydrophilic (purple). d.) Top view of PA pore and the ϕ-clamp. The ϕ-clamp is the constriction site in the PA pore. This figure was modified from (51) with permission from Nature.

1.2.8 Mechanism of LF/EF translocation

The translocation event is a complicated and cooperative process (see Figure 1.10). It involves two barriers: the unfolding of LF/EF, and the translocation of the proteins (55). It requires LF/EF binding sites in the PA pore, which are the α-clamps and the ϕ-clamp. The α-clamps can guide LF/EF into the lumen of the PA pore, and assist in protein unfolding. The ϕ-clamp is the constriction site in the PA pore which separates chemical gradients from the endosome to the cytosol (52,54). The proton gradient (ΔpH) across the membrane creates a

proton motive force (PMF) which serves as the driving force for translocation (54,56). There are two hypotheses that have been advanced for the mechanism of translocation including the extended chain Brownian-ratchet model, and the allosteric helix compression model (54,57,58). Both of them propose that LF must be unfolded, and that this unfolding is assisted by the low endosomal pH during translocation. However, the more recent model, the allosteric helix compression model, incorporates conformational changes in LF during translocation, and its interaction with the PA binding sites, features neglected in the Brownian-ratchet model (57). An overview of the two LF translocation models is depicted in Figure 1.10. According to the Brownian ratchet model (Figure 1.10a), LF is partially unfolded by the presence of an acidic pH in the endosome. LF contains negatively charged acidic residues which are protonated first before entering the negatively charged PA lumen. LF, by binding to the α-clamp, is guided into the lumen of the PA channel, and continues to unfold in order to pass through the narrow pore and its constriction site. Upon the arrival in the cytosol (where the pH is neutral), the acidic residues of LF are deprotonated, and hence regain their negative charges. This causes repulsion between LF and the PA channel, a feature which prevents the retro-translocation of LF (45,56). A recent crystal structure of PA revealed that the ϕ-clamp has only a diameter of 6 Å. It is therefore incapable of accumulating a secondary structure. In addition, the α-clamps were found to bind LF's helical structure non-specifically (51,54). As a consequence of these observations, the allosteric helix compression model has been forwarded (Figure 1.10b). According to this model, LF forms α-helices inside the PA channel before it passes through the ϕ-clamp. The α-clamps bind to these secondary structures non-specifically and allosterically, leading to a change or tightening in the size of the ϕ-clamp. The increasing amount of α-helices populating the channel force LF to unfold and translocate efficiently (57).

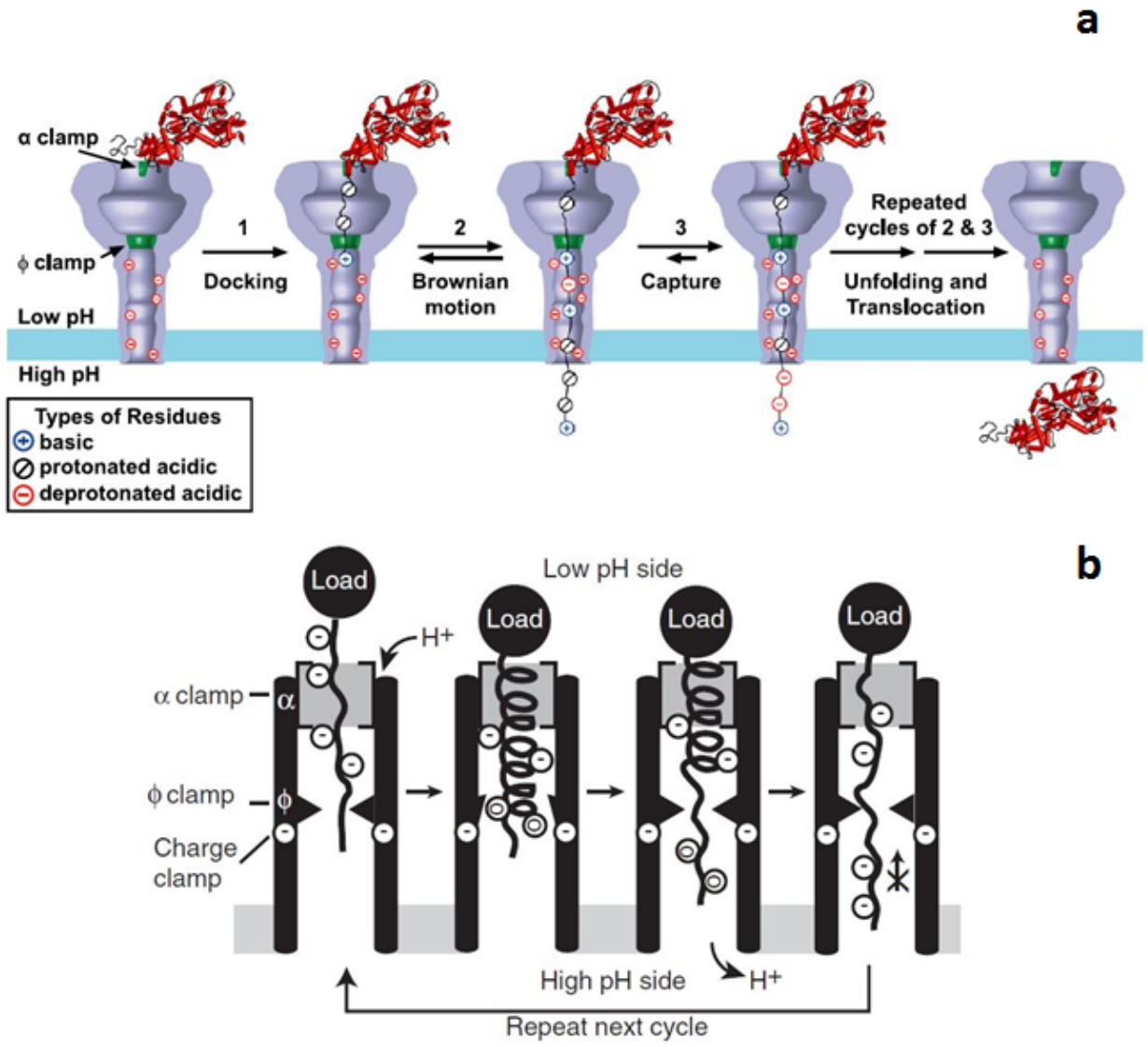

Figure 1.10: The two hypotheses for LF translocation. The proton gradient (ΔpH) across the endosomal membrane (Δ pH ~2) serves as the primary driving force for translocation. A.) Extended-chain Brownian-ratchet model. The partially unfolded LF molecule binds to the α-clamp, and translocates as a single polypeptide chain through the PA lumen. LF is captured at the ϕ-clamp to prevent bidirectional translocation, and hence, back-slipping. B.) Allosteric helix-compression model. The helical structure of LF is formed upon protonation inside the PA lumen. The helix binds to the α-clamps, and allosterically triggers conformational changes affecting the ϕ-clamp. At the ϕ-clamp, LF is forced to become a fully unfolded polypeptide. This figure was modified from (54,59).

1.2.9 Lethal factor (LF)

LF is a 776 amino acid (90 kDa) Zn^{2+}-dependent metallopeptidase which contains four domains (see Figure 1.11a). The N-terminal segment (domain I) containing 250 amino acids is homologous to that of EF, and is responsible for the binding to PA (36). Domain II takes part in the recruitment of the MAPKK substrate. Domain III shields the catalytic centre in domain IV, and is partly responsible for substrate binding. Domain IV is crucial to LF function because it houses the catalytic Zn^{2+} binding site (60,61). In the active site, one Zn^{2+} ion is coordinated to three amino acid residues (His686, His690, Glu735) and a water molecule (see Figure 1.11b). The histidine residues (His686, His690) are located on the 4α4 helix, while the glutamate residue (Glu735) is located on the 4α7 helix. These residues interact with the Zn^{2+} ion directly (60). According to mutagenesis studies, removal of any of the metal ligands results in the loss of LF's activity (62).

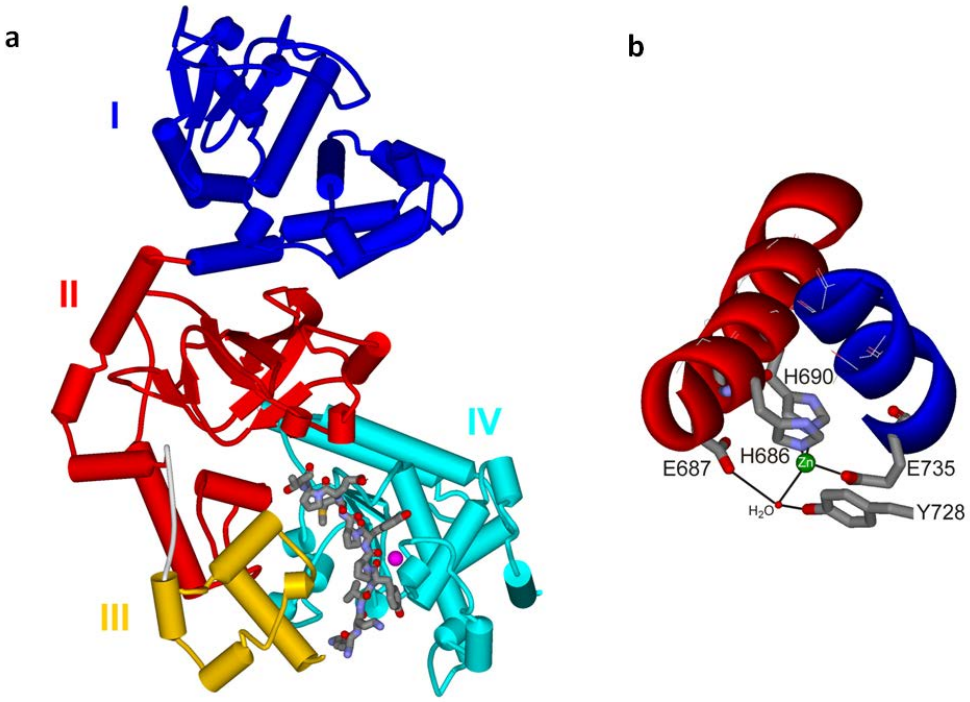

Figure 1.11: Structure of LF. a) The overall structure of LF. Domain IV contains one Zn^{2+} ion (highlighted in purple). A fragment of a MAPPK substrate located in the substrate binding groove between domains III and IV is shown as a stick model. b) The catalytic Zn^{2+} site is located between two separate helices (4α4 helix in red, and 4α7 helix in blue). The images were generated with Discovery Studio 3.5 (Accelrys, San Diego, CA) using the coordinates deposited under the pdb entry 1J7N (60).

The proposed mechanism of MAPPK hydrolysis by LF is shown in Figure 1.12 (62). LF contains a thermolysin-like H_{686}-E_{687}-x-x-H_{690}motif involved in metal binding and in the hydrolysis reaction (63). The Glu687 residue is located on the 4α4 helix and serves as a general base in the catalytic mechanism by binding and polarizing the Zn^{2+}-bound water molecule. A second shell residue, Tyr728, is located only 3.3 Å away from the Zn^{2+} ion, and also directly interacts with the Zn^{2+}-bound water molecule (62). The hydrolysis begins with the Zn^{2+}-bound water molecule nucleophilically attacking the carbonyl carbon atom of the cleavable peptide bond in the MAPPK substrate (see Figure 1.12). This reaction results in the cleavage of peptide bond. The amine leaving group is thought to be protonated and stabilized with the aid of Tyr728 (62,64).

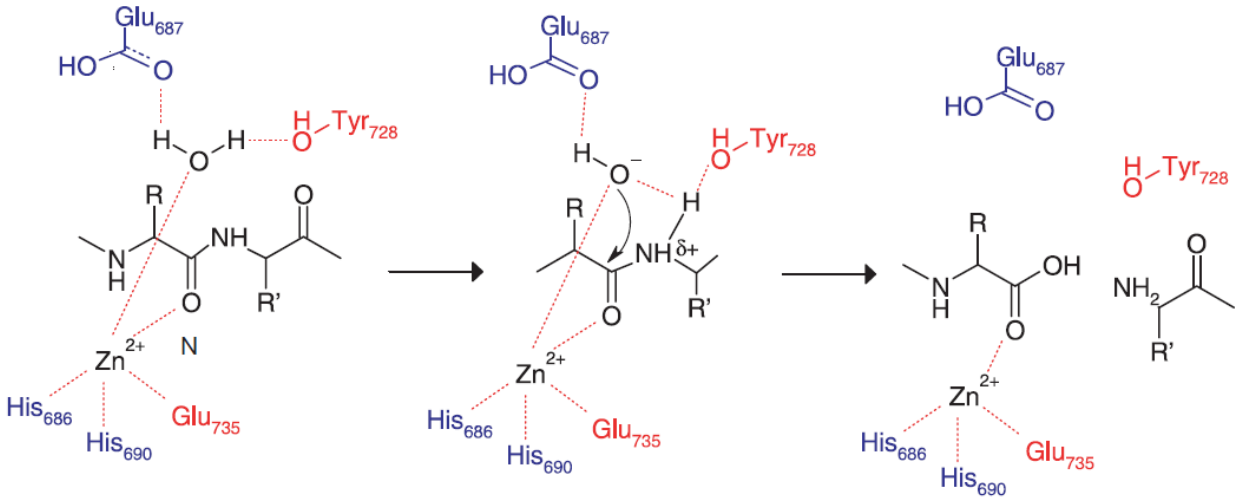

Figure 1.12: Proposed catalytic mechanism of LF. Residues highlighted in blue (Glu687, His686, His690) are part of thermolysin-like H-E-x-x-H motif. Two other residues essential for catalytic activity, and located downstream of the H-E-x-x-H motif, Tyr728 and Glu735, are depicted in red. The cleavage of MAPPKs is initiated by the attack of the Zn^{2+}-bound water molecule on the carbonyl carbon atom of the scissile peptide bond. This figure was taken from (62).

1.2.10 Fate of the catalytic Zn^{2+} site during LF translocation

The fate of LF's catalytic Zn^{2+} site during LF translocation is currently unknown. Regardless of whether translocation follows the extended chain Brownian-ratchet model or the allosteric helix compression model, LF must unfold to a single polypeptide chain in order to pass through the PA constriction site (51,54). Since the catalytic Zn^{2+} ion is anchored to two separate helices (see Figure 1.11b), it appears inevitable for the metal binding site to be disrupted during translocation. If LF loses its Zn^{2+} ion during translocation, then it must regain its metal ion somehow in the cytosol. However, free cytosolic Zn^{2+} levels are extremely low (in the picomolar range) (18), and it is questionable whether LF can effectively bind a Zn^{2+} ion in the cytosol without competing with other zinc proteins, a feature which may lead to an apparent zinc deficiency. Previous studies in our lab have revealed that LF has a high binding affinity (K_d = 1.2 pM) for its Zn^{2+} ion, and that the enzyme releases its metal ion at low pH (30% and 100% Zn^{2+} loss at pH 5.0 and 4.0, respectively) (65,66). In addition, a combination of chelator and tryptophan fluorescence spectroscopic studies has shown that the Zn^{2+} ion is not released when LF undergoes a change from the native to the unfolded state. As shown in Figure 1.13, LF was found to unfold at relatively low concentrations of GdnHCl, with the fully unfolded state of the protein being achieved at 0.75 M GdnHCl. At this concentration, however, there is only ~ 10-20% of Zn^{2+} released. In fact, a concentration of 3 M GdnHCl is required to release half of the enzyme's Zn^{2+} ions (53). Furthermore, the ability of the metal chelator 4-(2-pyridylazo)resorcinol (PAR) to access LF's active site and bind its Zn^{2+} ion was investigated in the same study (see Figure 1.14) (53). Overall, the data depicted in Figure 1.13 shows that (i) LF unfolds at low concentrations of GdnHCl as judged by fluorescence spectroscopy, (ii) at moderate denaturant concentrations, LF's metal ion becomes accessible to chelation by PAR, and (iii) only at high GdnHCl concentrations, the enzyme spontaneously loses its Zn^{2+} ion.

As outlined above, translocation through the PA pore requires a low endosomal pH and the unfolding of LF (or EF). Whether under those conditions the Zn^{2+} binding site of LF is disrupted, potentially resulting in the loss of the metal ion, is currently unknown. Hence, this thesis aims to investigate the effects of both chemical denaturants and pH on the fold, the accessibility of the active site Zn^{2+} ion to chelation, and the spontaneous release of the metal

ion. As mentioned earlier, the influence of urea and GdnHCl on LF's fold, Zn^{2+} accessibility and release at pH 7.4 has been documented previously (53). Thus, the studies described herein will extend the previous ones to cover pH values which mimic those encountered in endosomes, mainly using urea as the denaturant.

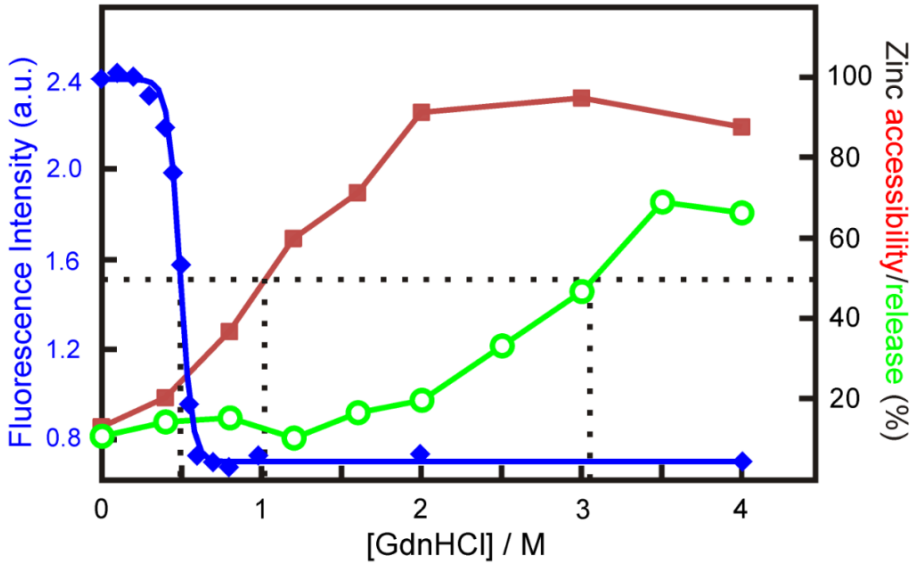

Figure 1.13: Unfolding and Zn^{2+} accessibility/release profiles recorded in the presence of GdnHCl at pH 7.4. The unfolding of LF (blue) was monitored by tryptophan fluorescence spectroscopy. The release of Zn^{2+} from LF is shown in green. The accessibility of LF's Zn^{2+} ion to chelation by4-(2-pyridylazo)resorcinol (PAR) is shown in red. This figure was prepared using the data reported in (53).

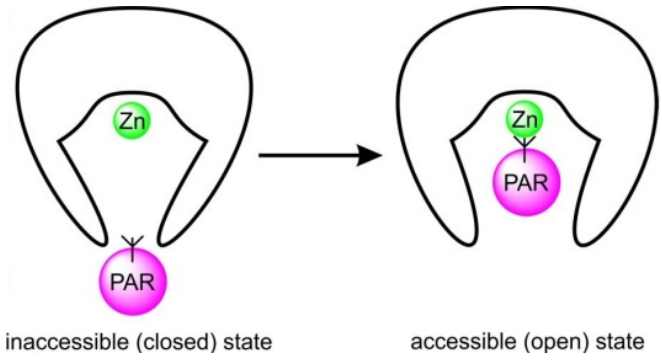

Figure 1.14: Model of accessibility of LF's Zn^{2+} ion to chelation by PAR. In the closed state (in the absence or at low concentrations of a denaturant), the chelator PAR is incapable of gaining access to the active site Zn^{2+} ion of LF. Upon an increase in the concentration of the denaturant, conformational changes in LF lead to an accessible, open state. Only in the open state, PAR is capable of penetrating the active site to bind to the enzyme's Zn^{2+} ion.

2 Hypotheses and Objectives

Hypotheses

It is hypothesized that at acidic pH values (mimicking those of the endosome), the structure of LF will be destabilized with respect to that found previously at pH 7.4 (i.e., lower concentrations of chemical denaturants are required to reach the unfolded state). Furthermore, it is hypothesized that lower pH values will more easily facilitate the release of the Zn^{2+} ion from LF's active site (compared to the neutral pH conditions (53)), and that the transition from the closed, PAR-inaccessible state to the open, PAR-accessible state will occur at lower denaturant concentrations at lower pH.

Objectives

The first hypothesis regarding the structural destabilization of LF at lower pH will be tested by monitoring the unfolding (or structural changes) of the protein in the presence of urea at different pH values by tryptophan fluorescence spectroscopy. The second hypothesis concerning the zinc release and accessibility will be tested by determining the dissociation of the metal ion from LF under acidic conditions by assessing (with the chelator PAR) the amount of Zn^{2+} in the filtrate following Amicon filtration of LF exposed to urea. In addition, the Zn^{2+} accessibility following exposure of LF to urea at different pH values will be measured spectrophotometrically using PAR. Finally, a fluorescence technique called red-edge excitation shift (REES) will be used to examine the degree of protein unfolding in LF to establish whether the protein is fully unfolded at higher denaturant concentrations.

3 Materials and methods

3.1 List of chemicals and laboratory equipment

Chemicals and laboratory equipment were purchased from the suppliers listed in Table 3.1 and Table 3.2.

Table 3.1: Chemicals

Chemical	Supplier
2-(*N*-morphoplino)ethanesulfonic acid (MES) 4-(2-Pyridylazo)resorcinol (PAR) 2-carboxy-2'-hydroxy-5'-sulfoformazylbenzene (Zincon)	Sigma-Aldrich, Oakville, ON
Acetic acid, glacial Acrylamide/Bis-acrylamide (37.5:1) 30% solution Ammonium persulfate	Bioshop, Burlington, ON
Antifoam Y-30 Emulsion	Sigma-Aldrich, Oakville, ON
Bio-tryptone Coomassie Brilliant Blue R-250 D-xylose	Bioshop, Burlington, ON
Dimethyl sulphoxide	Caledon Laboratory, Georgetown, ON
Glycerol (Biotechnology grade) Glycine (Biotechnology grade) Guanidine hydrochloride (Biotechnology grade) Guanidine thiocyanate (Biotechnology grade) *N*-2-Hydroxyethylpiperazine-*N*'-2-ethanesulfonic acid(HEPES)	Bioshop, Burlington, ON
Hydrochloric acid	Brenntag Canada Inc, Etobicoke, ON
LB agar (Miller) LB broth (Miller)	Bioshop, Burlington, ON
L-Tyrosine	Sigma-Aldrich, Oakville, ON
N,N,N'N'-Tetramethylethylenediamine (TEMED)	Bioshop, Burlington, ON
N-acetyl-L-tryptophanamide (NATA)	Sigma-Aldrich, Oakville, ON
PageRuler™ unstained protein ladder	Thermo Fisher Scientific, Burlington, ON
Polyethylene glycol 8000 (Biotechnology grade) Potassium phosphate dibasic (Anhydrous) Potassium phosphate monobasic (Anhydrous)	Bioshop, Burlington, ON
Q Sepharose™ Fast Flow	GE Healthcare, Peterborough, ON
Sodium chloride Sodium dodecyl sulfate (SDS) Sodium hydroxide	Bioshop, Burlington, ON
Sodium sulfate(Anhydrous)	BDH, Toronto, ON

Terrific broth (modified) Tetracycline (HCl form) Tris(hydroxymethyl)aminomethane (Tris) Urea (Molecular biology grade) Yeast extract	Bioshop, Burlington, ON
Zinc sulfate	Fisher Scientific, Ottawa, ON

Table 3.2: Laboratory equipment

Laboratory equipment	Company
Amicon® Ultra Centrifugal Filters	Millipore, Oakville, ON
AMSCO 3011 Gravity Pre Vacuum Single Door Sterilizer	Steris, Mississauga, ON
Avanti™centrifuge J-20XPI	Beckman Coulter, Mississauga, ON
Barnstead B-Pure water system	Thermo Fisher Scientific, Burlington, ON
BioFlo110 fermenter	New Brunswick Scientific Co, Enfield, CT
Cary 60 UV-Visspectrophotometer	Agilent, Santa Clara, CA
Centrifuge 5415C	Eppendorf, Mississauga, ON
ECHOtherm™ Benchtop Incubator – IN30	Torrey Pines Scientific, Carlsbad, CA
Epoch microplate spectrophotometer	Biotek Intruments, Winooski, VT
IEC multiRF refrigerated centrifuge	Thermo Fisher Scientific, Burlington, ON
Innova ™ 4300 incubator shaker	Eppendorf, Enfield, CT
Mini-Protean Electrophoresis System	Bio-Rad Laboratory, Mississauga, ON
Olis RSM 1000 spectrophotometer/fluorometer	OLIS, Bogart, GA
Tuttnauer autoclave-steam sterilizer 2340M	Tuttnauer, Hauppauge, NY

3.2 Preparation of stock solutions

3.2.1 AMT buffer (200 mM)

AMT is an aqueous three-component buffer system consisting of MES, Tris, and acetic acid. A 100 mL AMT stock solution with an ionic strength (I) of 200 mM was prepared by dissolving 1.952 g (0.1 M) MES, 2.423 g (0.2 M) TRIS, and 572 µL (0.1 M) acetic acid in ultrapure water from a Barnstead B-Pure water system (Thermo Fisher Scientific,

Burlington, ON). At room temperature, the pK_a values for acetic acid, MES, and Tris are 4.75, 6.15, and 8.1, respectively. Hence, AMT buffer can be used to maintain a constant ionic strength in the pH range of 4 to 9 (67).

3.2.2 Urea (8 M)

A 50 mL urea stock solution (8 M) was prepared by dissolving 24.023 g urea in either 25.75 mL Barnstead water supplemented with 6.25 mL AMT buffer (200 mM), or in 32 mL HEPES buffer (50 mM, pH 7.4). The pH was adjusted to the desired value using 1 M NaOH or 1 M HCl. Urea in AMT buffer (25 mM, desired pH) or HEPES buffer (32 mM, pH 7.4) can be kept at room temperature for at least one week.

3.2.3 Guanidine hydrochloride (GdnHCl) (8 M)

In a final volume of 50 mL, 38.212 g GdnHCl was dissolved in either 15.18 mL Barnstead water supplemented with 6.25 mL AMT buffer (200 mM), or in 21.43 mL HEPES buffer (50 mM, pH 7.4). The pH of the 8 M stock solution was adjusted to the desired value using 1 M NaOH or 1 M HCl. The stock solution was kept at room temperature.

3.2.4 Guanidine thiocyanate (GdnSCN) (5 M)

A 10 mL GdnSCN stock solution (5 M) was prepared by dissolving 5.908 g GdnSCN in either 5.42 mL HEPES buffer (50 mM, pH 7.4), or in 1.356 mL of AMT buffer (200 mM) supplemented with 8.644 mL of Barnstead water. The pH was adjusted to the desired value using 1 M HCl. The GdnSCN stock solution was kept at room temperature.

3.2.5 4-(2-Pyridylazo)resorcinol (PAR) (2 mM)

A 2 mM PAR stock solution was prepared by first dissolving 21.5 mg PAR in 2.5 mL DMSO, and then adding 47.5 mL of HEPES buffer (50 mM, pH 7.4) to achieve a final volume of 50 mL (53,68). The stock solution was covered with aluminum foil, and kept at 4 °C.

3.2.6 Tetracycline (10 mg/mL)

A stock solution of tetracycline (10 mg/mL) was prepared by dissolving 100 mg of tetracycline in 10 mL of 70 % (v/v) aqueous ethanol. The solution was kept at -20 °C.

3.3 Isolation of LF

3.3.1 LF expression system

The expression system for LF was obtained from Dr. J. Mogridge (University of Toronto, Canada), and contained the pWH1520 LF expression vector engineered into *Bacillus megaterium* (69). The plasmid contains a tetracycline resistance cassette, and the expression of LF is inducible by D-xylose. *B. megaterium* was stored at –80 °C in LB broth (Bioshop, Burlington, ON) supplemented with 20% (v/v) glycerol.

3.3.2 Preparation of starter cultures

All bacterial growth media were sterilized before being used to cultivate *B. Megaterium* cells. Sterilizations were carried out using a Tuttnauer 2340M steam sterilizer (Tuttnauer, Hauppauge, NY). Agar plates were prepared by dissolving 22.5 g LB agar (Miller) in 0.25 L of distilled water, and the starter culture was prepared by dissolving 3.75 g LB broth (Miller) in 0.15 L of distilled water. Tetracycline (10 μg/mL) was added to both solutions following sterilization. A few microliters of the *B. megaterium* stock solution (kept at -80 °C) were streaked onto an agar plate using a sterile loop. The plate was then placed for 24 h at 37 °C in an ECHOtherm IN30 incubator (Torrey Pines Scientific, Carlsbad, CA). A colony was then selected, placed in the starter culture, and incubated at 37 °C and 250 rpm for ~ 16 h in an Innova 4300 incubator shaker (Eppendorf, Enfield, CT). The absorbance at 600 nm ($O.D._{600nm}$) at the end of the cultivation period was measured on a Cary UV-Vis spectrophotometer (Agilent, Santa Clara, CA), and was found to be between 1.3 and 1.9.

3.3.3 Main culture

The main culture for the production of LF consisted of 2.7 L of Terrific broth, 0.3 L of potassium phosphate buffer, and 0.15 L of starter culture. The Terrific broth was prepared by dissolving 36 g biotryptone, 72 g yeast extract, and 12 mL glycerol in 2.7 L of distilled water. A mixture of 6.93 g monobasic potassium phosphate and 37.62 g dibasic potassium phosphate dissolved in 0.3 L distilled water was autoclaved separately. The Terrific broth was placed in a BioFlo110 fermenter (New Brunswick Scientific Co, Enfield, CT), and was

autoclaved in an AMSCO sterilizer (Steris, Mississauga, ON). To begin the cultivation of *B. megaterium*, the starter culture (0.15 L), Terrific broth (2.7 L), potassium phosphate buffer (0.3 L), and tetracycline (10 μg/mL) were mixed together inside the fermenter, and the temperature was set to 37 °C with moderate agitation (600 - 800 rpm) and aeration. After the first hour of growth, 75mL of sterile-filtered D-xylose (20% [w/v]) was added to the culture. The $O.D._{600nm}$ was monitored hourly with a UV-Vis spectrophotometer for a period of ~ 7 – 9 h or until an $O.D._{600nm}$ of 1.8 - 2.0 was reached. The bacterial culture was then transferred to 1 L centrifuge bottles and centrifuged using an Avanti J-20XPI centrifuge (Beckman Coulter, Mississauga, ON) at 7000 rpm and 4 °C for 25 min. Following centrifugation, the supernatant was carefully decanted into 3 L of a PEG-8000 solution (40% [w/v]), and the mixture was slowly stirred at 4 °C overnight.

3.3.4 Recovery of proteins

To recover the protein precipitate, the PEG-8000 protein mixture was centrifuged at 4 °C for 2 h at 7000 rpm. The supernatant was carefully discarded, and the protein pellet was transferred to a 50 mL centrifuge tube using a syringe. The pellet was then centrifuged at 4 °C at 7000 rpm using an IEC multiRF refrigerated centrifuge (Thermo Fisher Scientific, Burlington, ON) for 20 min. A volume of ~ 15 mL of Tris-HCl buffer (20 mM, pH 8.0) was added to re-solubilize the protein pellet. The solution was then centrifuged to recover the protein-containing supernatant. The remaining pellet/cell debris was supplemented with another ~ 15 mL of Tris-HCl buffer, and centrifuged as described above. All of the recovered supernatant was collected and kept on ice.

3.3.5 Purification of LF by anion exchange chromatography

A chromatography column was packed with 15 mL of Q-sepharose Fast Flow resin (GE Healthcare, Peterborough, ON) equilibrated with Tris-HCl buffer (20 mM, pH 8.0). The solubilized protein was loaded onto the column at a rate of 1 mL per min, and eluted using increasing concentrations of NaCl (150, 350, 550 mM) in Tris-HCl buffer (20 mM, pH 8.0). All eluted fractions (20 mL each) were collected on ice in centrifuge tubes. The 350 mM NaCl fraction was found to contain the majority (~ 90%) of LF.

3.3.6 Amicon filtration

Following purification, the 350 mM NaCl fraction containing LF was concentrated using a 30 kDa Amicon centrifugal filter at 4500 x *g*, and 4 °C. The retentate was supplemented with ~ 10 mL of HEPES buffer (50 mM, pH 7.4), and centrifuged. This step was repeated twice. Finally, LF was concentrated to ~ 1 mL, and the concentration (c) was determined spectrophotometrically using equation 1:

$$c = \frac{(\mathrm{Abs}_{280\mathrm{nm}} - (2 \times \mathrm{Abs}_{333\mathrm{nm}}))}{\varepsilon_{280}} \times 1\ cm \qquad (1)$$

where $\mathrm{Abs}_{280\mathrm{nm}}$ and $\mathrm{Abs}_{333\mathrm{nm}}$ represent the absorbances observed at 280 nm and 333 nm, respectively, and ε_{280} is the extinction coefficient of LF (74,200 $M^{-1}cm^{-1}$) (69). The yield of LF was typically ~3 mg LF per liter of cell culture. The LF stock solutions were then aliquoted into microcentrifuge tubes and stored at -80 °C.

3.3.7 SDS polyacrylamide gel electrophoresis (SDS-PAGE)

The purity of LF was assessed using SDS-PAGE. First, 10% polyacrylamide gels (resolving gel and stacking gel) were cast using the reagents listed in Table 3.3. Protein samples were supplemented with an equal volume of Laemmli buffer (see Table 3.4), boiled for 15 min, and then immediately placed on ice. A mini-PROTEAN Tetra Electrophoresis System (Bio-Rad Laboratory, Mississauga, ON) was filled with running buffer (see Table 3.5), and 10 µL of the protein sample was carefully loaded along with a PageRuler protein ladder (Thermo Fisher Scientific, Burlington, ON) into the wells of the stacking gel. The electrophoresis was performed at 75 mV for the first 15 min before increasing the voltage to 150 mV. When the bromophenol blue dye had passed through the gel, the resolving gel was retrieved and immersed in Coomassie Blue (see Table 3.6) for 20 min. The gel was then placed in destaining solution (see Table 3.7) until bands were visible against a clear background, a process which typically required 2 - 3 h.

Table 3.3: Composition of polyacrylamide gels

Reagent	Resolving Gel	Stacking Gel
30 % Acrylamide/Bis-acrylamide	4.5 mL	1.3 mL
1.5 M TRIS-HCl (pH 8.8)	3.75 mL	-
0.5 M TRIS-HCl (pH 6.8)	-	2.5 mL
10 % (w/v) Sodium dodecyl sulfate (SDS)	150 µL	100µL
10 % (w/v) Ammonium persulfate (APS)	50 µL	50 µL
TEMED	10 µL	10 µL
Water	6.75 mL	6.20 mL

Table 3.4: Composition of Laemmli Buffer (8 mL)

Reagent	Volume (mL)
10 % (w/v) Sodium dodecyl sulfate (SDS)	3.2
0.5 M TRIS-HCl (pH 6.8)	2.0
Glycerol	1.6
β-mercaptoethanol	0.8
0.1 % (w/v) Bromophenol blue	0.4

Table 3.5: Composition of running buffer (1 L)

Reagent	Amount (g)
Glycine	72
Tris	15.1
SDS	5

Table 3.6: Composition of the Coomassie Blue staining solution (1 L)

Reagent	Amount
Coomassie Brilliant Blue R-250	2 g
Methanol	455 mL
Water	452 mL
Acetic acid	91 mL

Table 3.7: Composition of the destaining solution (1 L)

Reagent	Volume (mL)
Methanol	300
Acetic acid	100
Water	600

3.3.8 Enzymatic activity assay

The activity of LF was assessed using the chromogenic anthrax lethal factor protease substrate II, S-*p*NA (Ac-GYβARRRRRRRRVLR-*p*NA, *p*NA=*para*-nitroanilide) (70,71), purchased from Biomatik (Cambridge, ON, Canada). The assay consisted of LF (50 nM) in HEPES buffer (50 mM, pH 7.4), and the S-*p*NA substrate at a final concentration of 10 μM was added to initiate the hydrolysis reaction. The changes in the absorbance at 405 nm ($O.D._{405nm}$) were monitored in a 100 μL quartz cuvette (Hellma, Concord, ON) for a period of 60 s on a Cary-60 UV-Vis spectrophotometer.

3.3.9 PAR assay

The zinc content of LF was determined with the chromogenic chelator 4-(2-pyridylazo)resorcinol (PAR) (68,72). The assay consisted of LF (5 μM) incubated in HEPES buffer (50 mM, pH 7.4) containing 4 M GdnHCl for 1 h prior to the addition of PAR at a final concentration of 50 μM, and measuring the absorbance at 500 nm ($O.D._{500nm}$). Zinc standards (0-10 μM) in HEPES buffer (50 mM, pH 7.4) containing 4 M GdnHCl were measured analogously, and served as the basis for calculating LF's zinc content.

3.4 Fluorescence spectroscopy

3.4.1 Tryptophan fluorescence spectroscopy

Chemical denaturants such as urea and GdnHCl can unfold LF (53), a process which can be monitored using the intrinsic fluorescence of LF's five tryptophan residues. In a typical assay, 900 μL LF (0.5 μM) was incubated with urea (0-6 M) in the three-component AMT buffer system (acetic acid, MES, and Tris; 25 mM, pH 5 - 7) containing 0.5 M NaCl or 0.5 M L-arginine for 1 h or 24 h at room temperature prior to recording tryptophan emission spectra using an OLIS RSM1000 spectrofluorometer (OLIS, Bogart, GA). The excitation wavelength was set to 295 nm with a bandpass of 5 nm. The emission spectra of LF were recorded from 300 to 400 nm in a mirrored quartz cuvette (Hellma, Concord, ON) in 0.5 nm increments (integration time of 0.5 s). The spectra of denaturant-containing buffer were measured analogously, and were subtracted from the LF spectra before being smoothed using the OLIS GlobalWorks software. LF spectra obtained using different pH conditions were subjected to normalization

prior to fitting or data analysis. The observed fluorescence intensities at 333 nm (Fl_{333nm}) were used to determine whether LF unfolded following a 2-state or a 3-state mechanism. The equation for a 2-state mechanism (native → unfolded) is shown in eq (2), and that of the 3-state mechanism (native→ intermediate→ unfolded) is indicated in eq (3):

$$FI_{obs} = \frac{FI_N + FI_U \times \exp(-\frac{\Delta G°_{N\to U} - m_{N\to U}C}{RT})}{1 + \exp(-\frac{\Delta G°_{N\to U} - m_{N\to U}C}{RT})} \qquad (2)$$

$$FI_{obs} = \frac{FI_N + FI_I \times \exp\left(-\frac{\Delta G°_{N\to I} - m_{N\to I}C}{RT}\right) + Fl_U \times \exp\left(-\frac{\Delta G°_{N\to I} - m_{N\to I}C}{RT}\right) \times \exp\left(-\frac{\Delta G°_{I\to U} - m_{I\to U}C}{RT}\right)}{1 + \exp\left(\frac{\Delta G°_{N\to I} - m_{N\to I}C}{RT}\right) + \exp\left(\frac{\Delta G°_{N\to I} - m_{N\to I}C}{RT}\right) \times \exp\left(\frac{\Delta G°_{I\to U} - m_{I\to U}C}{RT}\right)} \qquad (3)$$

where FI_{obs} is the observed fluorescence at 333 nm, N is the native state, I is the intermediate state, and U is the unfolded state, ΔG° represents the Gibbs free energy of a transition in the absence of denaturant, m is the denaturant dependence of ΔG°, c is the concentration of the denaturant, R is the gas constant (8.314 J $mol^{-1}K^{-1}$), and T is the temperature (293 K). The midpoint concentration (C_{mid}) of a transition was calculated by dividing ΔG° by m (73-75).

3.4.2 Red-edge excitation shift (REES)

The red-edge excitation shift (REES) was measured on an Olis spectrofluorometer. REES arises from slow relaxation of solvent molecules around tryptophan residues following their excitation (76,77). For each REES measurement, LF (5 μM) was excited at different wavelengths (280 nm, 285 nm, 290 nm, 295 nm, 300 nm, 303 nm, and 306 nm), and the emission spectra were recorded in a mirrored quartz cuvette from 300 to 400 nm with a bandpass of 1.9 nm. The settings for the wavelength increment and the integration time were identical to those indicated in Section 3.4.1. The samples consisted of LF incubated with a chemical denaturant in AMT buffer (25 mM, desired pH) for 1 or 24 h at room temperature prior to measurement. A standard containing 25 μM of *N*-acetyl-L-tryptophanamide (NATA) served as a control. All LF spectra were baseline-subtracted and smoothed by the OLIS GlobalWorks software. The REES was calculated by subtracting the wavelength of maximum emission (λ_{max}) recorded at λ_{exc} = 306 nm from that obtained at 280 or 295 nm.

3.5 Zinc accessibility

PAR has previously been shown to penetrate LF's active site at moderate denaturant concentrations, and to bind to the Zn^{2+} ion at pH 7.4 (53). The Zn^{2+} ion's accessibility to chelation under acidic conditions was studied in a total volume of 200 µL using LF (5 µM) incubated with urea (0 - 6 M) in AMT buffer (25 mM, pH 5.5 - 7) containing 0.5 M NaCl for 1 h at room temperature prior to the addition of PAR (10 µM). The $O.D._{500nm}$ was recorded immediately for a period of 60 min (10 s intervals) using an Epoch microplate spectrophotometer (Biotek Intruments, Winooski, VT). Zinc standards (0 - 10 µM) were measured analogously along with the samples, and served as the basis for the calculation of the amount of Zn^{2+} complexed by PAR.

3.6 Zinc release

The dissociation of Zn^{2+} from LF was monitored as a function of the concentration of chemical denaturant, and the pH value. The assay (final volume of 200 µL) consisted of LF (10 µM) incubated with urea (0-6 M) in AMT buffer (25 mM, pH 4 - 7) supplemented with 0.5 M NaCl for 1 h at room temperature. The LF samples were then added to a 0.5 mL Amicon Ultra Centrifugal Filter (10 kDa) and centrifuged at 13,000 rpm for 9 min in an Eppendorf 5415C Centrifuge (Eppendorf, Mississauga, ON). A volume of 100 µL of the filtrate was then transferred to a well of a 96-well microplate, and mixed with 90 µL of AMT buffer (192.5 mM, pH 7.6) to raise the pH to ~ 7.0. Finally, 10 µL of PAR (1 mM) was added, and the $O.D._{500nm}$ was recorded on an Epoch microplate reader. Zinc standards (0 - 10 µM) were prepared and measured in a similar manner to serve in the determination of the amount of Zn^{2+} released from LF.

4 Results

The experiments described in this thesis were aimed at investigating the effect of pH (mainly under acidic conditions) on the zinc release and structural changes in LF. Hence, the experiments were designed to be compared to the results obtained from previous studies reported by Lo and coworkers, where the effect of chemical denaturants (urea and GdnHCl) on the fold and zinc status of LF was monitored at neutral pH (pH 7.4) (53). The difference between previous and current studies was that instead of HEPES (50 mM, pH 7.4), a three-component buffer (25 mM AMT) was used in all pH studies (pH 4.0 – 7.0) to maintain a constant ionic strength.

4.1 LF aggregation at low pH

4.1.1 Effect of sodium chloride on protein aggregation

When LF is exposed to acidic conditions mimicking those of the endosome (i.e., between pH 5 and 6), aggregation of the protein is observed (65). As this phenomenon can interfere with the interpretation of spectroscopic measurements, initial experiments were aimed at finding conditions which suppress the formation of LF aggregates. At first, the effect of increasing the ionic strength of the buffer (by the addition of a salt) on protein aggregation was investigated. Since both cations and anions can influence protein structure, it was important to choose a salt which is neither chaotropic (structure breaking) nor kosmotropic (structure making). According to the Hofmeister series (see Figure 4.1), sodium chloride is a salt which would fulfill this requirement (78,79).

$SCN^- > ClO_4^- > I^- > NO_3^- > Br^- > Cl^- > F^- > H_2PO_4^- > S_2O_3^{2-} > SO_4^{2-} > CO_3^{2-}$

$Gdm^+ > Ba^{2+} > Ca^{2+} > Mg^{2+} > Li^+ > Cs^+ > Na^+ > K^+ > Li^+ > Rb^+ > NH_4^+ > H^+$

Chaotropic (structure breaker) ⟷ Kosmotropic (structure maker)

Figure 4.1: The Hofmeister series. Ions have the ability to control the structure and solubility of proteins. They can interact directly with proteins or with water molecules surrounding them (78-80). Gdm^+ denotes the guanidinium ion.

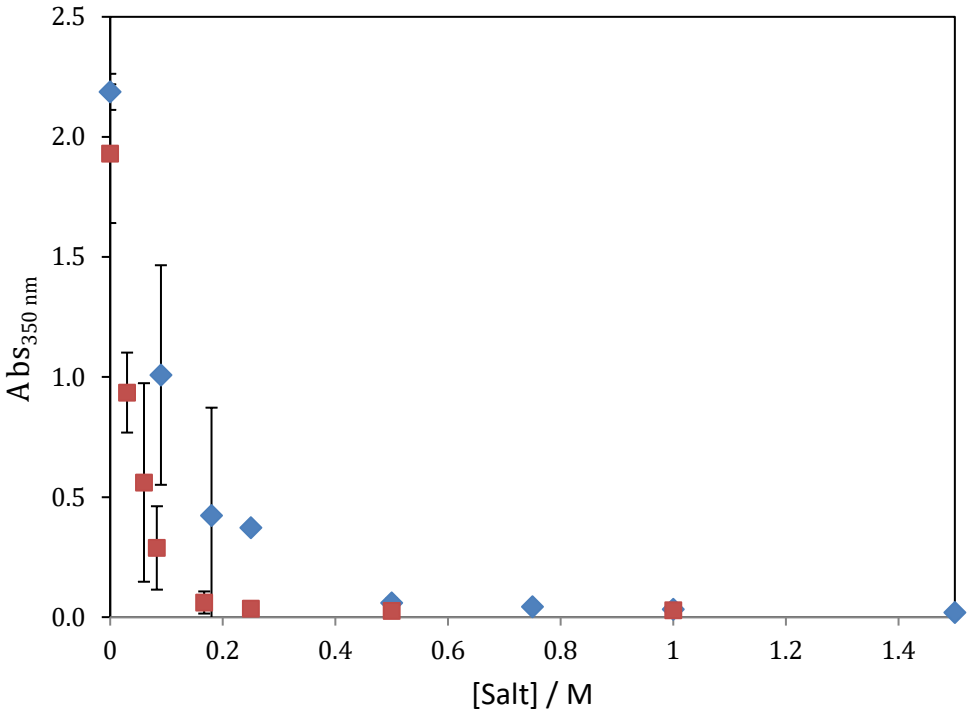

Figure 4.2: Effect of NaCl and Na_2SO_4 on LF aggregation at pH 5.0. LF (5 μM) was incubated with NaCl (diamonds) or Na_2SO_4 (squares) in AMT buffer (25 mM, pH 5.0) for 1 h prior to measuring the absorbance at 350 nm using a UV-Vis spectrophotometer. Values shown represent the mean (± 1 s.d.) of three independent measurements.

As shown in Figure 4.2, LF at pH 5.0 formed aggregates in the absence of salt as evidenced by the high absorbance values at 350 nm originating from light scatter. However, in the presence of salts (NaCl or Na_2SO_4), the $O.D._{350nm}$ value decreased, suggesting that the

formation of LF aggregates is suppressed. Due to the ionic strength of Na_2SO_4 being three times higher than that of NaCl, the former salt appears to be more effective in preventing protein aggregation. Nonetheless, a concentration of 0.5 M NaCl or Na_2SO_4 appears to be effective in minimizing light scattering, and thus, LF aggregation. Overall, the results demonstrate that increasing the ionic strength of the AMT buffer can help keep LF soluble under acidic conditions.

The pH-dependence of LF aggregation was also probed by intrinsic tryptophan fluorescence spectroscopy, which is typically more sensitive than UV-Vis spectroscopy. When LF's tryptophan residues are excited at 295 nm, a high degree of light scattering at 300 nm is observed when the protein aggregates (65).

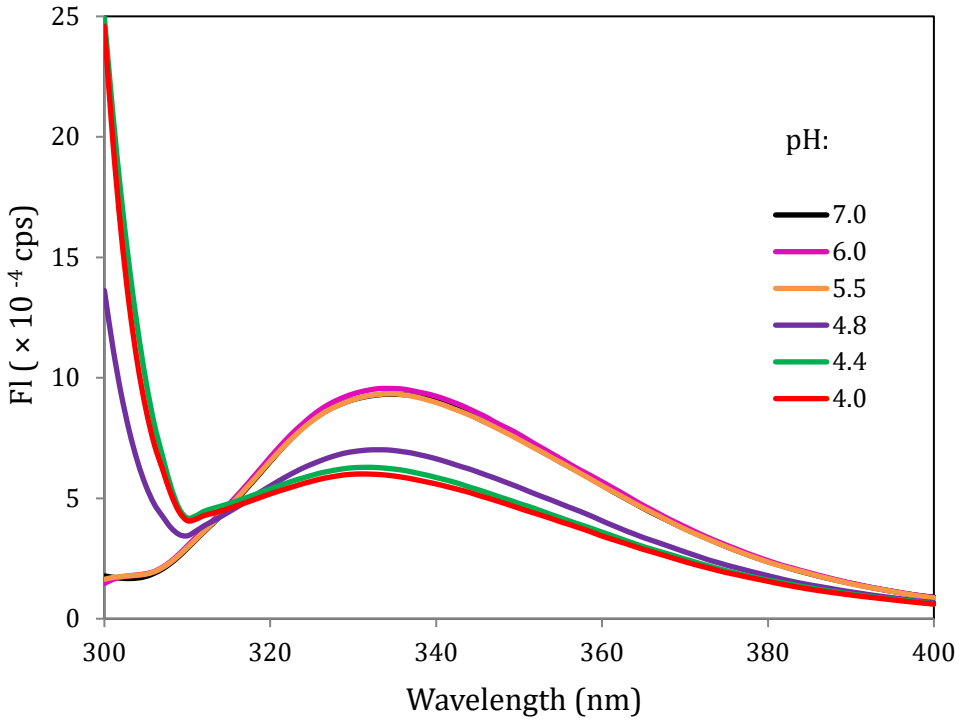

Figure 4.3: Trp fluorescence emission spectra of LF at different pH values. LF (0.5 μM) was incubated in AMT buffer (25 mM, pH 4 to 7) containing 0.5 M NaCl for 1 h at room temperature prior to recording emission spectra. The excitation wavelength was set to 295 nm.

As shown in Figure 4.3, the fluorescence intensity (FI) at 300 nm was high at pH < 5.5, an observation consistent with that reported in previous studies (65). The data indicate the presence of LF aggregates at low (endosomal) pH despite the addition of 0.5 M NaCl to the AMT buffer. Furthermore, the increase in Fl_{300nm} below pH 5.5 led to a decrease in Fl_{333nm} (the maximum emission wavelength for native LF). Although not tested experimentally, it is not unreasonable to suggest that this decrease in fluorescence intensity might be caused by an inner filter effect. In view of the emergence of light scattering below pH 5.5, the effect of increasing the concentration of NaCl on the fluorescence spectra of LF was investigated (see Figure 4.4).

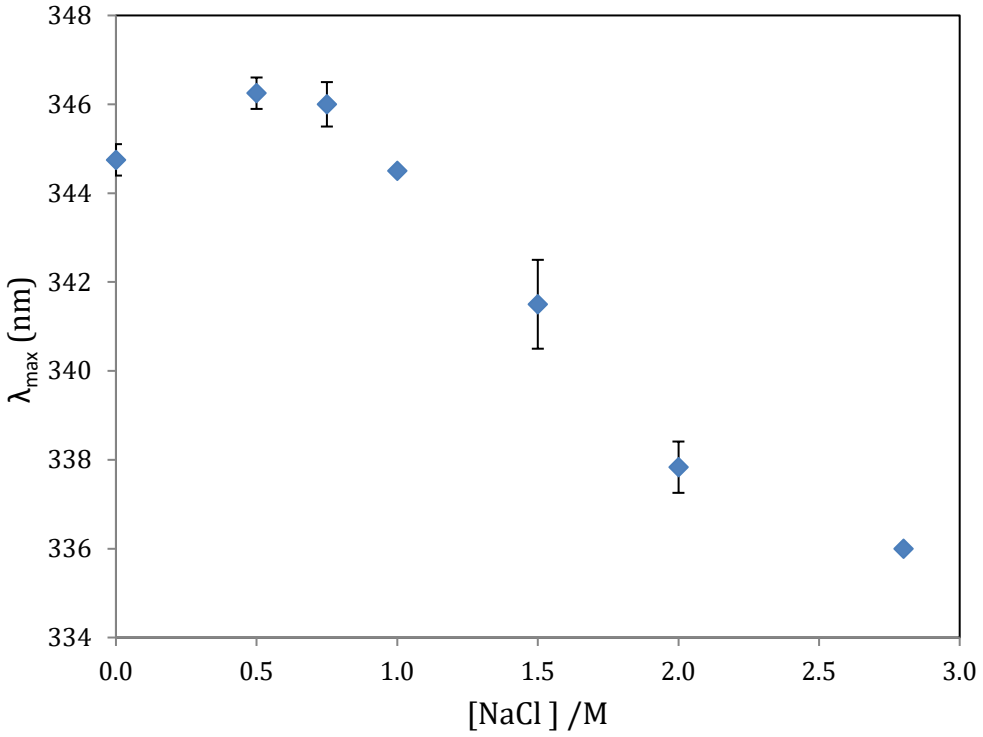

Figure 4.4: Effect of NaCl on λ_{max} in 6 M urea at pH 5.5. LF (0.5 μM) was incubated with NaCl (0 - 2.8 M) in 6 M urea in AMT buffer (25 mM, pH 5.5) for 1 h at room temperature prior to measurement. The excitation wavelength was set to 295 nm, and the emission spectra were recorded from 300 to 400 nm to determine the wavelength of maximum emission intensity (λ_{max}). Values shown represent the mean (± 1 s.d.) of three independent measurements.

As previously reported, LF is denatured by 6 M urea at pH 7.4 (in HEPES buffer) showing an emission maximum (λ_{max}) shift from 333 nm (native state) to 347 nm (unfolded state) (53). As shown in Figure 4.4, at pH 5.5, λ_{max} decreased with increasing amounts of NaCl in the AMT buffer. In the absence (or at low concentrations) of NaCl (0 – 1 M), λ_{max} remained high at ~ 345 – 346 nm, suggesting that LF remains in the denatured state. At a concentration of 2.8 M NaCl, λ_{max} was found to be 336 nm, a value close to that found for the native state of LF. These results clearly suggest that NaCl at concentrations > 1 M can influence the fold of LF.

As mentioned above, LF remained unfolded in 6 M urea (at pH 5.5) in the presence of 0.5 M and 0.75 M NaCl (see Figure 4.4). However, LF aggregation persisted at pH 5.0 in the presence of 0.5 M NaCl (see Figure 4.3). Therefore, it was investigated if 0.75 M NaCl can suppress aggregation and improve on the fluorescence intensity at 333 nm (see Figure 4.5).

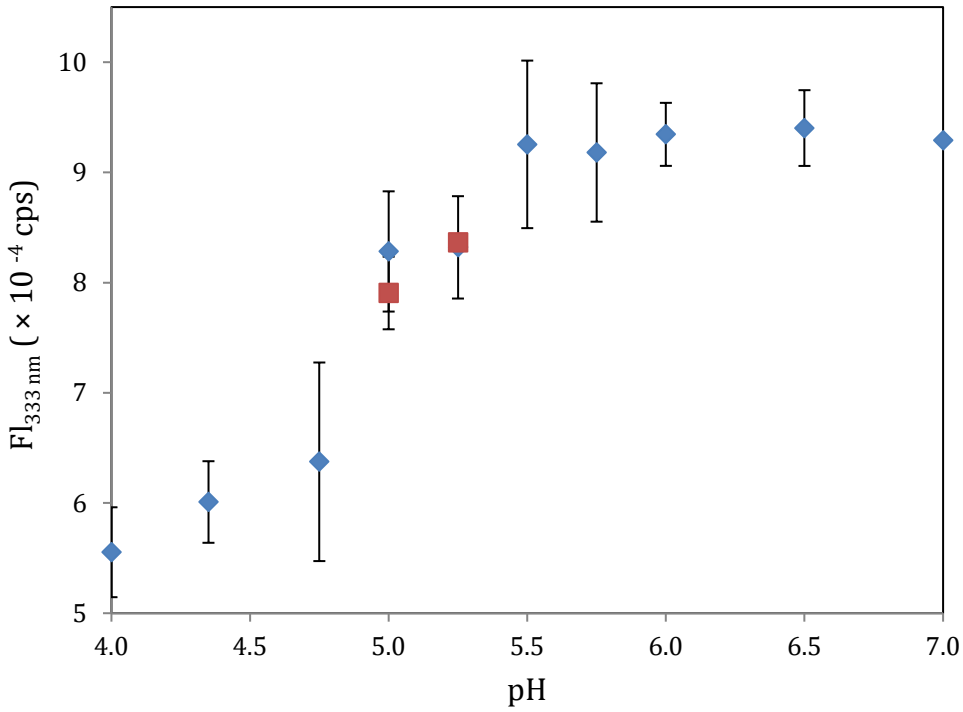

Figure 4.5: Influence of NaCl on the Fl_{333nm}. LF (0.5 µM) was incubated in AMT buffer (25 mM, pH 7.0 - 4.0) containing 0.5 M NaCl (blue diamonds) or 0.75 M NaCl (red squares) for 1 h at room temperature prior to recording emission spectra from 300 to 400 nm. The excitation wavelength was set to 295 nm. Values (FI_{333nm}) shown were extracted from the emission spectra, and represent the mean (± 1 s.d.) of three independent measurements.

In the presence of NaCl, FI_{333nm} was found to be constant from pH 7.0 – 5.5. The fluorescence intensity decreased slightly between pH 5.5 and 5.0, presumably as a consequence of the formation of LF aggregates. Below pH 5.0, a more substantial decrease in FI_{333nm} was observed, with only about 50% of the signal remaining at pH 4.0. Furthermore, increasing the amount of NaCl from 0.5 M to 0.75 M (at pH 5.0 or 5.25) did not lead to a change in the value of FI_{333nm}.

In summary, the addition of NaCl to the AMT buffer can suppress the formation of LF aggregates at endosomal pH. However, its use is limited to the concentration range of 0.5 M to 0.75 M because at higher concentrations, NaCl suppresses the unfolding of LF, and at lower concentrations, it is ineffective in preventing the aggregation of the protein at pH 5.0 (see Figure 4.3 and Figure 4.4).

4.1.2 Effect of L-arginine on LF aggregation at pH 5.0

L-arginine is a protein aggregation inhibitor, probably because its guanidinium group interacts with protein side chains (81,82). Hence, a range of concentrations of L-arginine was assessed with respect to its ability to suppress LF aggregation at pH 5.0 (see Figure 4.6).

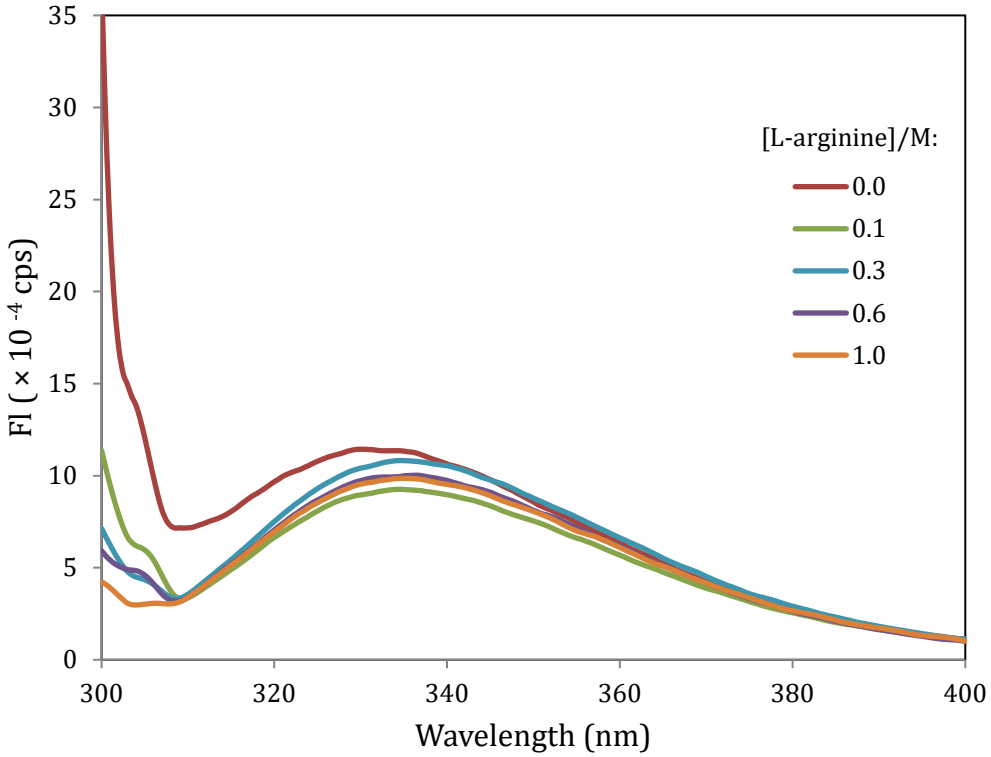

Figure 4.6: Trp fluorescence emission spectra of LF in the presence of L-arginine at pH 5.0. LF (0.5 µM) was incubated with L-arginine (0 - 1 M) in AMT buffer (25 mM, pH 5.0) for 1 h at room temperature prior to recording spectra. The spectrum recorded in the absence of L-arginine is depicted in red, and those measured with 0.1 M, 0.3 M, 0.6 M and 1.0 M L-arginine are shown in green, blue, purple and orange, respectively. The excitation wavelength was set to 295 nm.

In the absence of L-arginine, a high degree of light scattering (at 300 nm) was observed. In contrast, adding L-arginine to the LF samples significantly reduced the signal intensity at 300 nm, suggesting that inclusion of the amino acid helps to prevent LF aggregation at pH 5.0. To directly compare the effect of NaCl and L-arginine on the fluorescence of LF, emission spectra were recorded using the same concentration of NaCl and L-arginine (I = 0.5 M for both).

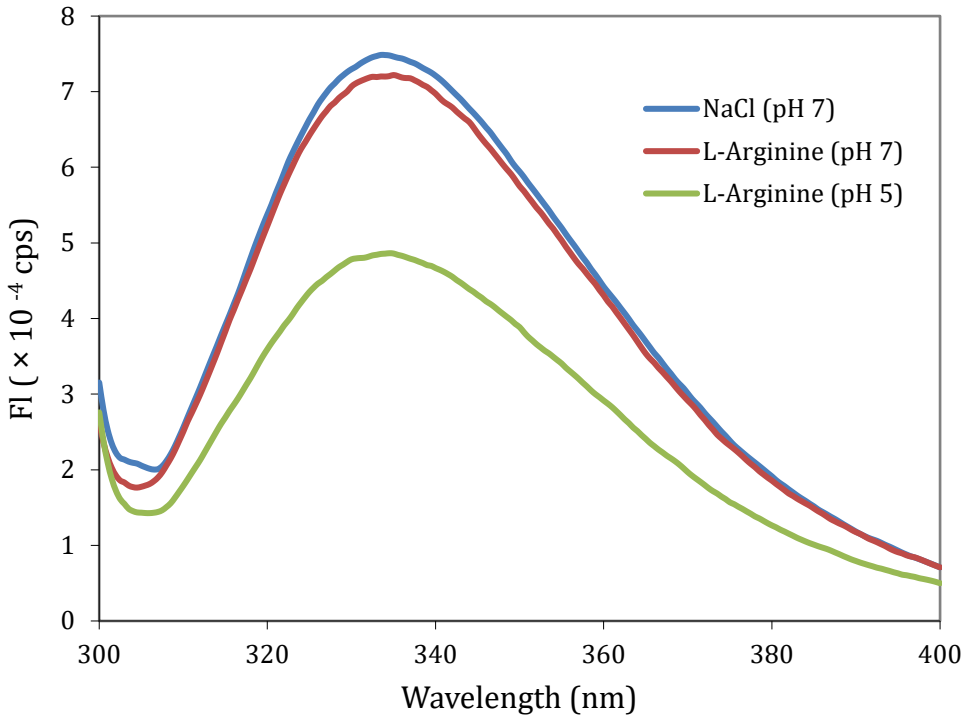

Figure 4.7: Trp emission spectra of LF with L-arginine at pH 7.0 and 5.0. LF (0.5 µM) was incubated with 0.5 M NaCl (blue), and with0.5 M L-arginine at pH 7.0 (red) or at pH 5.0 (green) in AMT buffer (25 mM) for 1 h at room temperature prior to recording spectra. The excitation wavelength was set at 295 nm.

As shown in Figure 4.7, the spectra for 0.5 M NaCl and 0.5 M L-arginine recorded at pH 7.0 were essentially identical with respect to their fluorescence intensities and their λ_{max} values at 335 nm. Furthermore, a decrease in the pH value from 7.0 to 5.0 led to a 30% reduction in the fluorescence intensity for LF exposed to L-arginine. Such decrease in the FI values can, most likely, be attributed to quenching caused by the protonation of amino acid residues (83). Overall, the addition of 0.5 M L-arginine to LF at pH 5.0 appears to suppress the aggregation of the enzyme, an effect not achievable with 0.5 M NaCl.

4.2 Tryptophan fluorescence studies

As shown in Figure 4.8, LF contains five tryptophan residues which can be selectively excited at a wavelength of 295 nm. Previous studies have shown that at neutral pH (pH 7.4), the native state of LF displays an emission maximum (λ_{max}) at 333 nm, and that upon unfolding it red-shifts to 347 nm (53).

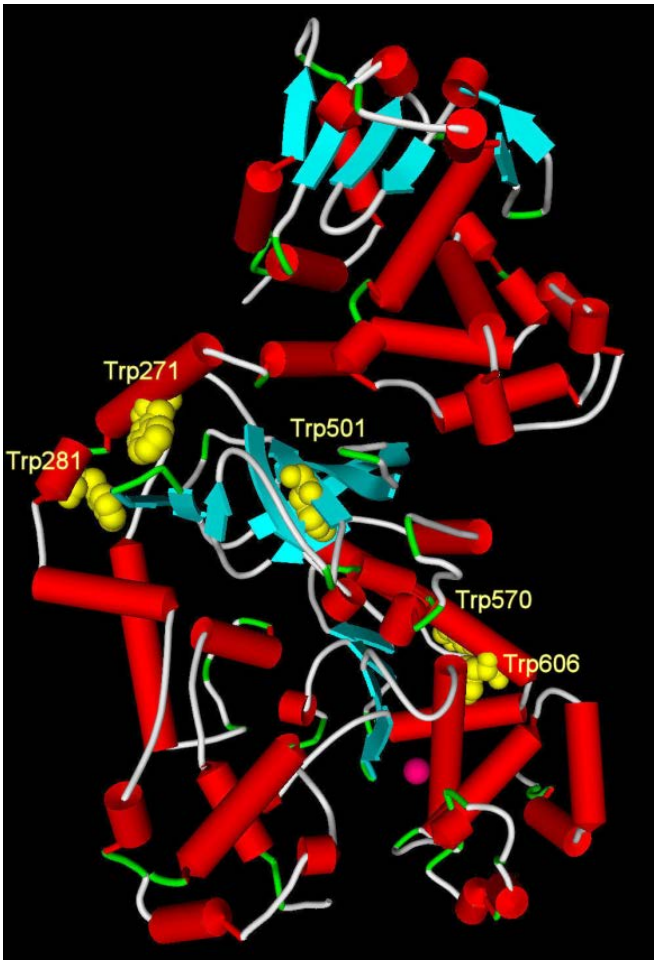

Figure 4.8: Tryptophan residues in LF. Four of LF's five Trp residues (Trp281, Trp501, Trp570, Trp606) are buried, and hence, solvent inaccessible. Trp271 is ~20% solvent accessible. The Zn^{2+} ion in the active site is depicted in magenta. This figure was taken from (53).

4.2.1 LF unfolding at neutral pH

The denaturation profiles of LF in the presence of urea (0 – 6 M) in AMT buffer at pH 7.0 and 6.5 are shown in Figure 4.9.

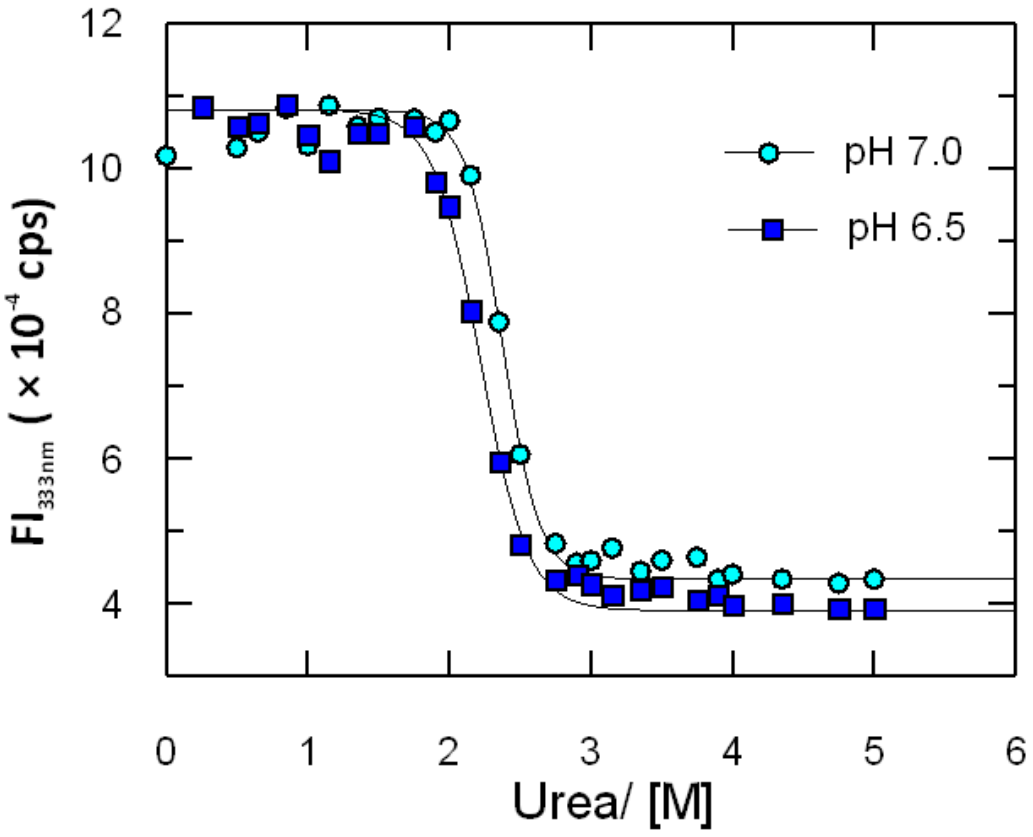

Figure 4.9: Urea-mediated LF unfolding at pH 7.0 and 6.5. LF (0.5 µM) was incubated with urea (0 – 6 M) in AMT buffer (25 mM) containing 0.5 M NaCl for 1h at room temperature prior to recording emission spectra. The excitation wavelength was set to 295 nm. The fluorescence intensity at 333 nm (Fl_{333nm}) recorded at pH 7.0 is depicted in light blue, while that monitored at pH 6.5 is shown in dark blue. The data was fit to a 2-state unfolding mechanisms (native state [N] → unfolded state [U]) as shown in the solid lines (see Methods section 3.4.1).

At pH 7.0 and 6.5, the unfolding of LF in the presence of urea followed a 2-state mechanism, a finding consistent with that recorded for the urea-mediated unfolding of LF at pH 7.4 (53). The C_{mid} values for the N → U transitions were 2.38 M for pH 7.0 and 2.22 M for pH 6.5. The slightly higher C_{mid} value at pH 7.0 indicates that at neutral pH LF is slightly more stable.

4.2.2 LF unfolding at low (endosomal) pH

The urea-mediated unfolding of LF at pH values mimicking those found in the endosome is shown in Figure 4.10.

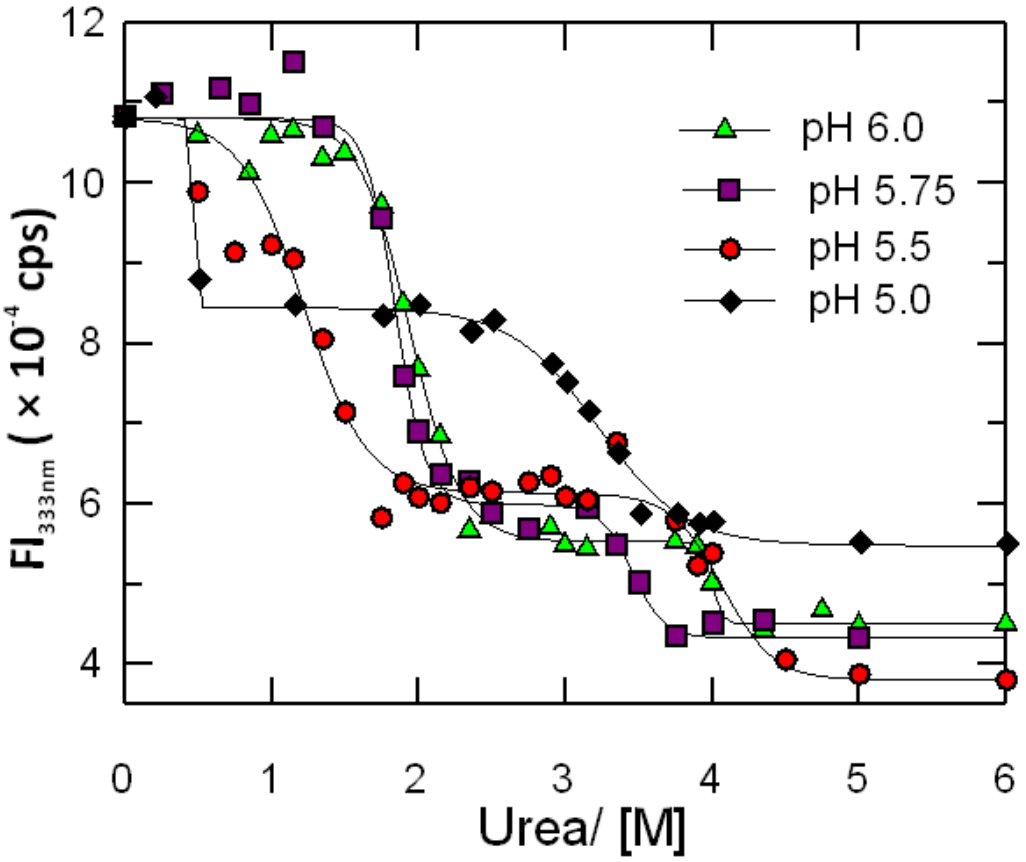

Figure 4.10: Urea-mediated LF unfolding at pH 6.0, 5.75, 5.5 and 5.0. LF (0.5 μM) was incubated with urea (0 – 6M) in AMT buffer (25 mM) containing 0.5 M NaCl (for pH 6.0 to 5.5) or 0.5 M L-arginine (for pH 5.0) for 1 h at room temperature prior to recording emission spectra. The excitation wavelength was set to 295 nm. The Fl_{333nm} values for pH 6.0 are depicted in green, for pH 5.75 in purple, for ph 5.5 in red, and for pH 5.0 in black. The data was fitted to a 3-state unfolding mechanism (native state [N] → intermediate state [I] → unfolded state [U]), as shown by the solid lines (see Methods section 3.4.1).

At pH values mimicking those of the endosome (pH 6.0, 5.75, 5.5, 5.0), LF unfolding appears to proceed via the formation of an intermediate state. Hence, the pathway of LF unfolding is different from that recorded at neutral pH (see Figure 4.9). Interestingly, the appearance of

an intermediate state in the titration profiles (as evidenced by the plateau in the mid-concentration range; see Figure 4.10) becomes more pronounced as the pH is lowered from 6.0 to 5.0. Since there are three distinct states (N, I, and U) in the unfolding of LF, there are two midpoint concentrations, one for the N → I transition (C_{mid1}) and one for the I → U transition (C_{mid2}). A summary of the C_{mid} values for the unfolding of LF in urea is shown in Table 4.1.

Table 4.1: Summary of the C_{mid} values for the urea-mediated unfolding of LF (pH 7.0 to 5.0).

	Two-state model		*Three-state model*			
	pH 7.0	pH 6.5	pH 6.0	pH 5.75	pH 5.5	pH 5.0
C_{mid1} (M)	2.38	2.22	1.94	1.83	1.18	n.d.
C_{mid2} (M)	n.a.	n.a.	4.00	3.46	4.09	3.23

n.a., not applicable. n.d., not determined. All values were calculated from the ΔG° and *m* parameters obtained by fitting of the recorded Fl_{333nm} values to Eq. (2) for the2-state model and Eq. (3) for the 3-state model.

As the table shows, the C_{mid} values of the first transition of LF unfolding (N → U for pH 7.0 and 6.5 [this is the only transition]; N → I for pH 6.0 - 5.5) were found to decrease with decreasing pH. Unfortunately, a reliable C_{mid1} value for the pH 5.0 measurement could not be obtained because of the lack data points at urea concentrations below 0.5 M. Nonetheless, as Figure 4.10 clearly shows, the C_{mid1} value at pH 5.0 is below 0.5 M, and hence smaller than that recorded at pH 5.5. These results suggest that the stability of the native fold of LF is decreased as the pH is lowered from 7.0 to 5.0. Regarding the second transition (I → U) observed at pH ≤ 6.0, the C_{mid2} values obtained from the fits for the pH 6.0, 5.75 and 5.5 measurements are to be taken with caution since the transition is not very pronounced and too few data points were recorded in this region.

4.3 Zinc release

Following the assessment of LF unfolding by Trp fluorescence spectroscopy, the ability of LF to retain its Zn^{2+} ion during urea-mediated unfolding was investigated.

4.3.1 Effect of NaCl on zinc release

As described in section 4.1, the aggregation of LF at acidic pH can be inhibited by NaCl. To investigate whether the release of Zn^{2+} in LF is affected by the presence of NaCl, the dissociation of the metal ion as a function of urea concentration and pH (from 4.0 to 6.0) was measured both in the absence and presence of NaCl.

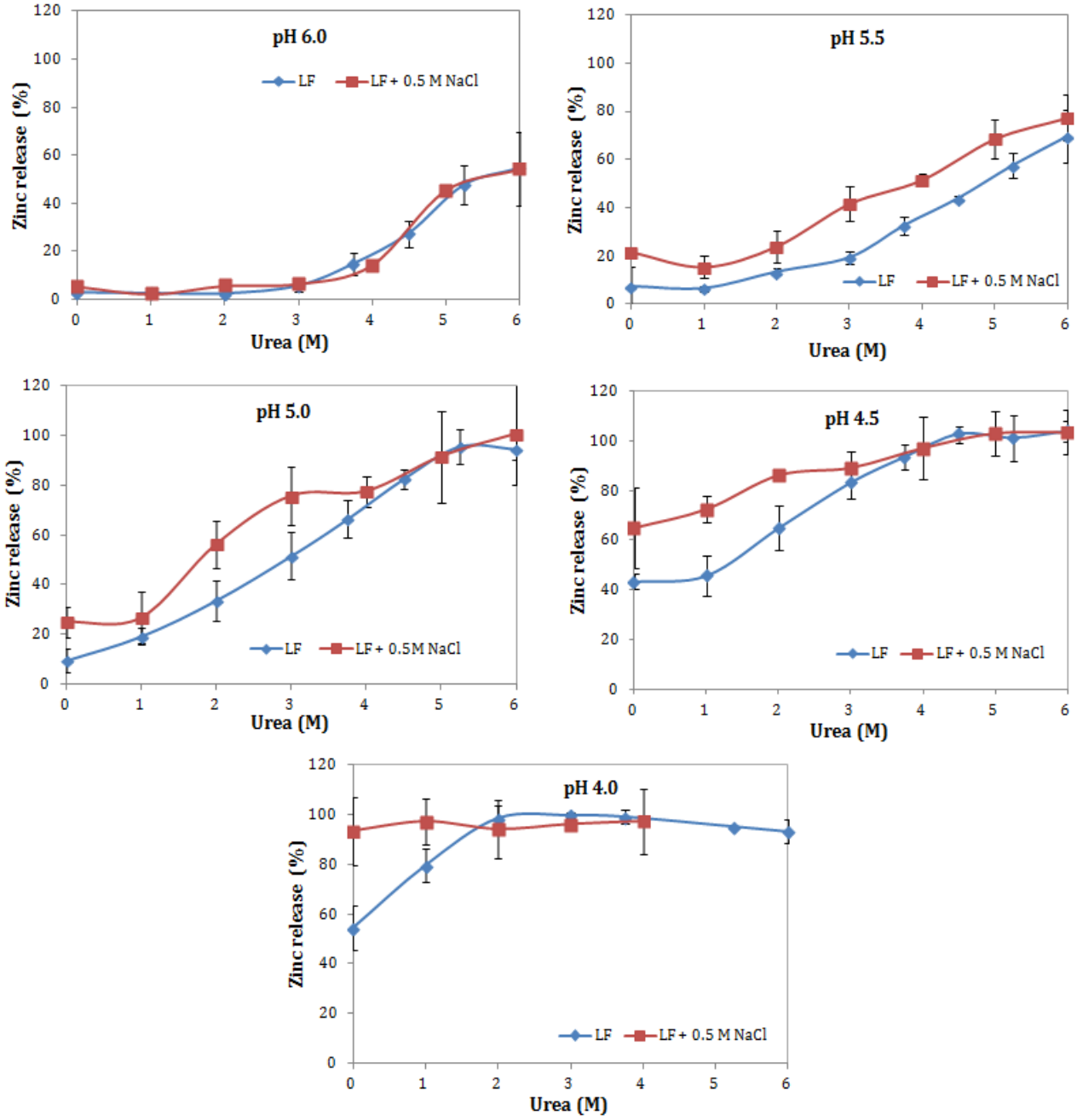

Figure 4.11: pH dependence of urea-induced zinc release from LF. LF (10 μM) was incubated with urea (0 - 6 M) in AMT buffer (25 mM) in the absence (blue) and presence of 0.5 M NaCl (red) for 1 h at room temperature prior to Amicon filtration, and determination of zinc in the filtrate(see section 3.6). Values shown represent the mean (± 1 s.d.) of three independent measurements.

As shown in Figure 4.11, under conditions where LF aggregation does not occur (i.e., at pH 6.0), the addition of NaCl did not lead to a change in the titration profile. However, the results

show that when LF aggregation is to be expected (between pH 5.5 and 4.0), the release of Zn^{2+} is typically slightly higher in the presence of NaCl. For instance, at pH 5.5, Zn^{2+} release from LF was ~10 - 20% higher when incubated with 0.5 M NaCl. Similarly, at pH 5.0, the Zn^{2+} release increased by > 10% in the presence of NaCl in the 0 – 4 M urea concentration range. At pH 4.0, the inclusion of NaCl resulted in a significant increase (from 52% to 93%) in the amount of Zn^{2+} released in the absence of urea. These results demonstrate that NaCl affects Zn^{2+} release. Since NaCl was shown to inhibit the formation of LF aggregates (see section 4.1), it seems that the aggregation of LF (observed in the absence of NaCl) reduces the release of Zn^{2+} from the enzyme.

4.3.2 Zinc release from LF as a function of pH

Since NaCl prevents LF aggregation, which as shown above interferes with the release of Zn^{2+} ions from the enzyme, all urea-induced Zn^{2+} release titrations from pH 7.0 down to pH 4.0 were performed in the presence of 0.5 M NaCl (see Figure 4.12).

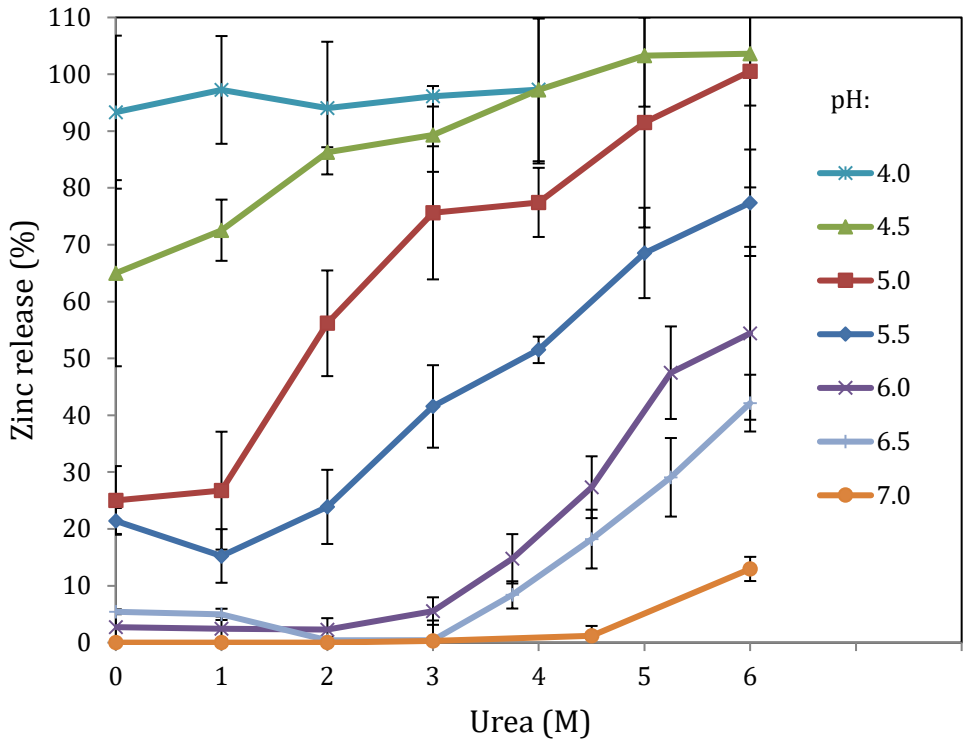

Figure 4.12: Zinc release of LF as a function of urea concentration and pH. LF (10 μM) was incubated with urea (0 - 6 M) in the presence of 0.5 M NaCl in AMT buffer (25 mM) for 1 h at room temperature prior to Amicon filtration, and determination of the zinc concentration of the filtrate (see section 3.6). Values shown represent the mean (± 1 s.d.) of three independent measurements.

As shown in Figure 4.12, the Zn^{2+} release from LF was highly dependent on the pH. In general, a lower pH induced a larger amount of Zn^{2+} to be released from LF. At pH 7.0, the Zn^{2+} release was essentially zero between 0 and 4.5 M urea, and only increased to ~ 10% in the presence of 6 M urea. In the endosomal pH range (6.0 – 5.0), the Zn^{2+} release gradually increased with increasing amounts of urea. At pH 6.0, the Zn^{2+} release was negligible at 0 M urea, and increased to 54% at 6 M urea. At pH 5.0, the degree of spontaneous Zn^{2+} release was 25% in the absence of urea, reaching 100% at 6 M urea. At pH values below 5.0, the majority of Zn^{2+} was found to be released in the absence of urea (65% at pH 4.5 and 95% at pH 4.0).

A summary of the pH dependence of Zn^{2+} release performed with 6 M urea (the highest concentration of the denaturant used) is shown in Table 4.2, illustrating that the amount of

Zn^{2+} released from LF changes significantly (from 13% to 100%) within a relatively small range of pH values (from 7.0 to 5.0). At pH 7.0, the Zn^{2+} release was 13%, a value slightly higher (by 3%) than that recorded previously at pH 7.4 in HEPES buffer (53).

Table 4.2: Zinc release from LF in the presence of 6 M urea.

pH	Zinc release (%)
≤5.0	100
5.5	77
6.0	54
6.5	42
7.0	13

From Section 4.2 and previous studies (53) it is apparent that the Trp fluorescence emission spectra show LF to be unfolded in the presence of 6 M urea regardless of the pH. Yet, the degree of Zn^{2+} release varied greatly in the pH range investigated (see Table 4.2). LF's Zn^{2+} ion is coordinated to two histidine residues (His686, His690) and one glutamate residue (Glu735) (see Figure 1.11b). The significant loss of Zn^{2+} from LF at pH ≤ 5.0 in the absence of urea is likely due to these amino acids becoming protonated, and thus losing their ability to bind the enzyme's metal ion.

4.3.3 Zinc release in the presence of GdnSCN

Previous studies have shown that LF's Zn^{2+} ion is not completely released at pH 7.4, even in the presence of GdnHCl, a denaturant much stronger than urea (53). To investigate whether it is possible to completely dissociate the Zn^{2+} ion from LF at neutral pH, GdnSCN, the strongest chemical denaturant known (78,84), was used in Zn^{2+} release titrations.

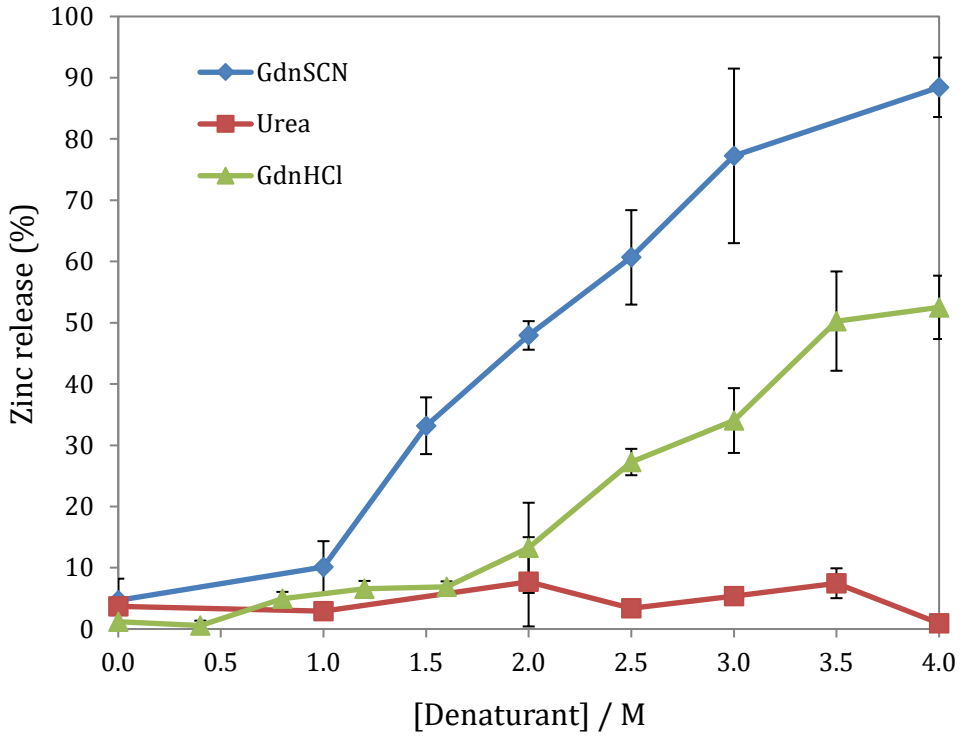

Figure 4.13: Zinc release from LF in the presence of chemical denaturants at pH 7.4. LF (5 μM) was incubated with GdnSCN (0 - 4 M) in HEPES buffer (50 mM, pH 7.4) for 1 h at room temperature prior to Amicon filtration, and determination of the zinc content of the filtrate (shown in blue). Data shown for the urea (red) and GdnHCl (green) titrations were obtained from (53). Values shown represent the mean (± 1 s.d.) of three independent measurements.

The results shown in Figure 4.13 demonstrate that LF released the largest amount of Zn^{2+} when GdnSCN was used as the denaturant. In the case of GdnSCN, the midpoint concentration (C_{mid}) for the release of Zn^{2+} was found to be 2.1 M, and ~90% of the metal ion dissociated at a concentration of 4 M. The second strongest chemical denaturant was GdnHCl, for which a C_{mid} value of 3.5 M was observed. Not unexpectedly, urea was the weakest chemical denaturant in this study, with the release of the metal ion being below 10% in the entire urea concentration range (up to 4 M). The denaturation of LF in the presence of GdnSCN will be described in more detail in Section 4.5.

4.4 Zinc accessibility

Previous studies on the unfolding and Zn^{2+} release of LF at pH 7.4 found that PAR has the ability to penetrate the active site of the enzyme, and bind to the metal ion (see Figure 1.14) (53). Therefore, it was of interest to investigate (i) the accessibility of Zn^{2+} to chelation by PAR under different pH conditions, and (ii) the propensity of the chelator to remove the metal ion from LF once bound to it.

4.4.1 Zinc accessibility determined with PAR

As shown in Figure 4.14, the results from the Zn^{2+} accessibility measurements at pH 7.0 in AMT buffer were similar to those reported in previous studies performed at pH 7.4 in HEPES buffer, in that the Zn^{2+} ion was complexed by PAR at denaturant concentrations smaller than those needed to induce the release of Zn^{2+} (53). For instance, at 3 M urea, no Zn^{2+} was released spontaneously (see Figure 4.12), however, the Zn^{2+} accessibility was found to be high at 20% at t = 0 min, and 53% at t = 60 min. The C_{mid} values were 4.0 M and 2.9 M, for the immediate and 60 min exposure to PAR, respectively. With the exception of the data recorded at 6 M urea, at least a ~10% increase in the Zn^{2+} accessibility was observed after 60 min of exposure to PAR.

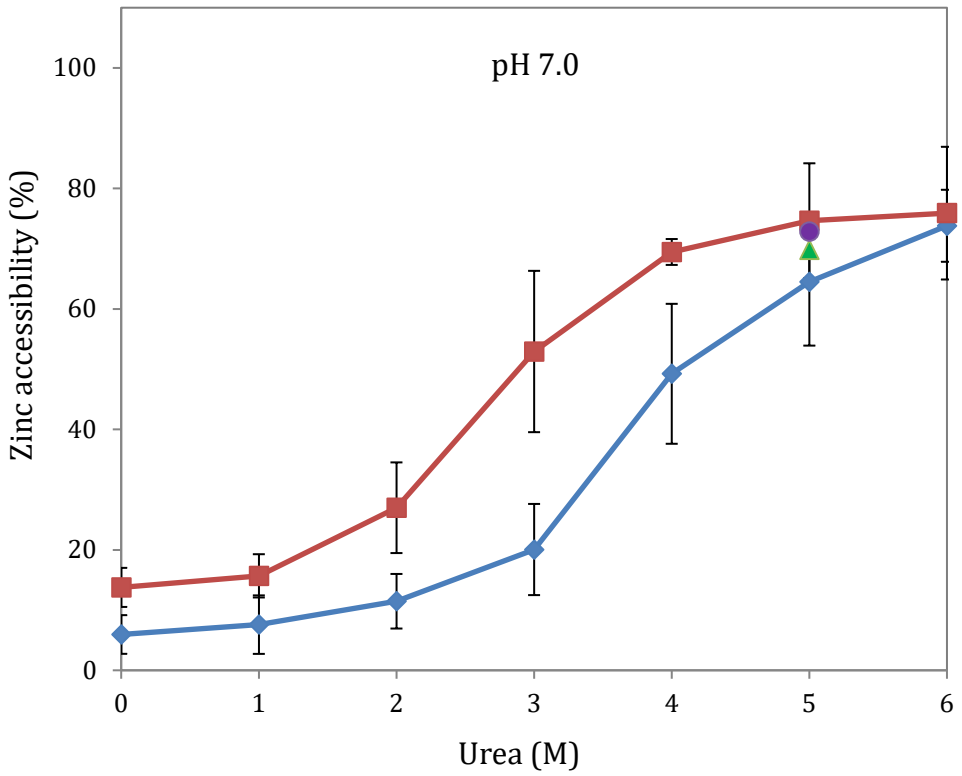

Figure 4.14: Effect of urea on the accessibility of Zn^{2+} to chelation by PAR at pH 7.0. LF (5 µM) was incubated with urea (0 - 6 M) containing 0.5 M NaCl in AMT buffer (25 mM, pH 7.0) for 1 h at room temperature prior to the addition of PAR (50 µM). The immediate degree of chelation by PAR (t = 0 min) is shown in blue, and that after 60 min of exposure to the chelator (t = 60 min) is depicted in red. Values shown represent the mean (± 1 s.d.) of three independent experiments. Two additional samples of LF, both incubated for 1 h in the presence of 5 M urea, were supplemented with PAR to initiate the complexation reaction. While one sample was immediately processed by Amicon filtration following the addition of PAR (green triangle), the other sample was allowed to incubate with the chelator for 60 min before Amicon filtration (purple circle), and prior to measurement of the amount of released Zn^{2+}.

The differences between the results obtained from the Zn^{2+} release and accessibility studies clearly suggest that PAR can penetrate the active site of LF and bind its metal ion at concentrations lower than those required to release Zn^{2+}. To address whether PAR merely binds the metal ion in the active site or whether the chelator removes Zn^{2+} from the enzyme after penetrating the active site, two additional protein samples were incubated for 1 h in 5 M urea before the addition of PAR. For one sample, the mixture was immediately subjected to Amicon filtration, and the concentration of the Zn^{2+}-PAR complex in the filtrate was

analyzed. As shown in Figure 4.14, the amount of Zn^{2+} released from LF in the form of the Zn^{2+}-PAR complex (green triangle) was found to be identical to that complexed by PAR (blue diamond). In addition, when the other sample (prepared analogously) was incubated with PAR for 60 min before processing by Amicon filtration, the concentration of the Zn^{2+}-PAR complex in the filtrate (purple circle) was identical to that recorded with the LF-containing sample (red square). These results clearly suggest that once PAR gains access to LF's active site, it binds and rapidly removes the Zn^{2+} ion from the protein. Furthermore, regardless of the time of exposure of LF to PAR (0 min or 60 min), the Zn^{2+} accessibility was found to be ~70%. This result suggests that at 5 M urea, the equilibrium between PAR-accessible (open) and –inaccessible (closed) states in LF is reached very rapidly.

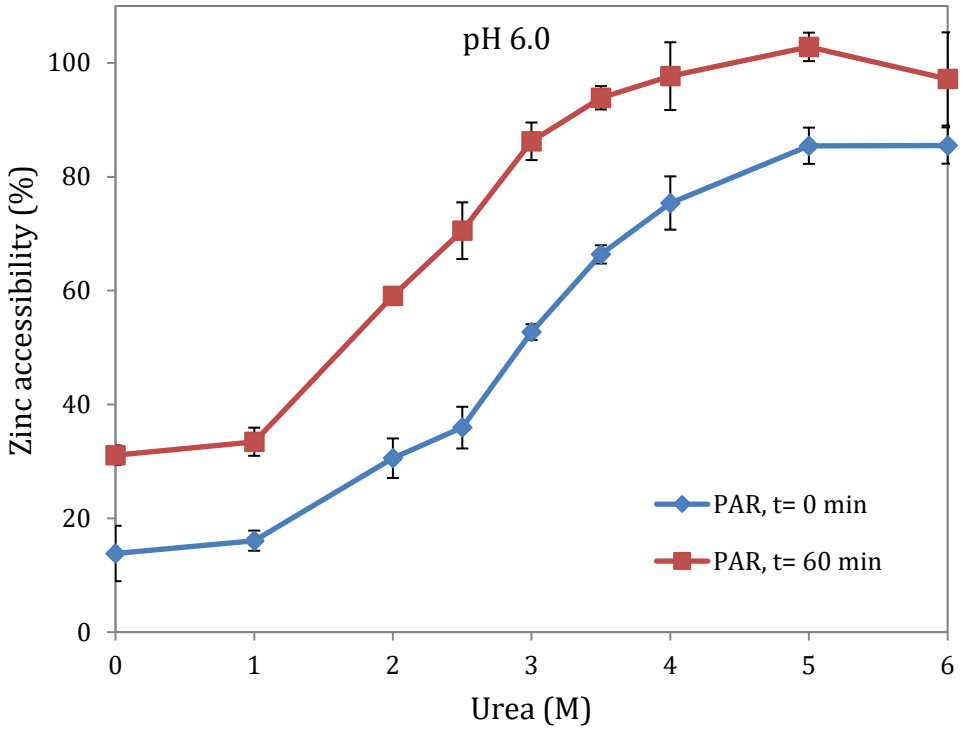

Figure 4.15: Effect of urea on the accessibility of Zn^{2+} to chelation by PAR at pH 6.0. LF (5 µM) was incubated with urea (0 - 6 M) containing 0.5 M NaCl in AMT buffer (25 mM, pH 6.0) for 1 h at room temperature prior to the addition of PAR (50 µM). The immediate degree of chelation by PAR (t = 0 min) is shown in blue, and that after 60 min of exposure (t = 60 min) is depicted in red. Values shown represent the mean (± 1 s.d.) of three independent measurements.

The effect of urea on the accessibility of Zn^{2+} to chelation by PAR at pH 6.0 is shown in Figure 4.15. Regardless of the urea concentration, the degree of Zn^{2+} chelation after 60 min of exposure to PAR was ~20% higher than that recorded for the t = 0 min values. The C_{mid} value was 2.9 M for immediate chelation (t = 0 min), and was 1.6 M after 60 min exposure to PAR (t = 60 min). These values are smaller than the C_{mid} values observed at pH 7.0, indicating a destabilization of LF at low pH.

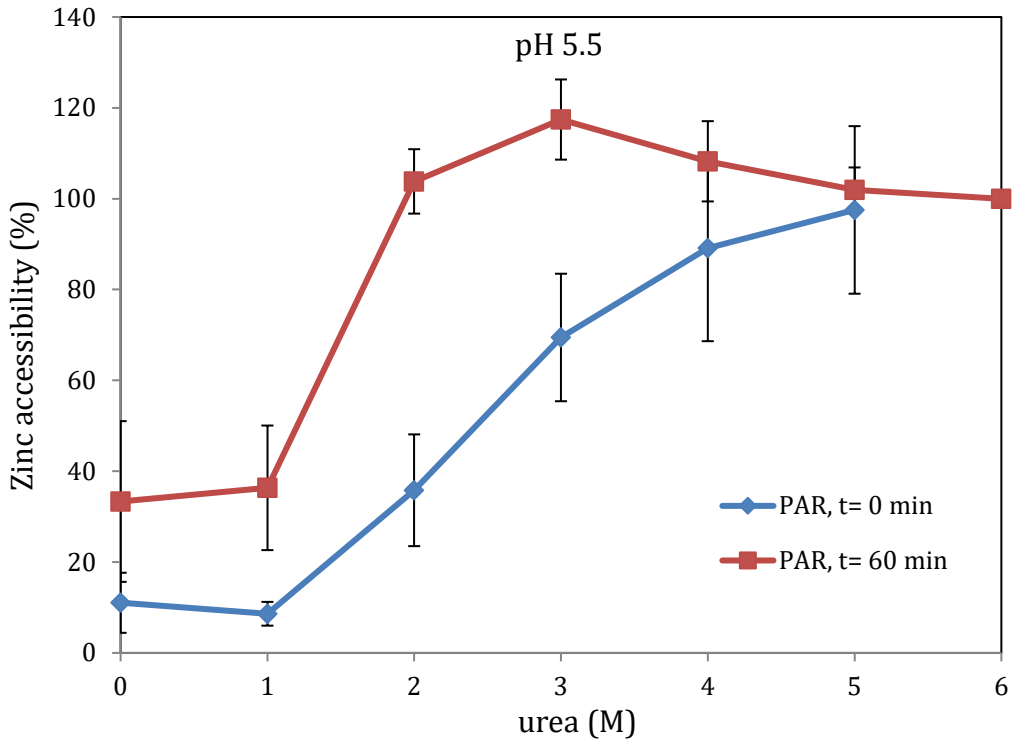

Figure 4.16: Effect of urea on the accessibility of Zn^{2+} to chelation by PAR at pH 5.5. LF (5 µM) was incubated with urea (0 - 6 M) containing 0.5 M NaCl in AMT buffer (25 mM, pH 5.5) for 1 h at room temperature prior to the addition of PAR (50 µM). The immediate degree of chelation by PAR (t = 0 min) is shown in blue, and that after 60 min of exposure to PAR (t = 60 min) is depicted in red. Values shown represent the mean (± 1 s.d.) of three independent measurements.

The effect of urea on the Zn^{2+} accessibility at pH 5.5, which could be considered a mid-endosomal pH, is shown in Figure 4.16. The relatively large error bars are a sign of PAR being not as sensitive in detecting/capturing Zn^{2+}at pH 5.5, a feature which is discussed further bellowed. After 60 min of exposure to PAR, the increase in Zn^{2+} accessibility compared to the t = 0 min value was much more pronounced that the increases observed at pH 7.0 or pH 6.0. For example, at 2 M urea, the Zn^{2+} accessibility increased from ~35% to 100% after 60 min of exposure to PAR, indicating that the Zn^{2+} accessibility is highly pH-and time-dependent. The C_{mid} values obtained from the accessibility studies using PAR between pH 7.4 and 5.5 are summarized in Table 4.3.

Table 4.3: Midpoint concentrations of urea for the accessibility of Zn^{2+} to chelation by PAR. The data for pH 7.4 were obtained from (53).

pH	C_{mid} (M)	
	t = 0 min	t = 60 min
7.4	4.4	3.1
7.0	4.0	2.9
6.0	2.9	1.6
5.5	2.4	1.2

As the table shows, the accessibility of Zn^{2+} to chelation by PAR was highly dependent on the pH value. The C_{mid} values recorded both at t = 0 min and t = 60 min of exposure of LF to PAR were found to decrease as the pH decreased. Prolonging the exposure time to 60 min also reduced the value of C_{mid}, indicating that PAR penetrates LF's active site gradually overtime to bind to the Zn^{2+} ion. Once PAR binds to the Zn^{2+} ion in the active site of LF, thus forming a Zn^{2+}-PAR complex, the metal ion is rapidly released from the enzyme.

4.4.2 Zinc accessibility studies with Zincon

Unfortunately, at pH values lower than 5.5, PAR is incapable of chelating Zn^{2+} because the compound becomes protonated, and therefore inefficient at binding metal ions (68). Hence,

all attempts to repeat the above-mentioned accessibility titrations with PAR at pH 5.0 failed (data not shown). However, 2-carboxy-2'-hydroxy-5'-sulfoformazylbenzene (Zincon) is another chromogenic chelator which has been shown previously to be an excellent agent to bind Cu^{2+} in the pH 5.0 to pH 11.0 range in the presence of urea (72). Because Zincon (similar to PAR) does not bind Zn^{2+} at pH 5.0 (72), the possibility of using Cu^{2+}-substituted LF to probe the enzyme's metal accessibility at pH 5.0 was explored. However, preliminary experiments to examine whether Zincon can penetrate the active site of ZnLF at pH 7.4 in a manner similar to that of PAR, were not successful (see Figure 4.17).

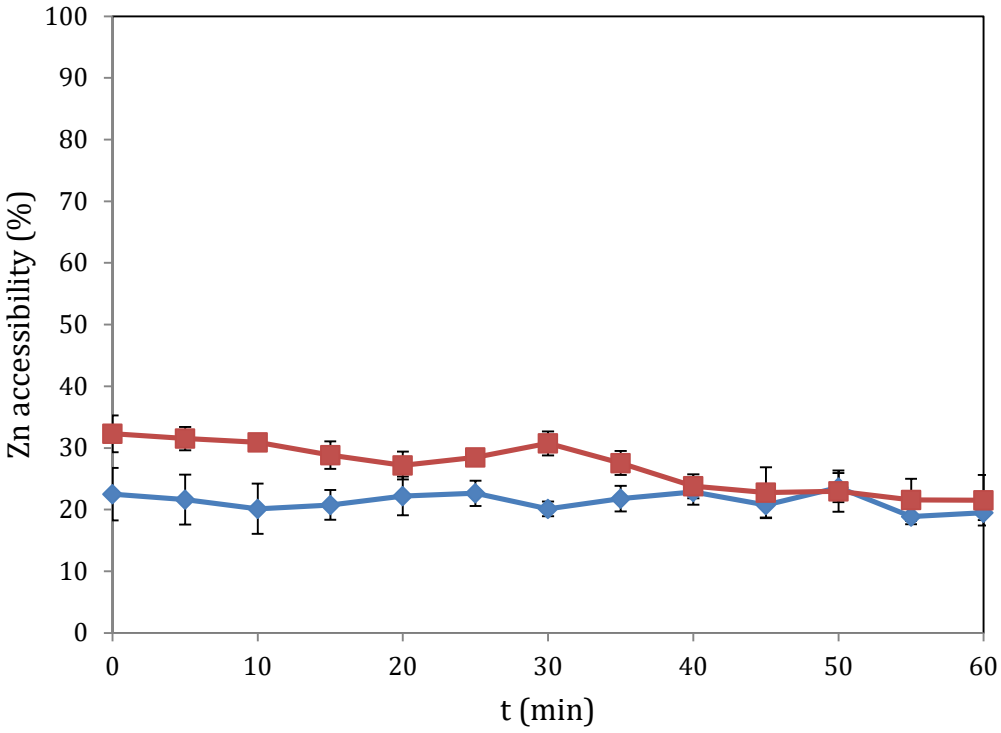

Figure 4.17: Time-dependence of the accessibility of Zn^{2+} to chelation by Zincon at pH 7.4. LF (5 μM) was incubated with 2.5 M (blue diamonds) or 5.0 M (red squares) urea in HEPES buffer (50 mM, pH 7.4) for 1 h at room temperature prior to the addition of Zincon (40 μM). The absorbance at 620 nm was recorded for 60 min in 5 min intervals. Values shown represent the mean (± 1 s.d.) of three independent measurements.

In fact, the Zn^{2+} accessibility remained constant and low during the duration of the experiment even at high urea concentrations. In previous studies on the accessibility of Zn^{2+}

to chelation by PAR using 2.5 M urea, the immediate chelation (t = 0 min value) was 20%, and was found to increase to ~ 40% after 60 min of exposure to PAR (53). In the case of Zincon, such increase in the Zn^{2+} accessibility was not observed (Figure 4.17). In addition, the Zn^{2+} accessibility recorded at 5 M urea was essentially identical to that found at 2.5 M, while in previous studies, the chelation by PAR was 80% (t = 0 and 60 min) (53). These results suggest that Zincon does not penetrate the active site of LF in a manner similar to PAR, and that, unfortunately, the chelator can therefore not be used as a probe to study the metal accessibility in LF at pH 5.0.

4.5 Red-edge excitation shift (REES)

As outlined earlier in Section 4.2, LF was found to unfold in the presence of relatively low concentrations of urea as evidenced by changes in the intrinsic tryptophan fluorescence spectra. However, the Zn^{2+} ion was shown to be retained even when LF was in the unfolded state (see Section 4.3), raising questions in regards to whether LF is really fully unfolded at moderate urea concentrations. To investigate whether LF can retain some (partial) fold at moderate urea concentrations, which may allow the protein to still interact and bind the Zn^{2+} ion, red-edge excitation shift (REES) measurements were performed. The presence of a REES effect (i.e., an increase in the maximum emission wavelength when λ_{exc} is increased) indicates a relatively slow rate of solvent relaxation around the examined fluorophores (typically Trp and Tyr residues in proteins). The rate or degree of solvent relaxation is directly related to the environment around the fluorophores. When the fluorophores are solvent-exposed, solvent relaxation is fast, and a REES is not observed. On the other hand, when fluorophores are buried (or solvent-inaccessible), the rate of relaxation is slow, and a REES is detectable (76,77,85).

4.5.1 REES measurements with LF

As mentioned earlier, the emission of tryptophan residues is highly sensitive to the polarity of their surroundings, affecting both the position of λ_{max} as well as the fluorescence intensity (FI) (83). *N*-acetyl-L-tryptophanamide (NATA), on the other hand, is a tryptophan analogue resembling the completely solvent-exposed amino acid. NATA is a useful (negative) control in REES studies because of this feature (i.e., NATA does not display a REES).

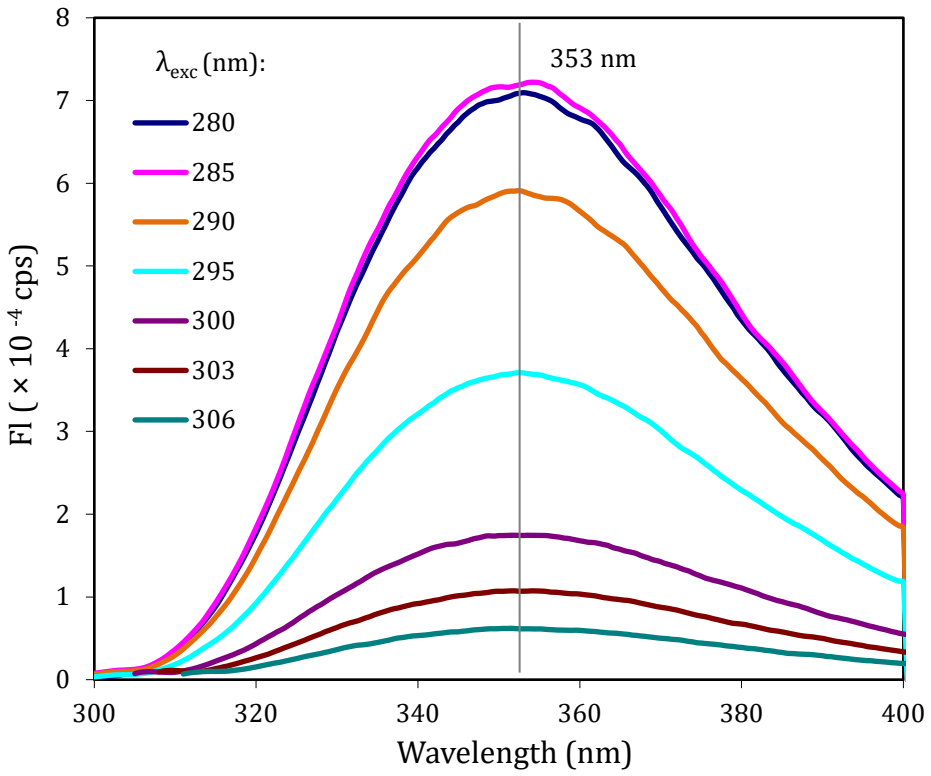

Figure 4.18: Emission spectra of NATA. NATA (25 µM) in AMT buffer (25 mM, pH 7.0) was excited at the wavelengths (λ_{exc}) indicated in the figure, and the emission spectra were recorded from 300 nm to 400 nm.

As shown in Figure 4.18, the emission maximum (λ_{max}) of NATA was found to be constant at 353 nm over the entire excitation wavelength range. As expected, a REES was not observed with NATA. The value of λ_{max} was higher than that recorded with unfolded LF (λ_{max} = 347 nm; see Section 4.2 and (53)), a feature which might indicate that LF is not fully unfolded at high denaturant concentrations.

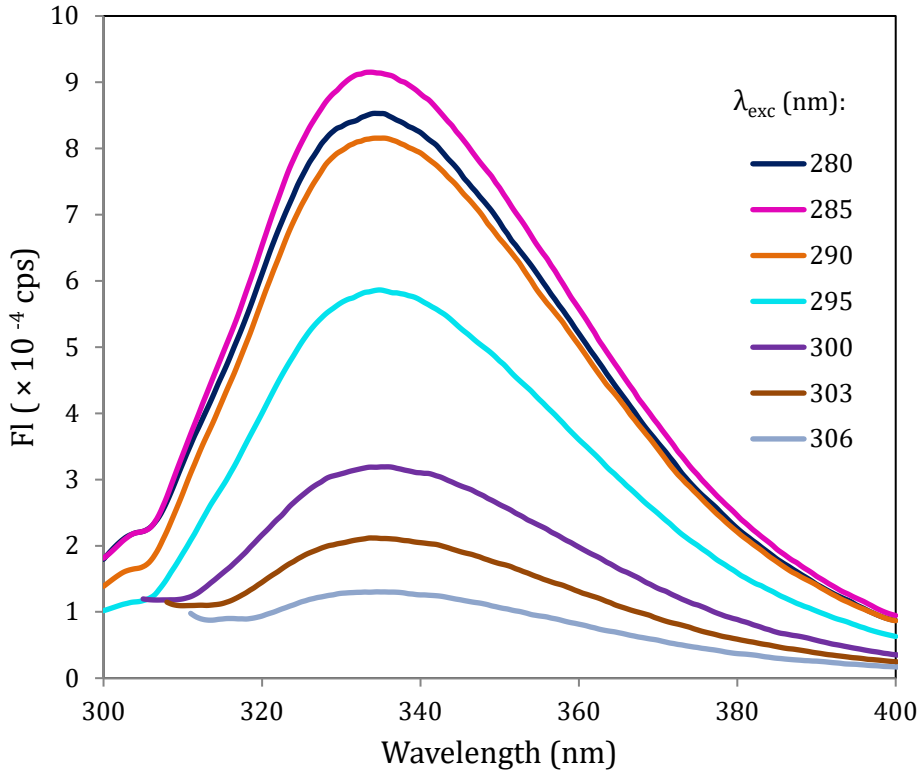

Figure 4.19: Emission spectra of native LF. LF (5 µM) was incubated in AMT buffer (25 mM, pH 7) for 1 h at room temperature prior to recording emission spectra following excitation at the wavelengths indicated in the figure.

In the case of native LF, excitation at 285 nm led to the highest emission intensity (an observation similar to that recorded with NATA; see Figure 4.18) at a wavelength of 334 nm (Figure 4.19). In general, as the excitation wavelength was increased from 285 nm to 306 nm, the FI value decreased. More importantly, the λ_{max} for native LF was found to increase from 334 nm (at λ_{exc} = 280 nm) to 338 nm (at λ_{exc} = 306 nm), indicating a REES of 4 nm. This result is expected since LF's five tryptophan residues are deeply buried in the protein's native state, and thus essentially solvent-inaccessible (see Figure 4.8). The fluorescence emission spectra of denatured LF (exposed to 6 M urea) are shown in Figure 4.20.

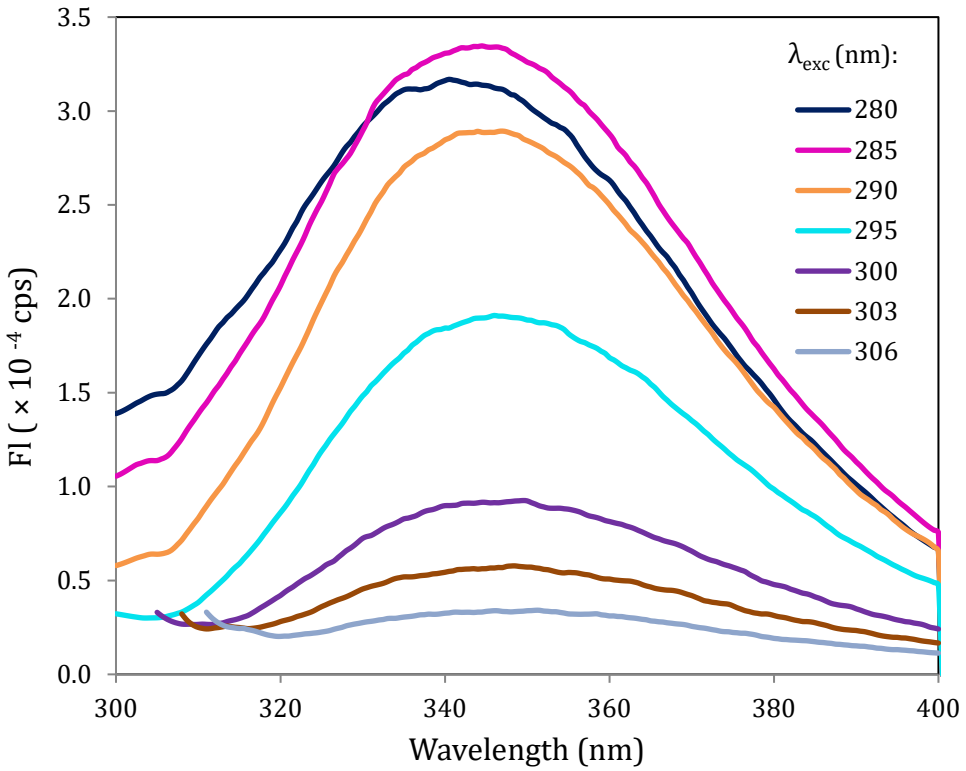

Figure 4.20: Emission spectra of LF in 6 M urea. LF (5 μM) was incubated with urea (6 M) in AMT buffer (25 mM, pH 5.5) for 1 h at room temperature prior to recording emission spectra. The range of excitation wavelengths used is indicated in the figure.

The overall emission intensities were found to be reduced by a factor of ~3 upon inclusion of the denaturant (see Figure 4.19 and Figure 4.20). The spectrum obtained at 280 nm was slightly blue-shifted (with respect to that recorded at 285 nm), a feature absent in the REES measurements with native LF.

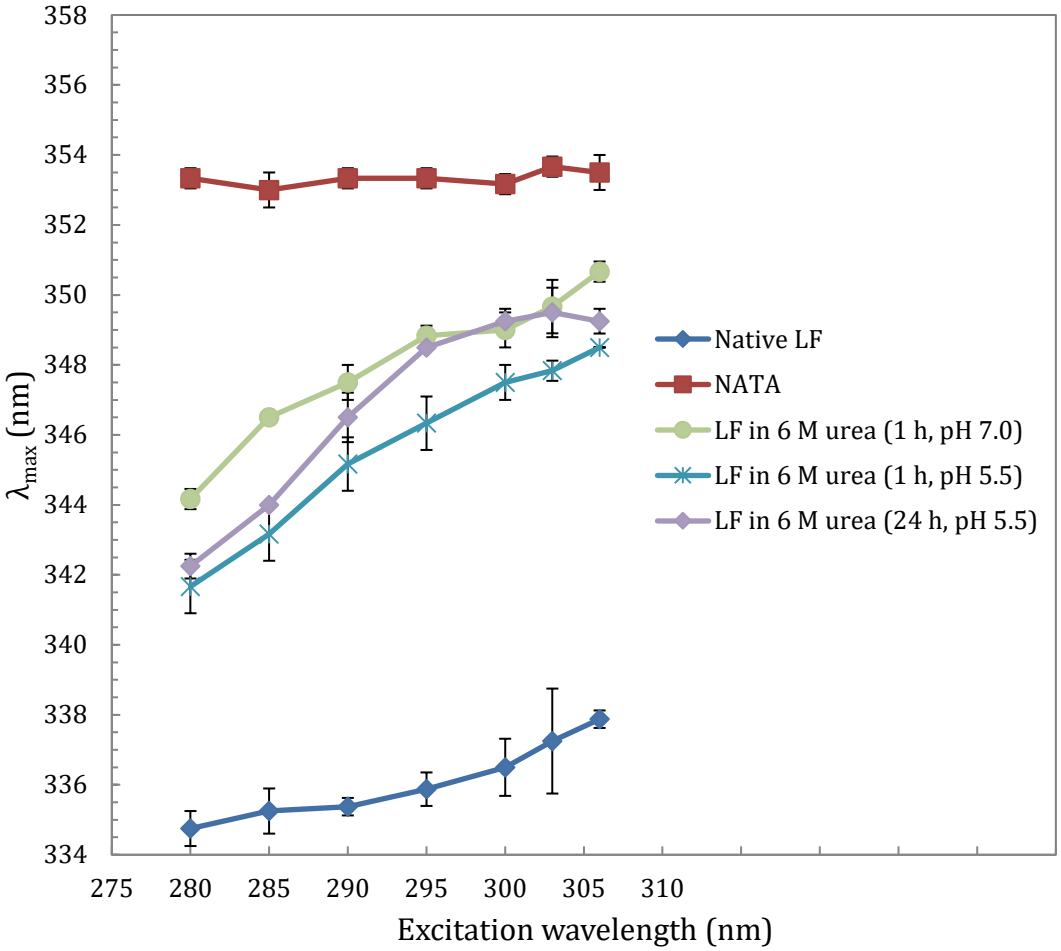

Figure 4.21: REES plot of urea-mediated unfolding of LF. LF (5 μM) was incubated with 6 M urea in AMT buffer (25 mM, pH 7.0 or 5.5) for 1 h or 24 h at room temperature prior to recording the emission spectra (excitation wavelength range: 280 - 306 nm). Data for NATA (red) and native LF (shown in Figure 4.18 and Figure 4.19) are included in this figure for reference, and are depicted in red and dark blue, respectively. Values shown represent the mean (± 1 s.d.) of three independent measurements.

As shown in Figure 4.21, native LF (as previously mentioned) displayed a REES of about 4 nm. Surprisingly, urea-exposed (for 1 h), unfolded LF at pH 5.5 showed a larger REES (~ 7 nm). To investigate whether changes in incubation time or pH can influence the magnitude of the REES, emission spectra were also obtained for LF incubated with 6 M urea at pH 5.5 for 24 h and at pH 7.0 for 1 h. As evident from Figure 4.21, neither an increase in the incubation time nor a change in the pH led to substantial changes in the REES.

The large REES for urea-exposed LF suggests that the enzyme is not fully unfolded. To probe whether harsher denaturing conditions could lead to the disappearance of a REES, LF was treated with the stronger denaturants GdnHCl and GdnSCN, and the emission spectra were recorded.

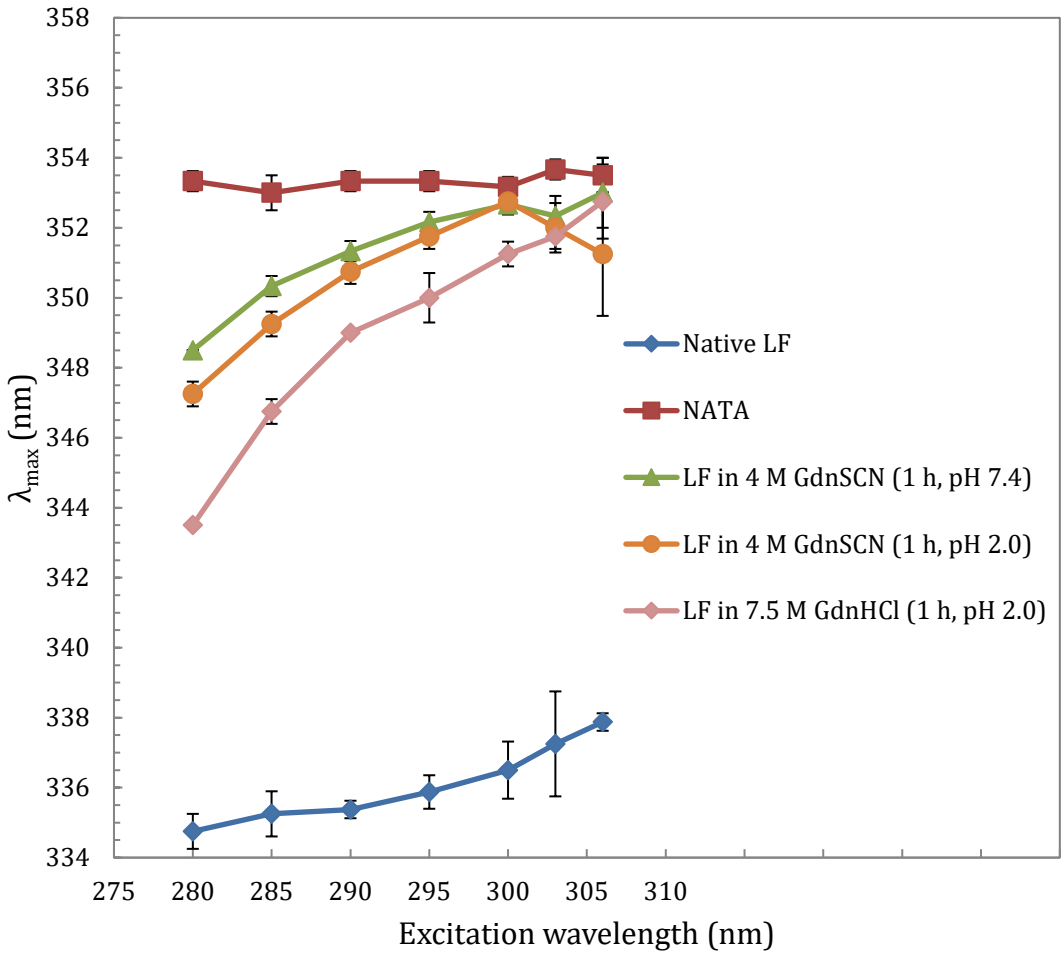

Figure 4.22: REES plot of GdnHCl- and GdnSCN-mediated unfolding of LF. LF (5 µM) was incubated with 4 M GdnSCN or 7.5 M GdnHCl in AMT (25 mM, pH 2.0) or HEPES buffer (50 mM, pH 7.4) for 1 h at room temperature prior to recording emission spectra (excitation wavelength range: 280 - 306 nm). Data for NATA (red) and native LF (shown in Figure 4.18 and Figure 4.19) are included in this figure for reference, and are depicted in red and dark blue, respectively. Values shown represent the mean (± 1 s.d.) of three independent measurements.

As shown in Figure 4.22, even though GdnHCl and GdnSCN are much stronger chemical denaturants than urea, a REES was observed, even at very low pH (pH 2.0). These results

indicate that LF might, even under very harsh conditions, retain part of its fold. However, the λ_{max} values were generally higher when GdnHCl or GdnSCN were used (see Figure 4.22) as compared to urea (see Figure 4.21). This result may suggest that LF is closer to a fully unfolded state with GdnHCl and GdnSCN than with urea. In addition, the position of λ_{max} for GdnHCl-treated LF was below that observed for the GdnSCN-exposed protein. Therefore, the degree of unfolding mediated by GdnSCN appears larger, a finding consistent with this salt being the strongest chemical denaturant known (78,79).

As mentioned earlier, the emission spectrum of LF exposed to 6 M urea and recorded at an excitation wavelength of 280 nm is significantly blue-shifted compared to that obtained at an excitation wavelength of 285 nm (see Figure 4.20). In addition, the increase in λ_{max} in the lower range of excitation wavelengths (i.e., 280 nm to 295 nm) was much more pronounced than that observed between 295 nm and 306 nm (see Figure 4.21 and Figure 4.22). This is rather surprising, and such effect is not observed with native LF. The fact that the emission wavelength increases most at excitation wavelengths below those selective for tryptophan residues (i.e., ≥ 295 nm) appears to indicate that the presence of tyrosine residues (there are 35 Tyr residues in LF) could interfere with the interpretation of REES data by "artificially" shifting λ_{max} to lower values. It is important to point out that typical REES measurements involve recording emission spectra using excitation wavelengths ranging from 280 nm to approximately 310 nm (76,85,86). Thus, at an excitation wavelength below 295 nm, both Tyr and Trp residues are excited, and as stated above, including excitation wavelengths below 295 nm in REES plots could potentially lead to an overestimation of the REES.

4.5.2 REES measurements with mixtures of tyrosine and NATA

Beside tryptophan, tyrosine is the most important intrinsic fluorophore found in proteins. Its emission is not as sensitive to changes in the polarity of its microenvironment as is the case with Trp residues, and the FI values are typically lower (83).

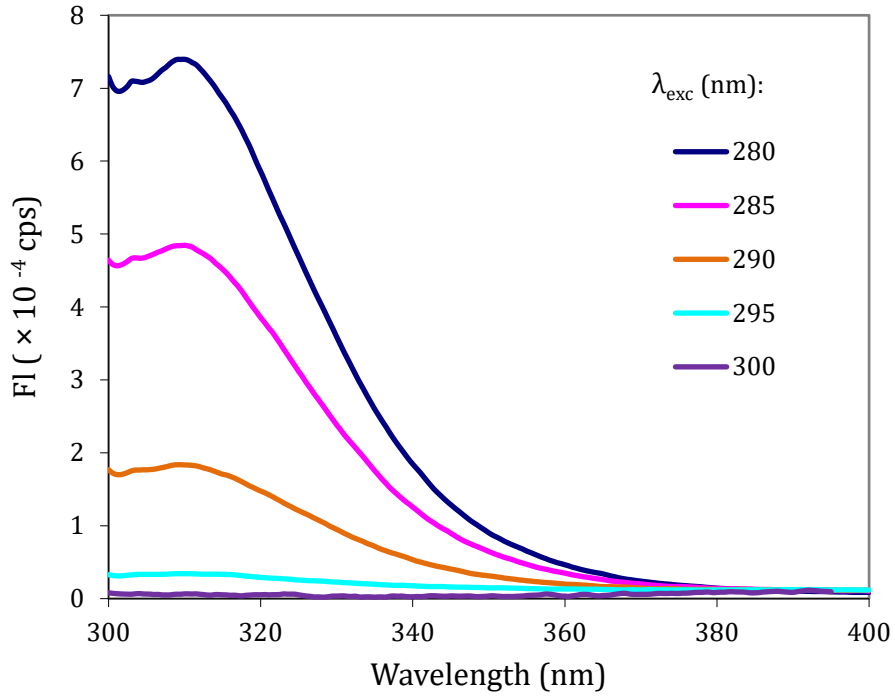

Figure 4.23: Emission spectra of L-Tyrosine. Tyrosine (150 µM) in AMT buffer (25 mM, pH 7.0) was excited at the wavelengths (λ_{exc}) indicated in the figure, and the emission spectra were recorded from 300 nm to 400 nm.

As shown in Figure 4.23, L-tyrosine can be excited at 280 nm, 285 nm, and 290 nm. The λ_{max} remained constant at 310 nm, a value 43 nm lower than that observed for NATA (Figure 4.18). As expected, the emission intensities were very low when the excitation wavelength was raised to 295 nm and above.

As mentioned above, LF contains five Trp and 35 Tyr residues (Y/W ratio of 7). To investigate how the presence of Tyr can affect the emission spectra, mixtures of NATA and L-tyrosine were excited at 280 nm, and their emission spectra were recorded.

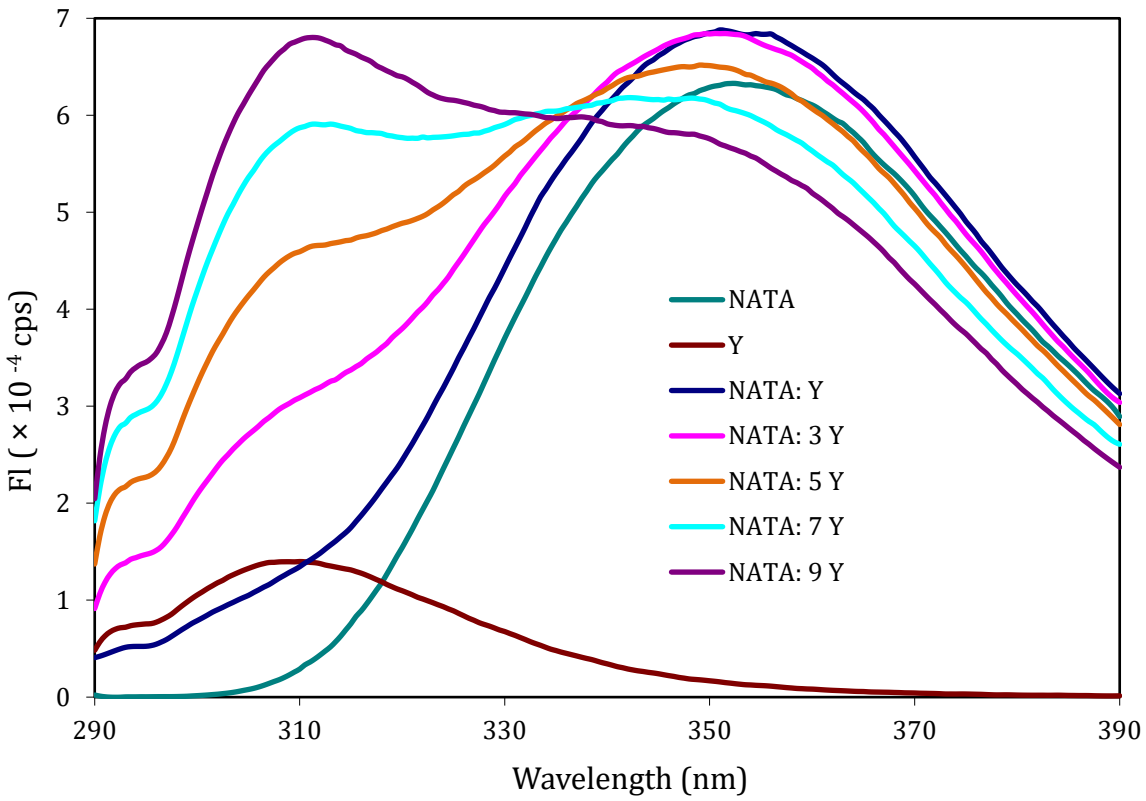

Figure 4.24:Emission spectra of NATA and L-Tyrosine mixtures (λ_{exc} = 280 nm). A mixture of NATA (25 µM) and L-tyrosine (1 to 9 equivalents; 25 - 225 µM) in AMT buffer (25 µM, pH 7.0) was incubated for 1 h at room temperature prior to recording emission spectra. The excitation wavelength was set to 280 nm.

Table 4.4: **Dependence of λ_{max} on the Y/NATA ratio.**

Y/NATA ratio	λ_{max} (nm)
0	352.5
1	351.0
3	350.5
5	349.0
7	342.0
9	311.5

As shown in Figure 4.24 and Table 4.4, an increase in the ratio of tyrosine and NATA (Y/NATA) from 0 to 9 led to a significant spectral blue-shift in the emission spectra with concomitant decrease in the λ_{max} value from 352.5 nm to 311.5 nm. At a Y/NATA ratio of 9, the emission spectrum was dominated by the emission of tyrosine at 310 nm. At a Y/NATA ratio of 7, which is identical to the Y/W ratio found in LF, the λ_{max} value (342 nm) was found to be decreased by approximately 10 nm with respect to that observed for NATA. This data strongly suggests that the presence of tyrosine residues in a protein can influence the emission spectra when the fluorophores are excited at 280 nm. This can consequently lead to substantial shifts (decrease) in the λ_{max} values, and thus, to an overestimation of the REES. These considerations are illustrated in Figure 4.25, which provides a summary of the REES data collected on LF. Even in the presence of chemical denaturants (urea, GdnHCl, or GdnSCN), LF was found to display a quite large REES, indicating that the protein is only partially unfolded. However, when the measurements at excitation wavelengths below 295 nm are omitted from the calculation of the REES (and therefore only the excitation of tryptophan residues are considered), the REES is much smaller (yellow bars in Figure 4.25). In fact, considering tryptophan fluorescence only, the REES obtained with LF incubated in the presence of 4 M GdnSCN at pH 2.0 was zero, suggesting that under these conditions LF is essentially fully unfolded. For all other conditions, the REES ranged from 0.8 – 2.8 nm regardless of the pH. This result clearly suggests that LF is not fully unfolded at high concentration of urea or GdnHCl. Overall, the REES studies showed that LF is very resilient, resisting complete unfolding even by strong chemical denaturants and at pH values in the endosomal pH range.

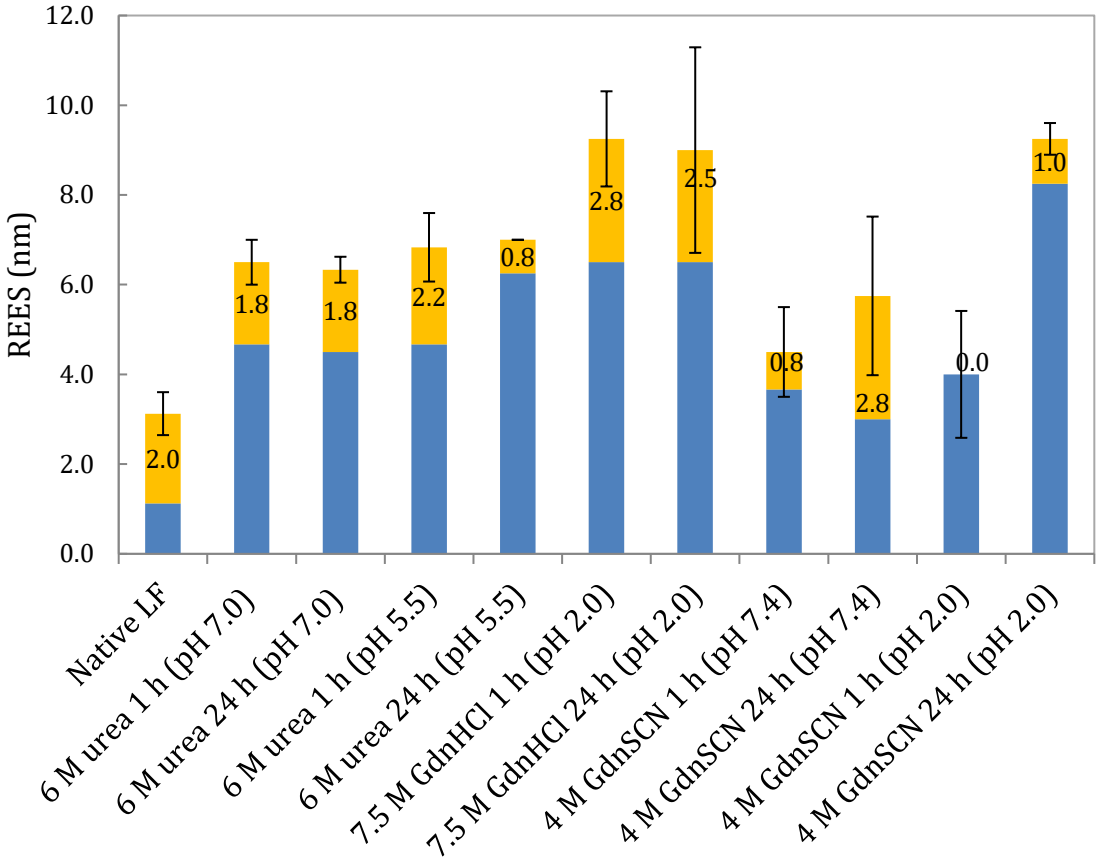

Figure 4.25: Summary of REES values. REES values were obtained from the recorded emission spectra shown in Figure 4.19 and Figure 4.20, and the REES plots shown in Figure 4.21 and Figure 4.22. The full bar represents the REES value obtained by subtraction of the maximum emission wavelength determined at 306 nm from that recorded at 280 nm. The yellow portion of the bar denotes the REES value (with numerical values included) obtained using the excitation wavelength range of 295 nm to 306 nm, whereas the blue portion represents the contribution in the 280 nm to 295 nm excitation range. Values shown represent the mean (± 1 s.d.) of three independent measurements.

5 Discussion

Anthrax is a lethal disease, and has the potential to be used as a biological weapon (28,29). In the era of rising antibiotic resistance, and in view of a current lack of a reliable treatment, a deeper understanding of the pathogenesis of anthrax is necessary. The mechanism of the translocation of the anthrax toxin components has been the main research focus in recent years (50-52,54,57). The anthrax toxin has three components: lethal factor (LF), edema factor (EF), and the pore forming protein protective antigen (PA). It was found that upon acidification of the endosome, PA forms a narrow pore which is inserted into the endosomal membrane (54). The PA channel is very narrow, and contains a constriction site only 6 Å in diameter (51). Hence, only LF (or EF) unfolded (or at least partially unfolded) to a single polypepetide chain can pass through this channel during the translocation event (51,54). LF is a Zn^{2+}-dependent metallopeptidase which contains one Zn^{2+} ion in the catalytic site essential for its cytotoxic activity (60). If LF must be (at least partially) unfolded during translocation, then its Zn^{2+}-binding site will most likely be disrupted.

This thesis investigated the unfolding of LF and its metal status at pH values which mimic those found in endosomes. Such studies were meant to provide knowledge of whether the Zn^{2+} ion in LF could be retained or lost during LF translocation. This is critical because the concentration of free cytosolic Zn^{2+} is very low (in the picomolar range) (18). If LF loses its metal ion during translocation and is forced to compete with other zinc proteins in the cytosol for available Zn^{2+}, an intracellular zinc deficiency could result.

5.1 LF aggregation at low pH

The first part of this thesis dealt with investigations on LF aggregation at acidic pH. The isoelectric point of LF is ~5.5, and LF aggregation is clearly measureable at ~pH 5.5 (65). The aggregation of LF was observed spectrophotometrically at 350 nm (see Figure 4.2), and by (more sensitive) light scattering analysis using a fluorometer (see Figure 4.3).

Protein aggregation is a common problem during pH studies. The addition of a protein aggregation inhibitor such as NaCl can change the ionic strength of the medium, and suppress the formation of protein aggregates (82,87). In the case of LF, sub-molar

concentrations of NaCl were found to significantly reduce protein aggregation at pH > 5.0. At NaCl concentrations > 1 M, the salt was found to stabilize the native fold of LF (see Figure 4.4), a feature which could interfere with the interpretation urea titration data. The stabilization of LF by higher concentrations of NaCl is interesting because, according to the Hofmeister series, NaCl is not strong structure maker (kosmotropic). On the other hand, Na_2SO_4 was shown in this study to be even more effective in preventing LF aggregation. This is surprising since the salt (along with its ammonium analogue) is used to precipitate proteins. In the case of LF, however, Na_2SO_4 seems to effectively prevent such precipitation. Although the reason for this is not known, it is possible that at low pH, charged surface patches on LF interact in a complementary fashion causing aggregation. In such case, NaCl or Na_2SO_4 might prevent aggregation of LF by disrupting this interaction.

The solubility of proteins is affected by both the ionic strength and the particular species of (Hofmeister) ions in solution (78,79,87). Unfortunately, the usefulness of NaCl in suppressing LF aggregation is limited to pH values above 5.0. As a consequence, another protein aggregation inhibitor, L-arginine, was investigated. Unlike NaCl, which increases the protein solubility by decreasing the surface tension (82), L-arginine contains a guanidine moiety which binds to the side chains of acidic and aromatic amino acid residues to suppress the formation of protein aggregates (82,88). As demonstrated in this study, LF aggregation was efficiently decreased at pH 5.0 in the presence of sub-molar concentrations of L-arginine (see Figure 4.6 and Figure 4.7).

5.2 LF unfolding monitored by tryptophan fluorescence spectroscopy

In this part of the study, structural changes in LF in the presence of urea at neutral and acidic pH were investigated using sodium chloride (for pH 7.0 - 5.5) and L-arginine (pH 5.0) as a means to suppress protein aggregation. According to the literature, acid denaturation rarely produces fully unfolded proteins in the absence of a chemical denaturant, and acidic conditions can lead to various effects on protein structure (89-91). Urea was chosen in this study because it is a relatively weak chemical denaturant in contrast to guanidine

hydrochloride which is too strong to observe subtle differences in the unfolding profiles of LF induced by slight acidification (53).

The unfolding of LF in HEPES buffer at pH 7.4 by urea has previously been found to follow a 2-state model, changing from the native state directly to the unfolded state (53). Such 2-state mechanism was also observed in the current studies performed at pH 7.0 and 6.5 (see Figure 4.9). However, the midpoint concentration (C_{mid}) of urea in AMT buffer at pH 7.0 was 2.38 M, which is slightly higher than that reported at pH 7.4 (1.89 M). This results might indicate that at pH 7.0, the fold of LF is slightly more stable, an observation which might be related to the addition of NaCl and the higher ionic strength (I = 0.5 M) of the buffer (see Figure 4.4). Using pH conditions mimicking those found in endosomes, the unfolding of LF followed a 3-state mechanism (see Figure 4.10). In this case, the native state of LF unfolds to an intermediate state before reaching the unfolded state. An intermediate state is often observed during acid-induced unfolding (89), and for LF, such state first appears at a pH of 6.0, and then gradually becomes more dominant as the pH reaches a value of 5.0 (late endosomal pH).

An unfolding mechanism involving more than two states under acidic conditions has also been observed previously with the N-terminal domain of LF, indicating that the unfolding of the protein domain (which binds to PA) under endosomal pH conditions involves different LF conformations (92). Although previous studies have shown LF unfolding to reach equilibrium after 24 h (53), measurements at pH ≤ 6.5 reported in this study were performed after 1 h of incubation with the denaturant because the fluorescence intensities after 24 h of exposure to the denaturant were found to have very large standard deviations, and a fit of the data was impossible. This observation might be related to the production of randomly coiled structures of LF, a feature which has been observed previously for other proteins (93). Nevertheless, for the 1 h measurements, the midpoint concentration of urea was found to decrease upon acidification from 2.38 M (pH 7.0) to 1.18 M (pH 5.5), and was below 0.5 M at pH 5.0, indicating that the native conformation of LF becomes more and more destabilized as the pH is lowered.

5.3 Zinc release

The release of metal ions, and Zn^{2+} in particular, from metalloproteins has been determined previously by adding a chromophoric chelator such as PAR directly to the protein sample (94,95). However, recent studies on LF have shown that spontaneous Zn^{2+} release cannot be determined by adding PAR directly to the LF-containing sample (53). Instead, spontaneously released metal ions need to be removed from LF by Amicon filtration before they can be quantified (in the filtrate), hence leading to a proper estimation of the amount of Zn^{2+} released (53). Previous investigations (performed at pH 7.4) on the Zn^{2+} release from LF using Amicon filtration followed by measurement of the Zn^{2+} concentration in the filtrate have revealed that LF resists metal ion release even when exposed to urea concentrations much higher than those required to induce unfolding (53). In the current studies, NaCl (0.5 M) was added to LF samples to prevent protein aggregation at low pH (see section 4.1). To investigate whether the addition of NaCl exhibits an effect on the amount of Zn^{2+} released, comparative studies were performed in the absence and presence of NaCl from pH 6.0 to 4.0 (see Figure 4.11). At pH 6.0, the addition of NaCl did not affect the amount of Zn^{2+} released from LF, a finding not surprising since the protein does not aggregate at this pH (65). However, as the pH was lowered from pH 5.5 to 4.0, the inclusion of NaCl resulted in a clear increase in the amount of Zn^{2+} released, especially under the most acidic pH conditions, and in the presence of urea at low concentrations. The results from early Trp fluorescence studies indicated that LF is less prone to aggregation at high urea concentrations. During the Zn^{2+} release studies using urea concentrations ranging from 4 to 6 M between pH 5.0 and 4.0, no aggregation was observable. Consequently, the inclusion of NaCl did not affect the degree of release of the metal ion from LF. Overall, the decreased Zn^{2+} release in the absence of NaCl is consistent with the formation of LF aggregates trapping the released metal ion, hence, leading to smaller amounts of Zn^{2+} in the Amicon filtrate.

The degree of Zn^{2+} release (in the presence of 0.5 M NaCl) was found to be a highly pH-dependent process (see Figure 4.12). Between pH 7.0 and 6.0, Zn^{2+} release was minimal until high concentrations of urea were reached. At pH values lower than 6.0 (and thus, lower than the *p*Ka value of histidine), a noticeable amount of Zn^{2+} (~25%; at pH 5.5) was released even in the absence of urea. This observation is likely related to the protonation of Zn^{2+}-

coordinating active site His residues in some of the LF molecules. Under late endosomal pH conditions (i.e., pH 5.0), Zn^{2+} was found to be fully released in the presence of 6 M urea. When the pH was further lowered to 4.0, the metal ion was fully released even in the absence of the denaturant, presumably due to the full protonation of active site metal ligands.

Studies on the effect of different chemical denaturants (GdnSCN, GdnHCl, and urea) on Zn^{2+} release from LF revealed that the strongest chemical denaturant (i.e., GdnSCN) caused the highest degree of metal release (~ 90% at 4 M; see Figure 4.13), whereas GdnHCl (4 M), the second strongest denaturant, was found to release only ~ 52% of the metal ion. Urea, the weakest of the three denaturants, did not trigger a significant release of the metal at neutral pH. Overall, these results demonstrate that GdnSCN is able to unfold LF and induce Zn^{2+} release more effectively than the other two denaturants.

5.4 Zinc accessibility

Since the spontaneous release of LF's Zn^{2+} ion required urea concentrations much larger than those to induce the unfolding of the protein, it was of interest to determine whether the denaturant could, at moderate denaturant concentrations, affect structural changes that allow a chelator to bind the active site metal ion. In this thesis, the chromophoric chelator PAR was used to study such changes at different pH values. For the measurements at pH 7.0, the results are similar to those obtained in previous studies performed at pH 7.4 (53) in that PAR was able to penetrate LF's active site to bind the metal ion with a midpoint of 4.0 M urea (at t = 0 min; see Figure 4.14). However, slightly more Zn^{2+} was bound immediately after PAR was added to LF, indicating that a slight decrease in the pH (by 0.4 pH units) can favour the open, metal-accessible conformation of LF. Lowering the pH successively to 5.5 led to a substantial decrease in the midpoint concentrations of urea (see Table 4.3) from 4.0 M to 2.4 M. This result is a clear indication that acidification facilitates the conversion of the closed (inaccessible) state of LF to the open form. In addition, incubation of LF with PAR for 60 min led to a marked decrease in the midpoint concentrations for all pH values investigated, reaching a value of 1.2 M urea at pH 5.5. The decrease in the midpoints upon prolonged exposure of LF to PAR (for 60 min) at pH 7.4 has been shown previously (53), and has been

attributed to the chelator being actively involved in shifting the equilibrium to the open, accessible state. At pH 5.5, and following exposure to PAR for 60 min, the fully (100%) open state was reached at 3 M urea. Therefore, acidic pH conditions such as those found in endosomes can facilitate conformational changes which assist PAR in gaining access to the Zn^{2+} binding site. Since PAR cannot be used to quantify Zn^{2+} at pH 5.0 because of the partial protonation of the chelator (68), the possibility of Zincon, an ideal chelator for Cu^{2+} at acidic pH (72), to replace PAR as an accessibility probe was explored. Unfortunately, the results show that Zincon does not gain significant access to LF's active site, and that this persists even at high denaturant concentrations. On the other hand, these results suggest PAR to be a rather unique accessibility probe to detect metal ions in proteins (53,96).

5.5 Summary of unfolding, zinc accessibility and release studies

A summary showing the results obtained from the LF unfolding profiles (determined by Trp fluorescence spectroscopy), and from the Zn^{2+} release and accessibility studies performed in the pH range of 7.0 to 5.0 in a comparative manner, is depicted in Figure 5.1 and Table 5.1.

At pH 7.0, the unfolding profile of LF shows that the native protein unfolds directly to the unfolded state. At a urea concentration of 3 M, LF appears to be fully unfolded. However, LF's Zn^{2+} ion is not released upon unfolding, and only very little Zn^{2+} ($\sim$ 10%) is released when the protein is exposed to 6 M urea. In contrast, the accessibility of Zn^{2+} to chelation by PAR, which is thought to penetrate to the enzyme's active site, changes significantly at urea concentrations larger than those required for unfolding, and much smaller than those necessary to induce spontaneous Zn^{2+} release. Hence, the transition midpoints for the unfolding, metal release and accessibility are clearly separated.

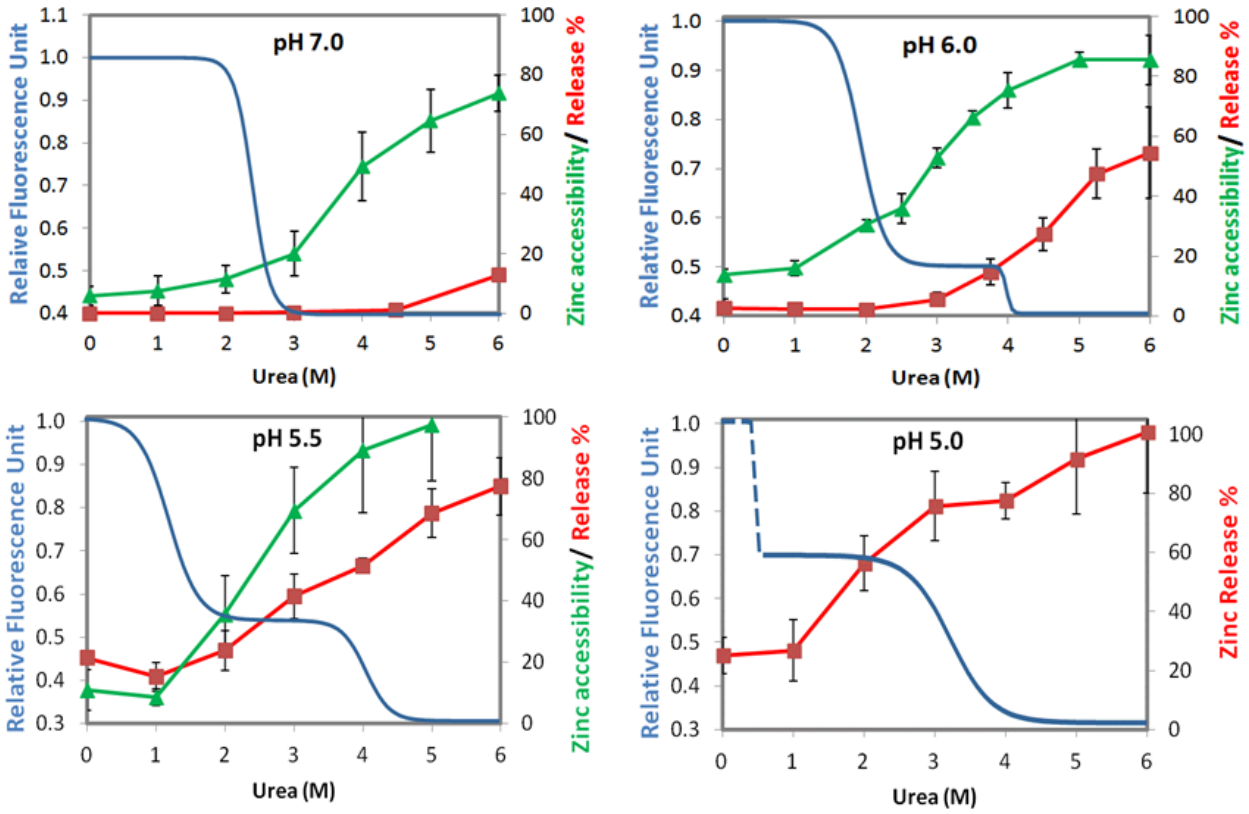

Figure 5.1: Summary of the LF unfolding profiles and the Zn^{2+} release and accessibility studies. Data shown was taken from the unfolding, release and accessibility profiles described in Sections 4.2, 4.3 and 4.4. For the unfolding profiles, only the fits of the data to the equations governing the 2-state (pH 7.0) and 3-state (pH 6.0 – 5.0) unfolding mechanism are shown.

Table 5.1: Summary of C_{mid} values.

pH	C_{mid} (M)		
	LF unfolding	Zinc accessibility	Zinc release
7.0	2.4	4.0	> 6.0
6.0	1.9	2.9	5.5
5.5	1.2	2.4	3.9
5.0	< 0.5 (n. d.)	n.d.	1.8

n.d., not determined. The C_{mid} values were obtained from Section 4.2 - 4.4, and the C_{mid} of LF unfolding represent the first transition N → U for a 2-state model (pH 7.0) or N → I for a 3-state model (pH 6.0 – 5.0).

Upon slight acidification to pH 6.0 (pH of early endosomes), the unfolding of LF appears to follow a 3-state mechanism, implying that the native state of the enzyme converts into an

intermediate state (at urea concentrations between 2 M and 3 M), and then to a fully unfolded state (at approximately at 4 M urea). As in the case of the pH 7.0 measurements, no Zn^{2+} release from native LF is observed. At moderate urea concentrations, and upon entering the intermediate state, only a modest release of the metal ion (~ 10% – 20%) is observed. The midpoint of metal release is at a urea concentration of ~ 5.5 M (see Table 5.1). As in the case of the pH 7.0 studies, the midpoint transition of the accessibility of the metal ion to chelation by PAR is between those recorded for the unfolding of LF and the release of the Zn^{2+} ion. However, the midpoint is significantly shifted towards lower urea concentrations (from 4.0 M to 2.9 M) when the pH is lowered from 7.0 to 6.0, suggesting that a lower pH facilitates a higher degree of metal ion accessibility.

Upon further acidification to pH 5.5, the unfolding of LF clearly followed a 3-state mechanism. The intermediate state is stable between 2 M and 3.5 M urea. Furthermore, the midpoint for the N → I transition is clearly lower at pH 5.5 than at pH 6.0, suggesting that the native state of LF is destabilized at lower pH values. Similarly, the midpoint for the release of Zn^{2+} is reduced to 3.9 M urea from 5.5 M observed at pH 6.0 (see Table 5.1). Interestingly, the midpoint for the release of Zn^{2+} from LF at pH 5.5 is close to that observed for the I → U unfolding transition. However, whether this finding is coincidental or whether it suggests that the release of the metal ion is triggered by the conversion of the intermediate state to the unfolded state needs to be determined in the future. As in the case of the pH 7.0 and 6.0 measurements, the midpoint of accessibility at pH 5.5 is between those determined for unfolding (C_{mid1}) and metal release. However, the midpoints are closer at pH 5.5.

At a (late endosomal) pH value of 5.0, the first (N → I) transition could not be resolved, but it is apparent that the native state of LF is destabilized, being essentially not observable at urea concentrations above 0.5 M (see the dashed line in Figure 5.1). This result clearly suggests that at pH 5.0, the native state of LF is the least stable. The intermediate state appears to be stable from 0.5 M to about 2.5 - 3 M urea. In addition, at pH 5.0, the native state of LF is prone to Zn^{2+} release even in the absence of urea (~ 30%), a finding in agreement with that reported previously (65). The midpoint of metal ion release was also found to be much lower than that observed at pH 5.5, indicating that LF releases Zn^{2+} more readily at lower concentrations of urea. The accessibility of Zn^{2+} to chelation by PAR could,

unfortunately, not be determined because the chelator is not able to bind Zn^{2+} at pH 5.0. The attempt to use the metal chelator Zincon instead of PAR also failed since, probably because Zincon is larger (bulkier) than PAR, and might not easily gain access to the active site of LF (see Section 4.4). Indeed, the exclusion of Zincon from the active site of the zinc-containing IMP-1 metallo-β-lactamase for steric reasons has been reported previously (96).

5.6 Red-edge excitation shift (REES)

As mentioned above, Zn^{2+} is not released when LF is unfolded, especially at neutral pH. To investigate whether LF is indeed fully unfolded at high concentrations of urea, red-edge excitation shift (REES) measurements using excitation wavelengths ranging from 280 nm to 306 nm were performed. A REES is observable only when the excited protein fluorophores are not fully exposed to the solvent (76,77). Native LF was found to display a REES of approximately 3 nm. Surprisingly, the results of this study show that the REES was observable even at high concentrations of very strong chemical denaturants including GdnSCN, and at very low pH. Furthermore, in some instances, urea- and GdnHCl-exposed LF showed a larger REES than that found for the native protein (see Figure 4.25). An analysis of tyrosine and tryptophan mixtures, however, revealed tyrosine residues to shift the wavelength of maximum emission to lower wavelengths when samples were excited below 290 nm (see Figure 4.23 and Figure 4.24). Thus, the overlapping emission spectra of tyrosine and tryptophan at low excitation wavelengths greatly affect the position of the emission maximum, leading to a rather artificial increase in the overall REES. This might explain why LF, even at high denaturant concentrations, displayed a rather large REES. It is important to point out, however, that such a large shift in λ_{max}, as observed in Y/NATA mixtures, is not expected in proteins containing tyrosine and tryptophan residues because, in proteins, the emission of tyrosine is significantly reduced due to tyrosine-to-tryptophan fluorescence energy transfer (97,98). Since, in Y/NATA mixtures, the molecules are much further away from each other (than is the case in proteins), such quenching of the tyrosine fluorescence is not expected. Hence, a distinct tyrosine emission band is clearly visible only in the fluorescence spectra of Y/NATA mixtures.

A few reports on protein conformational changes during denaturation show that a REES can be observed when the protein contains a fair amount of tyrosine residues (99-102). Tryptophan residues, on the other hand, can be selectively excited at wavelengths of 295 nm or above (76,85). When only the excitation wavelength range of 295 nm to 306 nm is considered, LF unfolded in the presence of GdnSCN at pH 2.0 does not show a REES, suggesting that the protein is fully unfolded under these conditions (Figure 4.25). In addition, these studies also clearly suggest that both tyrosine and tryptophan residues contribute to a REES in LF if excitation wavelengths between 280 nm and 290 nm are considered. Overall, the fold of LF appears to be very resilient to different chemical denaturants including urea, GdnHCl, and GdnSCN. In contrast to the intrinsic tryptophan fluorescence titrations, the REES studies clearly demonstrate that LF is not fully unfolded at low to moderate denaturant concentrations (see Figure 4.21). The residual fold under those conditions may then explain why Zn^{2+} is released (or accessible) far beyond the midpoint concentrations recorded in the unfolding profiles. It is therefore likely that the metal accessibility and release transitions correlate with structural or conformational changes in LF, which are not observable by tryptophan fluorescence spectroscopy.

6 Conclusions and future studies

In this thesis work, chemical denaturation in combination with acidification was used to study the unfolding of LF, and to monitor the Zn^{2+} ion status of the enzyme. During LF translocation, the protein is exposed to two stressors: a low (acidic) endosomal pH, and the PA pore, which (with the help of a pH gradient) forces LF to become unfolded. Whether some of the active site geometry can be maintained to allow the co-translocation of the catalytically important metal ion is not known. Previous studies at pH 7.4 using chemical denaturants have shown that the Zn^{2+} ion is tightly bound to LF's active site, and that the protein is capable of retaining the metal ion under conditions where the native structure of LF is unstable (53). In this study, the unfolding stress imposed by chemical denaturants was combined with a lowering of the pH so as to mimic the conditions of the endosome more closely. The results show that acidification leads to a significant destabilization of the native structure of LF, although the protein never appears to be fully unfolded, even at low pH and in the presence of denaturants at high concentrations. In addition, a decrease in pH leads to a much higher degree of Zn^{2+} release and metal accessibility to chelation by PAR. It is therefore clear that a combination of an unfolding stress and a low pH can destabilize the overall fold and the active site geometry responsible for metal binding in LF. It is therefore likely that the Zn^{2+} ion of LF is not co-translocated with the protein to the cytosol, but rather remains in the endosome. How the translocated, metal-deficient enzyme reinserts Zn^{2+} from a very limited pool of free Zn^{2+} ions to be catalytically functional (and display cytotoxicity) in the cytosol remains to be determined.

Future studies could be pursued to further probe the structural transitions occurring upon acidification and exposure to denaturants using circular dichroism (CD) spectroscopy, especially to investigate whether secondary structural elements remain in unfolded LF. However, to investigate such transitions by CD spectroscopy, the composition of the buffer would need to be altered since chloride ions are known to absorb strongly around 200 nm, a feature which would interfere with the interpretation of CD spectra (103,104).

Similar experiments could also be performed with PAR, using other zinc enzymes such as thermolysin, which contains the same active site motif as LF. Lastly, PAR appears to display unique characteristics as a metal accessibility probe, an aspect which should be further

studied with other metalloproteins. Such studies could provide further knowledge in the field of metalloprotein folding.

7 References

1. Lippard, S. J., and Berg, J. M. (1994) *Principles of Bioinorganic Chemistry*, University Science Books, Mill Valley, CA.

2. Maret, W. (2016) The Metals in the Biological Periodic System of the Elements: Concepts and Conjectures. *Int. J. Mol. Sci.* **17**, 66.

3. Palermo, G., Magistrato, A., Riedel, T., von Erlach, T., Davey, C. A., Dyson, P. J., and Rothlisberger, U. (2016) Fighting Cancer with Transition Metal Complexes: From Naked DNA to Protein and Chromatin Targeting Strategies. *ChemMedChem.* **11**, 1199-1210.

4. Albarede, F., Telouk, P., Balter, V., Bondanese, V. P., Albalat, E., Oger, P., Bonaventura, P., Miossec, P., and Fujii, T. (2016) Medical applications of Cu, Zn, and S isotope effects. *Metallomics* **8**, 1056-1070.

5. Salgado, E. N., Radford, R. J., and Tezcan, F. A. (2010) Metal-directed protein self-assembly. *Acc. Chem. Res.* **43**, 661-672.

6. Wilson, C. J., Apiyo, D., and Wittung-Stafshede, P. (2004) Role of cofactors in metalloprotein folding. *Q. Rev. Biophys.* **37**, 285-314.

7. Muller, F. L., Song, W., Liu, Y., Chaudhuri, A., Pieke-Dahl, S., Strong, R., Huang, T. T., Epstein, C. J., Roberts, L. J., 2nd, Csete, M., Faulkner, J. A., and Van Remmen, H. (2006) Absence of CuZn superoxide dismutase leads to elevated oxidative stress and acceleration of age-dependent skeletal muscle atrophy. *Free Radic. Bio. Med.* **40**, 1993–2004.

8. Igarashi, R. Y., and Seefeldt, L. C. (2003) Nitrogen fixation: the mechanism of the Mo-dependent nitrogenase. *Crit. Rev. Biochem. Mol. Biol.* **38**, 351-384.

9. Mairbaurl, H., and Weber, R. E. (2012) Oxygen transport by hemoglobin. *Compr. Physiol.* **2**, 1463-1489.

10. Welchen, E., and Gonzalez, D. H. (2016) Cytochrome c, a hub linking energy, redox, stress and signaling pathways in mitochondria and other cell compartments. *Physiol. Plant.* **157**, 310-321.

11. Stefanidou, M., Maravelias, C., Dona, A., and Spiliopoulou, C. (2006) Zinc: a multipurpose trace element. *Arch. Toxicol.* **80**, 1-9.

12. Maret, W. (2005) Zinc coordination environments in proteins determine zinc functions. *J. Trace Elem. Med. Biol.* **19**, 7-12.

13. Ward, R. J., Dexter, D. T., and Crichton, R. R. (2015) Neurodegenerative diseases and therapeutic strategies using iron chelators. *J. Trace Elem. Med. Biol.* **31**, 267-273.

14. Poujois, A., Devedjian, J.-C., Moreau, C., Devos, D., Chaine, P., Woimant, F., and Duce, J. A. (2016) Bioavailable Trace Metals in Neurological Diseases. *Curr. Treat Options Neurol.* **18**, 46.

15. Faller, P. (2009) Copper and Zinc Binding to Amyloid-β: Coordination, Dynamics, Aggregation, Reactivity and Metal-Ion Transfer. *Chembiochem.* **10**, 2837-2845.

16. Hane, F., and Leonenko, Z. (2014) Effect of metals on kinetic pathways of amyloid-β aggregation. *Biomolecules* **4**, 101-116.

17. Cristóvão, J. S., Santos, R., and Gomes, C. M. (2016) Metals and Neuronal Metal Binding Proteins Implicated in Alzheimer's Disease. *Oxid. Med. Cell Longev.* **2016.**, 9812178.

18. Colvin, R. A., Holmes, W. R., Fontaine, C. P., and Maret, W. (2010) Cytosolic zinc buffering and muffling: their role in intracellular zinc homeostasis. *Metallomics* **2**, 306-317.

19. Kaur, K., Gupta, R., Saraf, S. A., and Saraf, S. K. (2014) Zinc: The Metal of Life. *Compr. Rev. Food Sci. Food Saf.* **13**, 358-376.

20. Irving, H., and Williams, R. (1953) The stability of transition-metal complexes. *J. Chem. Soc.* **8**, 3192-3210.

21. Bonaventura, P., Benedetti, G., Albarede, F., and Miossec, P. (2015) Zinc and its role in immunity and inflammation. *Autoimmun. Rev.* **14**, 277-285.

22. Marger, L., Schubert, C. R., and Bertrand, D. (2014) Zinc: an underappreciated modulatory factor of brain function. *Biochem. Pharmacol.* **91**, 426-435.

23. Kochańczyk, T., Drozd, A., and Krężel, A. (2015) Relationship between the architecture of zinc coordination and zinc binding affinity in proteins–insights into zinc regulation. *Metallomics* **7**, 244-257.

24. Fukasawa, K. M., Hata, T., Ono, Y., and Hirose, J. (2011) Metal preferences of zinc-binding motif on metalloproteases. *J. amino acids* **2011**, 574816.

25. Roset, R., Inagaki, A., Hohl, M., Brenet, F., Lafrance-Vanasse, J., Lange, J., Scandura, J. M., Tainer, J. A., Keeney, S., and Petrini, J. H. (2014) The Rad50 hook domain regulates DNA damage signaling and tumorigenesis. *Genes Dev.* **28**, 451-462.

26. Doganay, M., and Demiraslan, H. (2015) Human anthrax as a re-emerging disease. *Recent Pat. Antiinfect. Drug Discov.* **10**, 10-29.

27. Mock, M., and Fouet, A. (2001) Anthrax. *Annu. Rev. Microbiol.* **55**, 647-671.

28. D'Amelio, E., Gentile, B., Lista, F., and D'Amelio, R. (2015) Historical evolution of human anthrax from occupational disease to potentially global threat as bioweapon. *Environ. Int.* **85**, 133-146.

29. Schwartz, M. (2009) Dr. Jekyll and Mr. Hyde: a short history of anthrax. *Mol. Aspects. Med.* **30**, 347-355.

30. Sternbach, G. (2003) The history of anthrax. *J. Emerg. Med.* **24**, 463-467.

31. Misgie, F., Atnaf, A., and Surafel, K. (2015) A Review on Anthrax and its Public Health and Economic Importance. *Acad. J. Anim. Diseases* **4**, 196-204.

32. Beyer, W., and Turnbull, P. C. (2009) Anthrax in animals. *Mol. Aspects. Med.* **30**, 481-489.

33. Al-Bayati, M. A. (2004) Severe hair loss induced by anthrax vaccine and reversed by the treatment with zinc. *Med. Veritas* **1**, 159-162.

34. Driks, A. (2009) The *Bacillus anthracis* spore. *Mol. Aspects Med.* **30**, 368-373.

35. Owen, J. L., Yang, T., and Mohamadzadeh, M. (2015) New insights into gastrointestinal anthrax infection. *Trends Mol. Med.* **21**, 154-163.

36. Moayeri, M., Leppla, S. H., Vrentas, C., Pomerantsev, A. P., and Liu, S. (2015) Anthrax Pathogenesis. *Annu. Rev. Microbiol.* **69**, 185-208.

37. Liu, S., Moayeri, M., and Leppla, S. H. (2014) Anthrax lethal and edema toxins in anthrax pathogenesis. *Trends Microbiol.* **22**, 317-325.

38. Young, J. A., and Collier, R. J. (2007) Anthrax toxin: receptor binding, internalization, pore formation, and translocation. *Annu. Rev. Biochem.* **76**, 243-265.

39. Moayeri, M., Sastalla, I., and Leppla, S. H. (2012) Anthrax and the inflammasome. *Microbes Infect.* **14**, 392-400.

40. Williamson, E. D., and Dyson, E. H. (2015) Anthrax prophylaxis: recent advances and future directions. *Front. Microbiol.* **6**, 1009.

41. Nestorovich, E. M., and Bezrukov, S. M. (2014) Designing inhibitors of anthrax toxin. *Expert opin. Drug Discov.* **9**, 299-318.

42. Chitlaru, T., Altboum, Z., Reuveny, S., and Shafferman, A. (2011) Progress and novel strategies in vaccine development and treatment of anthrax. *Immunol. Rev.* **239**, 221-236.

43. Zakowska, D., Bartoszcze, M., Niemcewicz, M., Bielawska-Drozd, A., Knap, J., Cieslik, P., Chomiczewski, K., and Kocik, J. (2015) *Bacillus anthracis* infections-new possibilities of treatment. *Ann. Agric. Environ. Med.* **22**, 202-207.

44. Artenstein, A. W., and Opal, S. M. (2012) Novel approaches to the treatment of systemic anthrax. *Clin. Infect. Dis.* **54**, 1148-1161.

45. Thoren, K. L., and Krantz, B. A. (2011) The unfolding story of anthrax toxin translocation. *Mol. Microbiol.* **80**, 588-595.

46. Geny, B., and Popoff, M. R. (2006) Bacterial protein toxins and lipids: pore formation or toxin entry into cells. *Biol. Cell* **98**, 667-678.

47. Bann, J. G. (2012) Anthrax toxin protective antigen-insights into molecular switching from prepore to pore. *Protein Sci.* **21**, 1-12.

48. Scobie, H. M., and Young, J. A. (2005) Interactions between anthrax toxin receptors and protective antigen. *Curr. Opin. Microbiol.* **8**, 106-112.

49. Gruenberg, J., and van der Goot, F. G. (2006) Mechanisms of pathogen entry through the endosomal compartments. *Nat. Rev. Mol. Cell Biol.* **7**, 495-504

50. Fabre, L., Santelli, E., Mountassif, D., Donoghue, A., Biswas, A., Blunck, R., Hanein, D., Volkmann, N., Liddington, R., and Rouiller, I. (2016) Structure of anthrax lethal toxin prepore complex suggests a pathway for efficient cell entry. *J. Gen. Physiol.* **148**, 313-324.

51. Jiang, J., Pentelute, B. L., Collier, R. J., and Zhou, Z. H. (2015) Atomic structure of anthrax protective antigen pore elucidates toxin translocation. *Nature* **521**, 545-549.

52. Schiffmiller, A., and Finkelstein, A. (2015) Ion conductance of the stem of the anthrax toxin channel during lethal factor translocation. *J. Mol. Biol.* **427**, 1211-1223.

53. Lo, S. Y., Säbel, C. E., Mapletoft, J. P., and Siemann, S. (2015) Influence of chemical denaturants on the activity, fold and zinc status of anthrax lethal factor. *Biochem. Biophys. Rep.* **1**, 68-77.

54. Brown, M. J., Thoren, K. L., and Krantz, B. A. (2015) Role of the α-clamp in the protein translocation mechanism of anthrax toxin. *J. Mol. Biol.* **427**, 3340-3349.

55. Thoren, K. L., Worden, E. J., Yassif, J. M., and Krantz, B. A. (2009) Lethal factor unfolding is the most force-dependent step of anthrax toxin translocation. *Proc. Natl. Acad. Sci. U. S. A.* **106**, 21555-21560.

56. Feld, G. K., Brown, M. J., and Krantz, B. A. (2012) Ratcheting up protein translocation with anthrax toxin. *Protein Sci.* **21**, 606-624.

57. Das, D., and Krantz, B. A. (2016) Peptide- and proton-driven allosteric clamps catalyze anthrax toxin translocation across membranes. *Proc . Natl. Acad. Sci. U. S. A.* **113**, 9611-9616.

58. Wynia-Smith, S. L., Brown, M. J., Chirichella, G., Kemalyan, G., and Krantz, B. A. (2012) Electrostatic ratchet in the protective antigen channel promotes anthrax toxin translocation. *J. Biol. Chem.* **287**, 43753-64374.

59. Brown, M. J., Thoren, K. L., and Krantz, B. A. (2011) Charge requirements for proton gradient-driven translocation of anthrax toxin. *J. Biol. Chem.* **286**, 23189-23199.

60. Pannifer, A. D., Wong, T. Y., Schwarzenbacher, R., Renatus, M., Petosa, C., Bienkowska, J., Lacy, D. B., Collier, R. J., Park, S., and Leppla, S. H. (2001) Crystal structure of the anthrax lethal factor. *Nature* **414**, 229-233.

61. Maize, K. M., Kurbanov, E. K., De La Mora-Rey, T., Geders, T. W., Hwang, D. J., Walters, M. A., Johnson, R. L., Amin, E. A., and Finzel, B. C. (2014) Anthrax toxin lethal factor domain 3 is highly mobile and responsive to ligand binding. *Acta. Crystallogr. D. Biol. Crystallogr.* **70**, 2813-2822.

62. Tonello, F., Naletto, L., Romanello, V., Dal Molin, F., and Montecucco, C. (2004) Tyrosine-728 and glutamic acid-735 are essential for the metalloproteolytic activity of the lethal factor of Bacillus anthracis. *Biochem. Biophys. Res. Commun.* **313**, 496-502.

63. Lipscomb, W. N., and Sträter, N. (1996) Recent advances in zinc enzymology. *Chem. Rev.* **96**, 2375-2434.

64. Tonello, F., and Montecucco, C. (2009) The anthrax lethal factor and its MAPK kinase-specific metalloprotease activity. *Mol. Aspects Med.* **30**, 431-438.

65. Montpellier, L. H., and Siemann, S. (2013) Effect of pH on the catalytic function and zinc content of native and immobilized anthrax lethal factor. *FEBS lett.* **587**, 317-321.

66. Sabel, C. E., Carbone, R., Dabous, J. R., Lo, S. Y., and Siemann, S. (2011) Preparation and characterization of cobalt-substituted anthrax lethal factor. *Biochem. Biophys. Res. Commu.* **416**, 106-110.

67. Ellis, K. J., and Morrison, J. F. (1982) Buffers of constant ionic strength for studying pH-dependent processes. *Methods Enzymol.* **87**, 405-426.

68. Kocyla, A., Pomorski, A., and Krezel, A. (2015) Molar absorption coefficients and stability constants of metal complexes of 4-(2-pyridylazo)resorcinol (PAR): Revisiting common chelating probe for the study of metalloproteins. *J. Inorg. Biochem.* **152**, 82-92.

69. Sabel, C. E., St-Denis, S., Neureuther, J. M., Carbone, R., and Siemann, S. (2010) Alkaline earth metals are not required for the restoration of the apoform of anthrax lethal factor to its holoenzyme state. *Biochem. Biophys. Res. Commun.* **403**, 209-213.

70. Tonello, F., Ascenzi, P., and Montecucco, C. (2003) The metalloproteolytic activity of the anthrax lethal factor is substrate-inhibited. *J. Biol. Chem.* **278**, 40075-40078.

71. Tonello, F., Seveso, M., Marin, O., Mock, M., and Montecucco, C. (2002) Screening inhibitors of anthrax lethal factor. *Nature* **418**, 386.

72. Sabel, C. E., Neureuther, J. M., and Siemann, S. (2010) A spectrophotometric method for the determination of zinc, copper, and cobalt ions in metalloproteins using Zincon. *Anal. Biochem.* **397**, 218-226.

73. Santoro, M. M., and Bolen, D. (1988) Unfolding free energy changes determined by the linear extrapolation method. 1. Unfolding of phenylmethanesulfonyl α-chymotrypsin using different denaturants. *Biochemistry* **27**, 8063-8068.

74. Morjana, N. A., McKeone, B. J., and Gilbert, H. F. (1993) Guanidine hydrochloride stabilization of a partially unfolded intermediate during the reversible denaturation of protein disulfide isomerase. *Proc. Natl. Acad. Sci. U. S. A.* **90**, 2107-2111.

75. Eftink, M. R. (1994) The use of fluorescence methods to monitor unfolding transitions in proteins. *Biophys. J.* **66**, 482-501.

76. Chattopadhyay, A., and Haldar, S. (2014) Dynamic insight into protein structure utilizing red edge excitation shift. *Acc. Chem. Res.* **47**, 12-19.

77. Demchenko, A. P. (2002) The red-edge effects: 30 years of exploration. *Luminescence* **17**, 19-42.

78. Baldwin, R. L. (1996) How Hofmeister ion interactions affect protein stability. *Biophys. J.* **71**, 2056-2063.

79. Zhang, Y., and Cremer, P. S. (2006) Interactions between macromolecules and ions: the Hofmeister series. *Curr. opin. Chem. Biol.* **10**, 658-663.

80. Schneider, C. P., Shukla, D., and Trout, B. L. (2011) Arginine and the Hofmeister Series: the role of ion-ion interactions in protein aggregation suppression. *J. Phys. Chem. B.* **115**, 7447-7458.

81. Lange, C., and Rudolph, R. (2009) Suppression of Protein Aggregation by L-Arginine. *Curr. Pharm. Biotechnol.* **10**, 408-414.

82. Nuhu, M. M., and Curtis, R. (2015) Arginine dipeptides affect insulin aggregation in a pH- and ionic strength-dependent manner. *Biotechnol. J.* **10**, 404-416.

83. Lakowicz, J. R. (2013) *Principles of fluorescence spectroscopy*, Springer, Baltimore, Maryland, U. S. A.

84. Mason, P. E., Neilson, G. W., Dempsey, C. E., Barnes, A. C., and Cruickshank, J. M. (2003) The hydration structure of guanidinium and thiocyanate ions: implications for protein stability in aqueous solution. *Proc. Natl. Acad. Sci. U S A.* **100**, 4557-4561.

85. Haldar, S., Chaudhuri, A., and Chattopadhyay, A. (2011) Organization and dynamics of membrane probes and proteins utilizing the red edge excitation shift. *J. Phys. Chem. B.* **115**, 5693-5706.

86. Kumar, C. S., Sivaramakrishna, D., Ravi, S. K., and Swamy, M. J. (2016) Fluorescence investigations on choline phospholipid binding and chemical unfolding of HSP-1/2, a major protein of horse seminal plasma. *J. Photochem. Photobiol. B, Biology* **158**, 89-98.

87. Inouye, K., Kuzuya, K., and Tonomura, B. (1998) Effect of Salts on the Solubility of Thermolysin: A Remarkable Increase in the Solubility as Well as the Activity by the Addition of Salts without Aggregation or Dispersion of Thermolysin. *J. Biochem.* **123**, 847-852.

88. Shah, D., Li, J., Shaikh, A. R., and Rajagopalan, R. (2012) Arginine-aromatic interactions and their effects on arginine-induced solubilization of aromatic solutes and suppression of protein aggregation. *Biotechnol. Prog.* **28**, 223-231.

89. Fink, A. L., Calciano, L. J., Goto, Y., Kurotsu, T., and Palleros, D. R. (1994) Classification of acid denaturation of proteins: intermediates and unfolded states. *Biochemistry* **33**, 12504-12511.

90. Goto, Y., Takahashi, N., and Fink, A. L. (1990) Mechanism of acid-induced folding of proteins. *Biochemistry* **29**, 3480-3488.

91. Goto, Y., Calciano, L. J., and Fink, A. L. (1990) Acid-induced folding of proteins. *Proc. Natl. Acad. Sci. U. S. A.* **87**, 573-577.

92. Krantz, B. A., Trivedi, A. D., Cunningham, K., Christensen, K. A., and Collier, R. J. (2004) Acid-induced unfolding of the amino-terminal domains of the lethal and edema factors of anthrax toxin. *J. Mol. Biol.* **344**, 739-756.

93. Pace, C. N., and Hermans, J. (1975) The Stability of Globular Protein. *CRC Crit. Rev. Biochem.* **3**, 1-43.

94. Mulligan, V. K., Kerman, A., Ho, S., and Chakrabartty, A. (2008) Denaturational Stress Induces Formation of Zinc-Deficient Monomers of Cu,Zn Superoxide Dismutase: Implications for Pathogenesis in Amyotrophic Lateral Sclerosis. *J. Mol. Biol.* **383**, 424-436.

95. Peroza, E. A., dos Santos Cabral, A., Wan, X., and Freisinger, E. (2013) Metal ion release from metallothioneins: proteolysis as an alternative to oxidation. *Metallomics* **5**, 1204-1214.

96. Siemann, S., Brewer, D., Clarke, A. J., Dmitrienko, G. I., Lajoie, G., and Viswanatha, T. (2002) IMP-1 metallo-β-lactamase: effect of chelators and assessment of metal requirement by electrospray mass spectrometry. *Biochim. Biophys. Acta.* **1571**, 190-200.

97. Weber, G. (1960) Fluorescence-polarization spectrum and electronic-energy transfer in proteins. *Biochem. J.* **75**, 345-352.

98. Weber, G. (1960) Fluorescence-polarization spectrum and electronic-energy transfer in tyrosine, tryptophan and related compounds. *Biochem. J.* **75**, 335-345.

99. Catici, D. A., Amos, H. E., Yang, Y., van den Elsen, J. M., and Pudney, C. R. (2016) The red edge excitation shift phenomenon can be used to unmask protein structural ensembles: implications for NEMO-ubiquitin interactions. *FEBS J.* **283**, 2272-2284.

100. Kelkar, D. A., Chaudhuri, A., Haldar, S., and Chattopadhyay, A. (2010) Exploring tryptophan dynamics in acid-induced molten globule state of bovine α-lactalbumin: a wavelength-selective fluorescence approach. *Eur. Biophys. J.* **39**, 1453-1463.

101. Chaudhuri, A., Haldar, S., and Chattopadhyay, A. (2010) Organization and dynamics of tryptophans in the molten globule state of bovine α-lactalbumin utilizing wavelength-selective fluorescence approach: comparisons with native and denatured states. *Biochem. Biophys. Res. Commun.* **394**, 1082-1086.

102. Chattopadhyay, A., Rawat, S. S., Kelkar, D. A., Ray, S., and Chakrabarti, A. (2003) Organization and dynamics of tryptophan residues in erythroid spectrin: novel structural features of denatured spectrin revealed by the wavelength-selective fluorescence approach. *Protein Sci.* **12**, 2389-2403.

103. Kelly, S. M., Jess, T. J., and Price, N. C. (2005) How to study proteins by circular dichroism. *Biochim. Biophys. Acta.* **1751**, 119-139.

104. Greenfield, N. J. (2006) Using circular dichroism spectra to estimate protein secondary structure. *Nat. Protoc.* **1**, 2876-2890.